Contributions to Smart Metering: Protocol Design and Data Analytics

Yue Yang

A dissertation submitted in partial fulfillment of the
requirements for the degree of

Doctor of Philosophy

University of Washington

2015

Reading Committee:

Sumit Roy, Chair

Daniel Kirschen

James Ritcey

Baosen Zhang

Program Authorized to Offer Degree:
Electrical Engineering

University of Washington

Abstract

Contributions to Smart Metering: Protocol Design and Data Analytics

Yue Yang

Chair of the Supervisory Committee:
Professor Sumit Roy
Electrical Engineering

The next generation Advanced Metering Infrastructure (AMI), with the aid of two-way Smart Metering Network (SMN), is expected to support many advanced functions, such as remote reading and control, demand response, etc. In order to satisfy the communication requirements of these applications, the information transportation protocol design and data analytics are of fundamental importance to the design of SMN and associated research topics that need to be discussed.

A suitable and well-designed Multiple Access Control (MAC) protocol is critical to the transportation of information in SMN. First, SMN traffic may be classified according to their communication requirements; thus each type may require a different MAC protocol which is specially designed for it. Furthermore, as discussed in Chapter 2, because the number of Smart Meters (communication nodes) involved in such a single SMN is much larger than those in today's local area networks, the traditional MAC protocols are unlikely to perform well in SMN.

In order to solve this scalability issue for event-driven traffic, in Chapter 3, we propose two grouping based MAC protocols: TDMA-DCF and Group Leader DCF-TDMA. Both of them reduce the competitive random channel contentions in SMN effectively by dividing all the Smart Meters into several groups. The group division and management schemes are also clearly presented. We conduct comprehensive throughput and delay analysis on these two schemes for unsaturated traffic conditions and hidden node events. From the numerical

results, we observe that the performance of these two grouping based MAC protocols are significantly better than those of traditional random access protocols.

In order to solve the scalability issue for periodic data transportation, in Chapter 4, we propose a modified PCF scheme with the aid of cognitive radio technology, in which the Smart Meters are allowed to use the white space to report the periodic data to the data aggregator as secondary users. The comprehensive throughput analysis is also presented. The numerical and simulation results through NS-3 show that the modified PCF with cognitive radio significantly outperforms the traditional one in SMN.

In Chapter 5, we focus on a specific type of periodic reporting data, power factor measurement, which is an important information to the power grid security and infrequently changing. Therefore, we exploit the time-invariant nature of this measurement and propose a new MAC protocol by using compressive sensing, a famous signal processing and reconstruction technique. The simulation results show that this proposed scheme can solve the scalability issue effectively and outperform the traditional MAC protocols.

An effective analysis of Smart Metering data is critical to demand response, one of the most important applications in SMN, whereby customers use aggregated power consumption data (available locally via Smart Meters) and real-time pricing information (send pre-emptively from the utility) to schedule their future energy use to enhance conservation goals. This requires enabling customers to determine *disaggregated* consumption at individual appliance level from aggregated power consumption data. Therefore, in Chapter 6, we propose a real-time disaggregation algorithm based on a new Markov Chain model for the power consumption of individual electrical appliances. The model incorporates both temporal and inter-device correlations which are used to estimate the appliance-level disaggregated power consumption through the application of the Viterbi Algorithm. The performance is vetted through significant testing with real minute-resolution power consumption data and proves the accurate estimation.

TABLE OF CONTENTS

LIST OF FIGURES

LIST OF TABLES

GLOSSARY

AMI: Advanced Metering Infrastructure

AMR: Automatic Meter Reading

AP: Access Point

CFP: Contention Free Phase

CR: Cognitive Radio

CP-PCF: PCF Scheme with CR

CS: Compressive Sensing

DCF: Distributed Coordination Function

DCFT: DCF-TDMA Scheme

EMS: Energy Management System

EV: Electric Vehicle

GMAC: Group-based MAC Protocol

HAN: Home Area Network

IED: Intelligent Electronic Device

LAN: Local Area Network

LC: Local Collector

MAC: Multiple Access Control

MDM: Meter Data Management

NAN: Neighborhood Area Network

PCF: Point Coordination Function

PHEV: Plug-in Hybrid Electric Vehicle

PLC: Power Line Carrier

PU: Primary User

RTP: Real Time Price

SG: Smart Grid

SM: Smart Meter

SMN: Smart Metering Network

SU: Secondary User

TDCF: TDMA-DCF Scheme

TDMA: Time Division Multiple Access

TMAC: Token-coordinated random access MAC Protocol

WAN: Wide Area Network

ACKNOWLEDGMENTS

The author wishes to express sincere appreciation to everyone who has kindly offered help during my Ph.D. study.

First of all, I would like to express my heartfelt gratitude to my Ph.D. advisor, Prof. Sumit Roy. His immense knowledge and insightful guidance are always leading me towards the promising direction. His idea have supported me during the most difficult moment in my research and study. It is my pleasure to have him as my advisor.

In addition, I want to thank all the members of my Ph.D. Committee, Prof. Daniel Kirschen, Prof. James A. Ritcey, Prof. Baosen Zhang, and Prof. Archis Ghate, for their generous help and valuable suggestions.

Furthermore, I would like to thank all my UW professors, labmates and friends who have helped me with my research and study. Prof. Radha Poovendran, Prof. Payman Arabshahi, Prof. Miguel A. Ortega Vazquez, Prof. Sreeram Kannan, Hamed Firooz, Ling Luo, Fei Ye, Linda Bai, Colby Boyer, Abdulmohsen Mutairi, Farzad Hessar, Hossein Safavi, Chang Wook Kim, Shwan Ashrafi, Yoshikazu Nishida, Benjamin Morgan, De Meng, Zixia Hu, Xiang Zou, Chou-Chang Yang, Xuhang Ying, all supported my work in various ways.

At last I want to sincerely thank my family - my parents Hualong Yang and Xiuying Qiu, and my girl friend Xinyu Xie. Without their support, I will not be able to finish this work.

DEDICATION

to my Family

Chapter 1

INTRODUCTION

Traditionally, the collection of power data from end-customer premises has been accomplished using conventional power meters. Even if such meters could be remotely read as in Automated Meter Reading (AMR) systems, such capabilities were limited to one-way, infrequent data upload. The next generation - Advanced Metering Infrastructure (AMI) - is based on a *two-way* network, Smart Metering Network (SMN), which is comprised with the communications transceivers integrated into Smart Meters. Therefore, in addition to the remote reading function, AMI may also support remote control, load management and demand response by sending down-link control information from the utility. We provide a high-level comparison of these three generations of power metering systems in the Fig.1.1 and introduce the AMI applications and SMN architecture in more details in Chapter 2. In order to satisfy the communication requirements of those advanced applications in A-MI, the information transportation protocol design and data analytics become the most two significant parts in the SMN design and associated research topics that need to be investigated.

1.1 MAC Protocols Design for Smart Metering Network

In the past few years, how to transport the information to the data destinations in SMN quickly, reliably and efficiently attracts researchers' attentions a lot. A large amount of literature discusses the selection of suitable bi-directional communication/networking technology to take the responsibility of data transportation [53], [50]. The unlicensed wireless technologies, such as 802.11 Wireless LANs (WiFi), appear to be preferred options, for their low cost and widespread prior adoption, given the fact that no new licensed spectrum will be available for AMI. Furthermore, in order to solve some potential challenges unique to SMN scenarios, a new IEEE Standardization Task Group (IEEE 802.11ah TG) [4] is currently

Generation	System	Comm. Network	Terminal Device	Function
Last	Traditional Power Metering System	No Comm. Network	Conventional Meters	Manual Reading
Current	Automatic Meter Reading (AMR)	One-way Comm. Network	Conventional Meters Coupled with One-way Comm. Infrastructure	Remote Reading
Current/ Next	Advanced Metering Infrastructure (AMI)	Two-way Comm. Network (SMN)	Smart Meters	Remote Reading and Control, Load Management, Demand Response, Fault Detection

Figure 1.1: Comparison among three Generations of Power Metering Systems

engaged in creating a modified 802.11 based standard that operates at the frequencies below 1 GHz.

In addition to that, a well designed Multiple Access Control (MAC) protocol also plays a big role in the SMN wireless transportation work, due to the following reasons:

First, SMN traffic may be classified into two categories according to their communication requirements. The event-driven data is generated unpredictably in response to some urgent events and thus must be communicated as soon as possible, while the periodic data can be scheduled and is usually quite delay tolerant. Therefore, each type of traffic may require a different MAC protocol which is specially designed for it.

Furthermore, as discussed more in the Chapter 2, both the coverage of network and the number of Smart Meters involved in SMN significantly exceed those in indoor WiFi networks for which application they were originally designed. For example, IEEE 802.11ah TG requires one data collector to support a network with upto 6000 Smart Meters as a benchmark [2], while the average number of communications node served by a single WiFi BSSID is on the order of 20-30. Therefore, the traditional WiFi MAC protocols do not perform well in the application of SMN.

In order to solve the scalability issue for the event-driven traffic, in Chapter 3, we pro-

pose two grouping based random access MAC protocols: TDMA-DCF and Group Leader DCF-TDMA scheme. These two schemes divide all Smart Meters into several groups to reduce the competitive channel access and are both directed at 802.11 type networks operating at the frequencies below 1GHz, that has been adopted by the IEEE 802.11ah TG. We also conduct comprehensive throughput and delay analysis on these schemes for unsaturated traffic conditions and hidden node events. The numerical results show that these two grouping based MAC protocols significantly outperform the traditional random access protocol DCF in a densely populated network with large coverage like SMN.

In order to solve the scalability issue for periodic data transportation, in Chapter 4, we propose a modified PCF scheme with the combination of cognitive radio technology, in which the Smart Meters may use the white space to report power consumption measurements to the data aggregator when the primary users are not occupying the channels. We also conduct comprehensive throughput analysis on the proposed scheme. The numerical and simulation results through NS-3 show that the PCF scheme with cognitive radio significantly outperforms the traditional one.

Furthermore, in Chapter 5, we focus on a specific kind of periodic reporting data, power factor measurement, which is one of the most important information for the future power grid security. Different with other periodic traffic, such as power consumption data, power factor measurement is infrequently changing. Therefore, in order to solve the scalability issue for this specific data report, we exploit the time-invariant nature of this measurement and propose a MAC protocol with the aid of compressive sensing, a well-known signal processing and recovery technique. The simulation results show that this proposed method significantly outperforms the traditional MAC protocols in a densely populated network like SMN.

1.2 Real-time Disaggregation of End-use Power Consumption

Future in-building power management systems will incorporate *demand response* as a key application to improve energy utilization. Increasingly, Smart Meters located on premises will record the aggregate power consumptions and periodically report them to the data aggregator. Based on this temporal power consumption data record, the utility will anticipate

the load in the next forecast period, and broadcast a real-time energy price for that period back to the consumer. The consumer will use the price signal to determine appliance level actions (i.e. which ones to turn on/off during which period) to lower power consumption and cost.

Presently, the customer only has access to aggregated power consumption from the S-mart Meter. As a result, it is difficult for the customers to determine what appliances are responsible for their main loads. For example, according to [33],[54], consumers easily underestimate the energy consumed by heating or cooling devices and overestimated the energy used by other appliances. Therefore, as mentioned in [25], any data driven algorithm that allows the consumer access to *disaggregated power consumption at individual appliance level* will be a key component of enabling future demand response type mechanisms. Current disaggregation algorithms suffer either from limited accuracy or costly installation and maintenance. Furthermore, many do not achieve sufficiently low disaggregation delay implying constraints on (near) real-time operation necessary for Demand Side Management. In Chapter 6, we propose a real-time disaggregation algorithm based on Markov Chain model and implement it with Viterbi Algorithm. The model captures the inherent two dimensional correlations of minute-resolution power consumption behavior of each individual electrical appliance, that allows reliable estimation of their disaggregation power consumption status with short delay.

1.3 Thesis Organization

The rest of the dissertation is organized as follows. In Chapter 2, we introduce the AMI network features, including AMI applications, SMN architecture, candidate communication technologies and traffic types. The scalability issue within the SMN is also explained in details. The Grouping based MAC protocol design for event-driven data transportation is illustrated in Chapter 3. The proposed MAC protocols for periodic data reporting with the aid of cognitive radio and compressive sensing are explained in Chapter 4 and Chapter 5 respectively. The real-time power consumption disaggregation algorithm using Markov Chain model and Viterbi Algorithm is presented in the Chapter 6. We concludes the entire dissertation in 7.

Chapter 2

ADVANCED METERING INFRASTRUCTURE AND SMART METERING NETWORK FEATURES

2.1 AMI Applications and Benefits

We briefly summarize several representative applications of AMI and their resulting benefits.

2.1.1 Outage Detection and Management

Traditionally, outage may only be detected by a report from customers and other monitoring at the control center. With the aid of SMN, the utility can devise a more efficient way to detect the outage and improve response time. For example, once the voltage drops below a threshold for a duration, the Smart Meter may report a warning message and enable the control center to detect and locate the source of an impending outage event.

2.1.2 Demand Response

With SMN, the customers will be able to acquire their own real-time energy usage data and use dynamic pricing information sent by the utility, to make better decisions or manage automatically on use of the electric appliances within the premises, so as to conserve energy and cost.

2.1.3 Power Quality Monitoring

The status of monitoring of the distribution segment (from the distribution substation to customers) is currently very limited. AMI enables collection of various types of real-time data at many more points - such as feeder voltage and current, power quality within a customer premise etc. This will lead to more efficient and accurate power quality monitoring.

2.1.4 Remote Connect and Disconnect

With the aid of SMN, a utility may remotely enable or disable the energy delivery to certain customers, so as to smooth consumption peaks or automatically react to some emergency events.

The above is only a partial list of applications and benefits from AMI. In summary, with the help of the bi-directional communication network, AMIs can improve operational efficiency, reliability and security.

2.2 Smart Metering Network Architecture

Fig.2.1 presents an SMN system based on the Smart Grid Architecture given in [10]. A short overview of its main components follows:

- *Smart Meter (SM):* This device has three different roles. First, the Smart Meter is a multi-utility instrument measuring electric power consumption (and possibly in future, gas, water and heat). It can thus act as an energy control center, i.e. as a point of aggregation for usage information collected by using a Home Area Network (HAN) that connects home appliances. Finally, the Smart Meter also serves as the gateway between HAN and external network; it reports on energy consumption, sends out urgent data, receives remote commands from the utility and is responsible for security of the above transactions.

- *Home Area Network (HAN):* This is composed of multiple inter-connected electric appliances, such as air conditioner, dish washer, plug-in hybrid electric vehicles (PHEV) etc. and the Smart Meter. All the components inside HAN share information or deliver control commands to each other. For example, the dish washer may send a signal to Smart Meter, requesting it to send a 'postpone' command to the charging PHEV, so that it may operate without incurring excessive energy cost at that time.

- *Local Collector (LC):* Between the Smart Meter and Utility Center, there could be multiple layers of intelligent electronic devices that act as data concentrators. For

example, a data collection node closer to customer premises - named as Local Collector - collects SM data from multiple premises and relays it to the Central Collector. Additional functions at the Local Collector may include simple data processing and distributed decision and intelligence using it's own data. The network segment between Smart Meter and Local Collector is called Neighborhood Area Network (NAN), while that above Local Collector belongs to Wide Area Network (WAN).

- *Central Collector:* A centralized data repository for the entire region operated by the utility that acts as the interface with Control Center, Billing Center and Asset Management Center. These centers may use this data to conduct analysis and evaluate system status, and make decisions or deliver control commands to other components.

The mapping between the SMN components and their prospective physical deployments is also shown in the Fig.2.1. For example, the Local Collector could be located at a Distribution Transformer because it would be easy to power the Collector and obtain measurements from other feeder devices. On the other hand, the independent deployment for Local Collector may provide more flexibility to adjust its coverage range. The Central Collector is likely to be deployed closer to the centers. If the utility's coverage region is not very large, only one Central Collector located close to the centers may suffice. Otherwise, Collectors may be placed at the Distribution Substation as the second tier data relay. The network from the Local Collector to the Central System simply transports the data collected in the NAN segment, and as such we focus on the design of MAC protocols at the Local Collector (NAN).

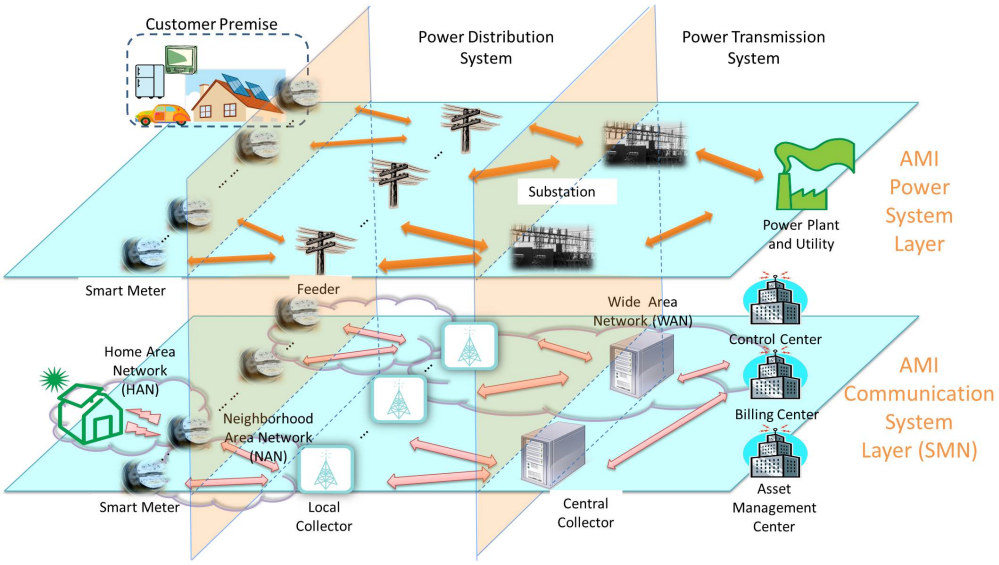

Figure 2.1: AMI Power and Communication System Architectures

2.3 Communication Technologies

A large amount of literature discusses the feasibility of several optional bi-directional communication technologies applied on the SMN. We summarize the various options and highlight their pros/cons in Fig.2.2.

In Power Line Carrier (PLC), the data is transmitted over electricity transmission lines along with electrical power [41]. Its communication performance depends on several factors, such as frequency, propagation distance and existence of transformers because the data signals cannot go through the transformers. PLC has gained a lot of attractions because it uses the existing power lines as signal carrier and no extra cabling fee is needed. Therefore, many countries (e.g. Singapore) adopted it for broadband communication services. However, PLC also suffers from several disadvantages, such as high signal attenuation, high noisy medium and lower scalability, which leads to the termination of deployment in some countries (e.g. US) [52].

WiFi is a communication technology that allows devices to exchange data wirelessly based on IEEE 802.11 Standards. Its popularity and better reliability than other wireless communication technologies make it on the top of the candidate technology list. Further-

Technology	Applications	Benefits	Limitations
Power Line Carrier	WAN, NAN, HAN	No Extra Cabling Fee, High Security	High Noisy Medium, Low Scalability
Messaging over Cellular Network	HAN, NAN, WAN	Mature Development, Long Range	Low Data Rate, Low Robustness, Low Security, Costly Spectrum Fees, Low Scalability
WiFi	HAN, NAN, WAN (with multi-hop)	Mature Development, Free License, High Robustness	Low Security, Low Scalability
ZigBee	HAN	Low Cost	Short Range, Low Security, Low Data Rate

Figure 2.2: Comparison among optional Communication Technologies for SMN

more, it is also a cost efficient network with dynamic self-healing and distributed control. On the contrary, the capacity and security are the main challenges for its application on the SMN. Therefore, the IEEE 802.11ah TG is creating a new WiFi-based standard that operates at the frequencies below 1GHz [2]. They are trying to solve the possible challenges of traditional WiFi applied on SMN, such as scalability and power saving.

ZigBee is a wireless communication technology that consumes low power at the device side [57]. Thanks to its low cost and easy implementation, this technology has already been widely used in the Smart Home network by many AMI vendors, such as Itron and Landis Gyr. They produce smart meters and measuring devices integrated with ZigBee protocol to monitor and control the Home Energy Status. On the other hand, there are still some constraints on ZigBee for its practical application on the SMN. For example, its short range confines this protocol in the application domain of HAN. Furthermore, the processing capabilities and memory size of the ZigBee device are expected to be improved for more advanced functions and communication requirements of the SMN.

Messaging over Cellular Network allows the Smart Meters and Local Collector to exchange information via short message service, which has been supported by multiple mature cellular network standards, such as GSM, CDMA, LTE [22]. It is the popularity and easy implementation that make this technology become an attractive candidate option. Furthermore, the long range and high data rate provide the utility more flexibility to design and

implement the SMN. However, the concern about reliability and delay performance makes a barrier for the implementation of this technology in practice, especially under the condition of heavy traffic load.

2.4 Traffic Types

The data transmitted over SMN may be classified according to latency requirements. For example, energy consumption information is delay tolerant compared to fault reports or other control actions in response to some urgent events, that must be communicated as soon as possible [49]. Broadly, the above corresponds to two different classes of traffic: periodic and event-driven data. The former includes energy consumption information while the latter is largely data from protection devices (relays, reclosers etc. that monitor local fault status) or from electric vehicle charging stations. We thus select two representative examples

- Periodic Data: Energy Consumption Information
- Event-driven Data: Electric Vehicle Charging Data

and conduct a simple calculation of the resulting traffic generated using the following:

$$\begin{aligned}
&\text{Data Load per House} = \text{App Header} + \text{Tran Header} \\
&+\text{Network Header} + \text{Related Table Payload} \;\Rightarrow \\
&\begin{bmatrix} \text{Energy Consumption} \\ \text{EV Charging Data} \end{bmatrix} = \text{Header} + \begin{bmatrix} \text{Table 23} \\ \text{Table 75,27,28,115} \end{bmatrix} \\
&= \begin{bmatrix} \text{115722 byte per 15 mins} \\ \text{66727 byte per charging} \end{bmatrix},
\end{aligned}$$

where all the parameters in the equations are referred to ANSI C12.19 Standard [8] and listed in the Fig.2.3.

Data	Data Amount	Data	Data Amount
App Header	57 byte	Tran Header	40 byte
Network Header	40 byte	Table 75: Event Control	238 byte
Table 23: Current Register Data	115585 byte	Table 27: Present Register Selection	12 byte
Table 28: Present Register Value	4 byte	Table 115: Condition based Load Control	66336 byte

Figure 2.3: Parameter List for Data Load Calculation

2.5 Scalability Issue

Scalability requires that MAC protocols continue to perform well as the number of SMs offering data scales. Referring to [2], one Local Collector is required to support a network with upto 6000 SMs when considering MAC performance. According to [3], the urban outdoor path loss model for 900MHz RF in dB is $P_{L,dB}(r) = 8 + 37.6log_{10}(r)$, where r denotes the distance between the Smart Meter and Local Collector. Then based on the parameters listed in the table (Fig.2.4) [4], the received power and noise power at the receiver terminal are given as:

$$\begin{aligned} P_{RX,dB}(r) &= P_{TX,dB} + G_{dB} - P_{L,dB}(r) \\ &= 0 + 3 - (8 + 37.6log_{10}(r)), \end{aligned}$$

$$P_N = k \times T \times W = 1.3 \times 10^{-23} J/K \times 290K \times 2MHz. \tag{2.1}$$

Referring to the AWGN capacity derivation with BPSK modulation in [26], we may draw a figure of the transmission rate and received power with respect to r. As shown in the Fig.2.5, the RX received power at $1200m$ satisfies a reasonable received power threshold ($-120dB$) and achievable transmission rate at $4500m$ exceeds $100kbps$, the minimal required data rate set in IEEE 802.11ah Use Case [2]. This implies that one Local Collector may need to communicate with individual Smart Meters located $1200m$ away using a star topology. Given typical SM density ρ (1000-6800 SMs per km^2) [24],[1], it is possible to have in excess

Parameter	Value	Parameter	Value
Channel Bandwidth W	2 MHz	Transmitter Power $P_{TX,dB}$	30 dBm
Antenna Gain G_{dB}	3 dB	Temperature T	290 K
Transmission Frequency	900 MHz	Boltzmann's Constant k	1.38×10^{-23} J/K
SM Density ρ	1000 per km^2	Cell Radius R	1200 m
$SINR_{dB,th}$	14 dB	$P_{RX,dB,th}$	-129 dB

Figure 2.4: Parameter List for Transmission Rate and Hidden Node Calculation

of 6000 Smart Meters communicating to one Local Collector. Clearly, the design of MAC protocols for such large number of nodes, invites challenges about scalability of any chosen MAC protocol for SMN as discussed next.

For random access protocols based on carrier sensing - such as DCF (CSMA/CA) in IEEE 802.11 - such a large coverage area corresponding to a single Collector cell will lead to significant hidden nodes. In the traditional random access protocols, such as CSMA/CA, all nodes listen to estimate channel status (busy/idle) based on energy thresholding. If the node observes the channel to be continuously idle for a specific interval, it starts contending for the channel via a random back-off process. However, when the coverage of the Local Collector is enlarged, one Smart Meter (hidden node) may not be able to detect ongoing transmission of other meters due to the degenerated radio channel condition. Then this hidden node may initiate its own transmission because it determines the channel as idle, which leads to a collision.

In order to investigate the number of hidden nodes with growing Local Collector coverage, we consider the network topology of a disk with radius of R and uniformly distributed SM density ρ (Fig.2.6), the distribution of Smart Meter deployment with respect to r is $f(r) = \frac{2r}{R^2}$, where $0 \leq r \leq R$. Since the down-link communication from Local Collector may cover all the Smart Meters successfully, thus the hidden node only exits in up-link communications where Smart Meter is always the transmitter (TX) and Local Collector is

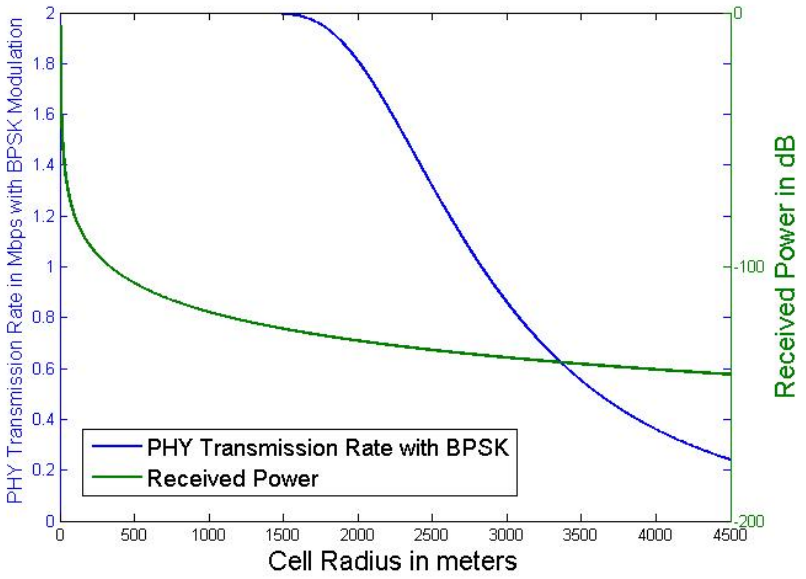

Figure 2.5: PHY Transmission Rate of the Communication with BPSK Modulation and Received Power at Local Collector with respect to Their Distance

always the receiver (RX). According to [21], the area inside the interference range of the receiver I and outside the carrier sensing range of the transmitter X is defined as the hidden area $A(r)$ (shadowed zone) for a given Smart Meter, which is given as:

$$A(r) = \begin{cases} 0 & (r \leq X - I), \\ \beta I^2 + rX|sin(\alpha)| - \alpha X^2 & (r > X - I), \end{cases} \tag{2.2}$$

where $\alpha = cos^{-1}\left(\frac{X^2+r^2-I^2}{2rX}\right)$ and $\beta = \pi - cos^{-1}\left(\frac{r^2+I^2-X^2}{2rI}\right)$.

The Carrier Sensing Range X can be calculated based on the equation $P_{TX,dB} + G_{dB} - P_{L,dB}(X) = P_{X,dB,th}$, where $P_{X,dB,th}$ is the carrier sensing threshold for the received power such that the received signal can be detected. Furthermore, the Interference Range I can be derived based on the following equation:

$$I(r) = min \left[\begin{array}{ll} R, & \{y|P_{RX,dB}(r) - 10log_{10}(P_N + P_{RX}(y)) \\ & = SINR_{dB,th}\} \end{array} \right], \tag{2.3}$$

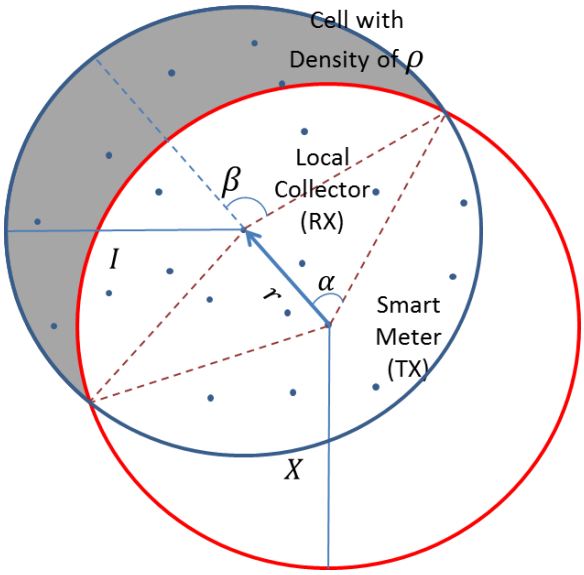

Figure 2.6: Network Topology for Hidden Node Calculation

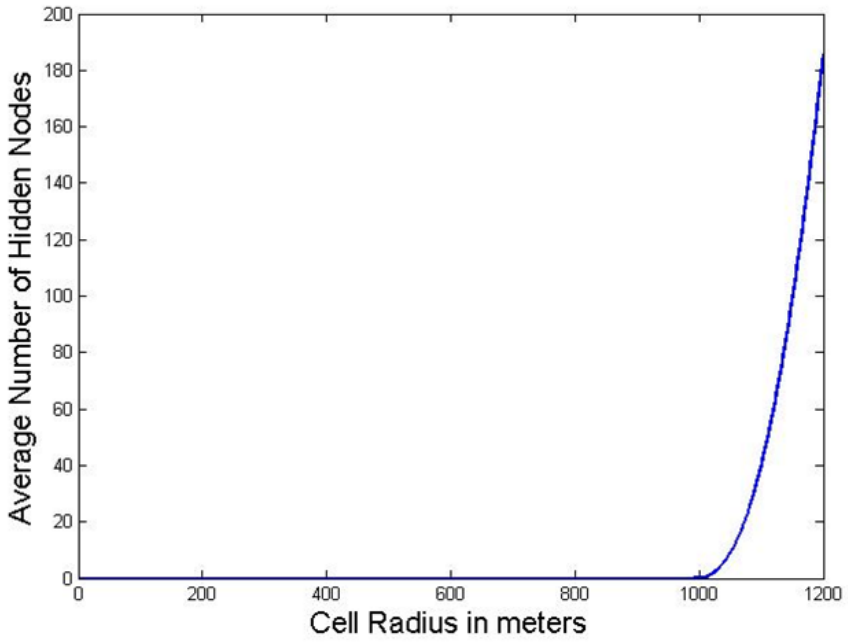

Figure 2.7: Results for Hidden Node Calculation

where $SINR_{dB,th}$ is the threshold for Signal Noise Interference ratio such that received signal can be decoded successfully.

After that, we use $N_{hidden} = \int_0^R \rho A(r) f(r) dr$ to obtain the mean number of hidden nodes inside the network and plot it with respect to cell radius R based on the parameters listed in Fig.2.4. As shown in the Fig.2.7, the number of hidden nodes increases dramatically when the coverage of the network is enlarged. Although the DCF in 802.11 proposes the RTS/CTS algorithm to reduce the occurrence probability of hidden nodes event, its effect on such a large area network still needs to be investigated. On the other hand, the increasing number of Smart Meters may also increase the data load in the SMN, which basically results in stronger competition for the medium access. Then the collisions and following retransmissions happen more frequently, which directly aggravate the performance. Therefore whether the MAC protocols may guarantee the latency requirements of the event-driven and delay sensitive data under the case of large network is also a critical metric to evaluate the designed MAC protocols.

Chapter 3

GROUPING BASED MAC PROTOCOLS DESIGN FOR EV CHARGING DATA TRANSMISSION IN SMART METERING NETWORK

3.1 Introduction

A fundamental change in power system loading is underway as the result of the increasing adoption of plug-in electric vehicles. According to [28], the market share of Electric Vehicles (EVs) is anticipated to be 30% and the electrical consumption for charging EVs may take up to 5% of the total electrical consumption by 2030. Traditionally, the charging of EV is operated according to a business-as-usual (BAU) scenario [29] where the charging starts upon plugging in the EV and happens at a constant rate until the vehicle is fully charged. This scenario in the absence of any intelligent coordination or communication may create new load peaks. In order to address this, the authors in [29] proposed the following energy control strategy to optimize EV charging operations - whenever any EV is connected for charging, the associated Smart Meter sends a message to the local collector and reports the charging parameters. Based on the network load information at that time, an optimal charging schedule for all requesting EVs is determined to smooth out loading. Such EV charging may be considered as a (relatively) continuous control procedure with charging parameters modified by the customer based on scheduling information received; in turn, the Smart Meter reports the modification and enables the local collector to update the charging schedules. As a result, the uplink EV charging data is treated as event-driven and somewhat delay tolerant, based on the updating time constant for the loop. Clearly, the uplink data traffic from the Smart Meters are modeled as independent and randomly distributed (according to customer behavior). The intensity of such traffic increases with network scale and EV adoption. In this Chapter, our primary aim is to design and evaluate an effective MAC protocol for such event-driven random data.

However, traditional random access MAC protocols such as DCF in IEEE 802.11, do

not work well on event-driven data in SMN due to the *scalability* issue. As shown in last chapter, both the coverage of network and the number of Smart Meters involved in SMN significantly exceeds those in indoor Wireless LAN (WiFi) networks for which application they were originally designed. Accordingly, the base 802.11 random access MAC (called Distributed Coordination Function or DCF) needs appropriate modifications for a large cell-size/number of stations such as SMN. The authors of [59] proposed Token-coordinated random access MAC (TMAC) by dividing all the stations into several groups and separating network channel access into two-tiers: inter-group and intra-group tier. The coordinating AP distributes to each group a non-overlapping interval (slot) and allows the stations in each group to compete for the channel only within their allocated interval. On the other hand, the Group-based MAC (GMAC) proposed in [60] assigns a group leader to each group and only allows the group leaders to contend for the channel in the contention phase. Once a generic leader wins the competition and captures the channel, it schedules the transmissions of all stations inside its group by broadcasting a scheduling message. Then the stations in this group start to transmit their respective data to AP according to the schedule. After completion of the intra-group tier of transmissions, the leaders compete for the channel again (intra-group tier). However, these two prior works may still suffer following limitations for the special use case of SMN:

- These only undertake performance analysis based on throughput and ignore average packet delay - the primary metric of interest in our case;

- The group division algorithms presented in these papers targeted at mobile nodes, may not be suitable for SMN where the client nodes (Smart Meters) are static and deployed in a lattice-like network;

- They assume no hidden nodes (their network size is a few hundred feet), which is much smaller than that of SMN.

- They only consider performance under saturated traffic condition, which does not match the EV charging data traffic for Smart Meters.

- These works are based on IEEE 802.11n standard, which provides very high PHY transmission rate ($> 100Mbps$) with $20/40MHz$ channel bandwidth. In contrast, the SMN based on IEEE 802.11ah uses only $1/2MHz$ channel bandwidth, as befits the low PHY transmission rate. Therefore, the performance of the grouping based random access protocols with low PHY transmission rate needs investigation, to assess it's impact on MAC protocol performance.

In summary, we extend TMAC and GMAC, and propose two new random access MAC protocols that support efficient transport of event-driven data for large-cell networks, based on the notion of grouping: TDMA-DCF (TDCF) and Group Leader DCF-TDMA (DCFT), whose operation details are presented in Section 3.2. From the Section 3.3 to Section 3.5, we improve the original two-dimensional Markov process model [18] for DCF for unsaturated traffic [9],[16] to incorporate hidden node events [37] and conduct performance analysis, whose results are presented and discussed in Section 3.6. This chapter is concluded in 3.7.

3.2 Grouping Based Schemes Description

In this section, we describe the implementation of traditional DCF and two grouping based schemes for the NAN. The associated group division algorithms are also introduced.

3.2.1 Traditional DCF Scheme

As a baseline NAN protocol, we consider the traditional DCF (IEEE 802.11) MAC with channel Bandwidth $1MHz$. Because of the significant hidden node problem, it is reasonable to assume that the traditional DCF scheme includes RTS/CTS mechanism to try to alleviate the effect of increasing hidden nodes on the performance.

3.2.2 TDMA-DCF Scheme (TDCF Scheme)

Grouping is one of the proposed ideas in IEEE 802.11ah TG to solve the scalability issue for SMN. Similar to the scheme in [59], we first divide all the SMs into several groups with group size n_1 according to the rules mentioned in the following subsection. Since each group includes many SMs, it is reasonable to assume that each group has at least one

Control Packet Format				
Sub-frame Duration	Group ID	Member IDs	Timestamp	Other Necessary Parameters

Figure 3.1: Control Packet Payload Format

packet to transmit at any time. Therefore it is preferable for the LC to operate TDMA at the inter-group tier. During each periodic frame in the contention phase, the LC allocates one mutually exclusive sub-frame to each group by broadcasting a control message, whose format is shown in Fig.3.1

Once a generic group has been allocated the sub-frame and obtains the transmission rights, all the SMs inside this group compete for the channel by DCF. Therefore, the number of meters involved in the contention concurrently is n_1 at most. The random access at intra-group tier lasts until the sub-frame duration T_G passes or the channel keeps idle for a continuous interval T_I, defined as 'idle interval'. After that, the LC broadcasts another control packet to allocate a new sub-frame to another group. It is noted that there may exist some communications not finishing at the end of sub-frame, then it may collide with the random access of next group nodes if they do not detect the ongoing transmission. Therefore, in order to avoid such collision, the sub-frame allocation is only controlled by the LC's broadcasting message. The scheme is operated as shown in Fig.3.2.

3.2.3 Group Division and Management for TDCF Scheme

In order to reduce the hidden node events of the random access at intra-group tier, we divide all the SMs into several groups according to their deployment proximity and optimal group size n_1. For conciseness, we use d to denote the maximal allowed distance between any two SMs in one group within which all the transmissions may be detected. Actually, as shown in the Section 3.6, the group size n_1 has more significant effect on the performance of the grouping based schemes. Therefore, we may consider n_1 as priority when initializing the group division. The details of the group division algorithm are described in the Fig.3.5. After the division, as shown in the Fig.3.3, the grouping status is recorded in the Regis-

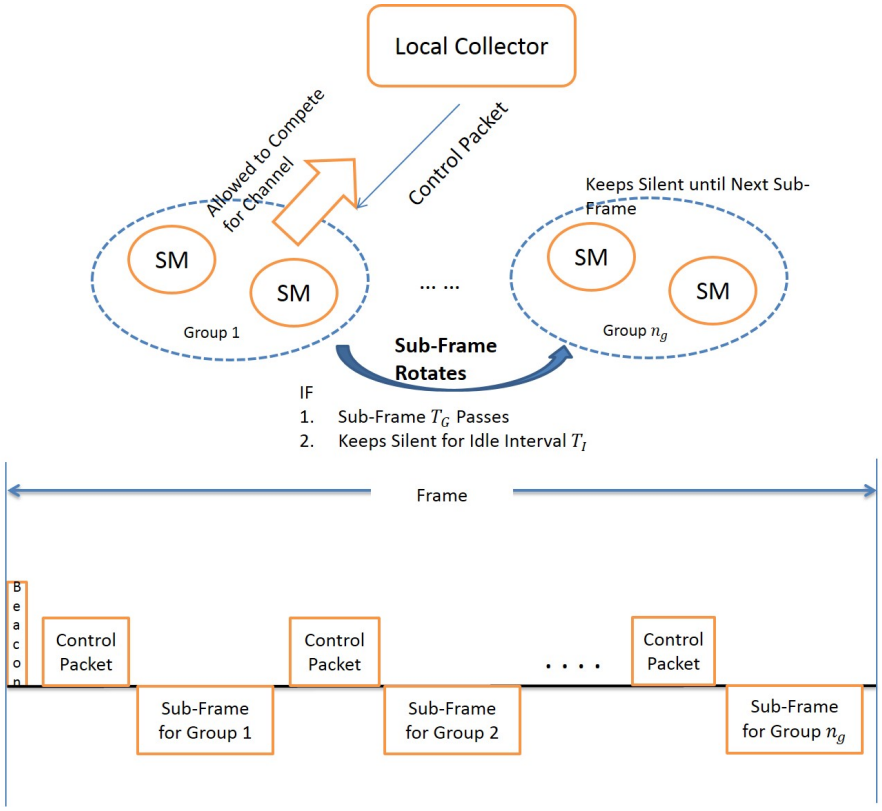

Figure 3.2: TDMA-DCF Scheme Operations

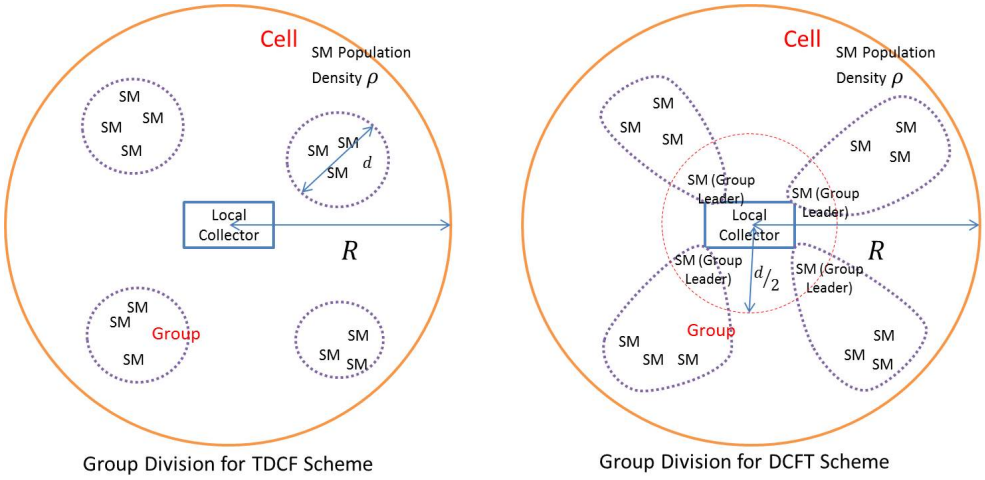

Figure 3.3: Network Topology after Group Division

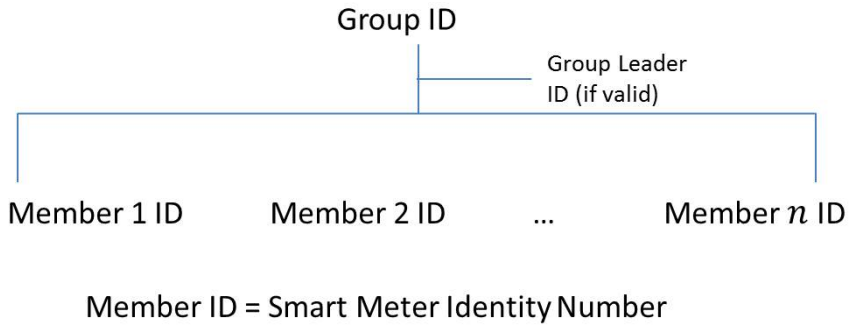

Figure 3.4: Registration Table

tration Table, which is displayed in Fig.3.4. Furthermore, whenever one new SM s_{new} is installed into the coverage of the LC or another SM s_{leave} is uninstalled, the association and disassociation procedure are also described in Fig.3.5. It is noted that the group division mechanism in [60] for mobile stations is not applicable because the SMs are located fixed.

3.2.4 Group Leader DCF-TDMA Scheme (DCFT Scheme)

We divide all the SMs into groups with group size n_2 according to a different rule which is mentioned below. Furthermore, the Group Leader DCF-TDMA scheme applies DCF at the

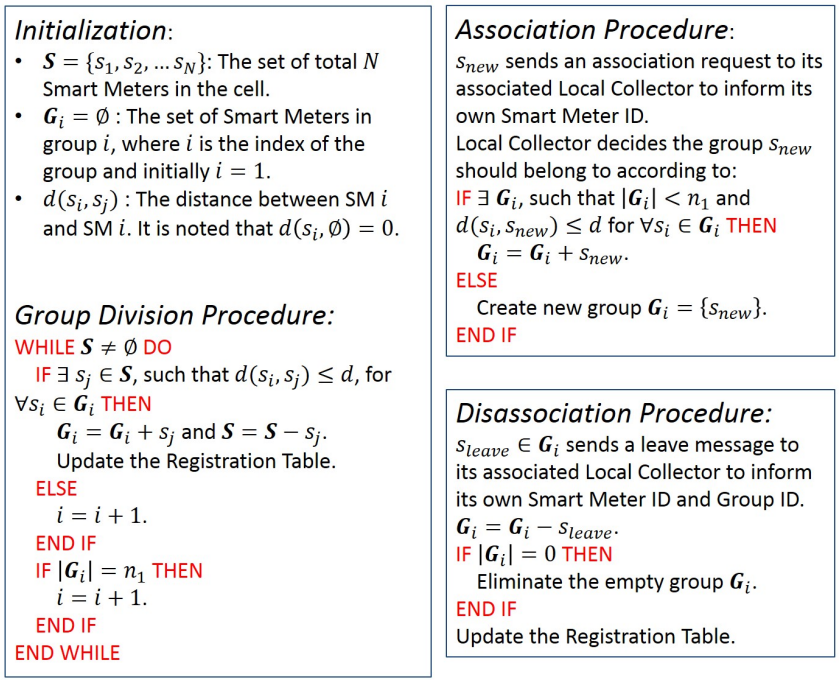

Figure 3.5: Group Division and Management Algorithms for TDCF Scheme

inter-group tier and Polling protocol at the intra-group tier, which is opposite to the TDCF scheme. First, LC assigns a group leader for each group. At the beginning of the periodic frame of the contention phase, all the group leaders compete for the channel via RTS/CTS exchange based on the DCF scheme. Therefore the number of SMs involved concurrently in the random access at most equals to the number of groups which is much less than the total number of meters. If a generic group leader wins the competition, i.e. this leader reserves a sub-frame for its associated group via the RTS message and informs other group leaders of the expected duration via the CTS responded by the LC, then the LC polls all the meters inside the 'winner' group one by one; the SM replies to the LC with its own data sequentially. The reserved sub-frame lasts until the LC broadcasts an 'END' message when all the meters inside the group finish the transmissions. If any meter in the group has nothing to transmit and keeps silent to the polling message, the LC is able to detect this case and starts to poll next sequential meter after two continuous idle SIFS. Accordingly, the collector may broadcast the 'END' signal earlier. After that, all the group leaders start

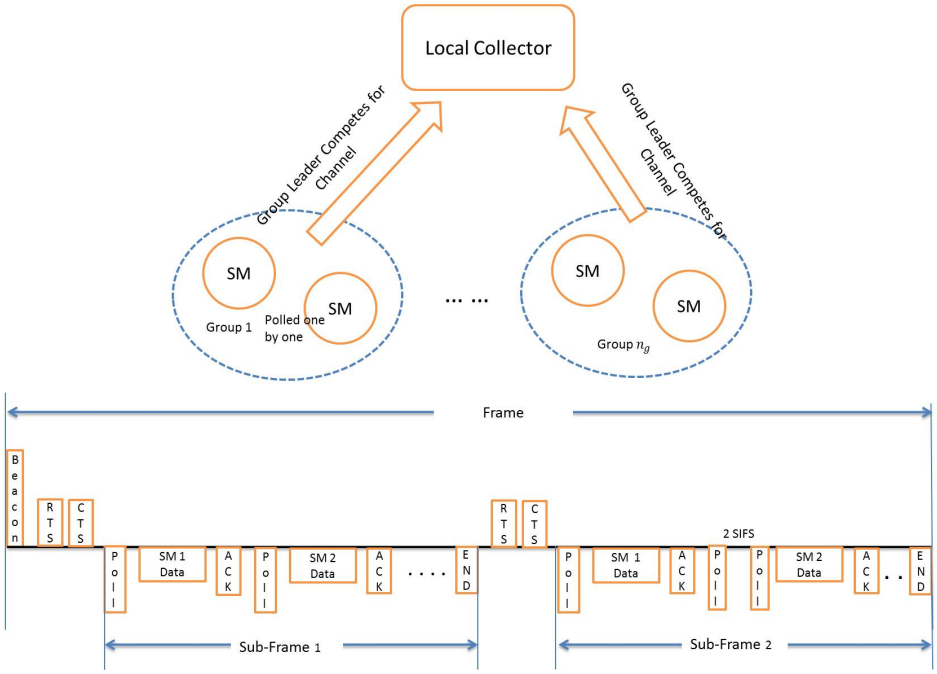

Figure 3.6: Group Leader DCF-TDMA Scheme Operations

to compete for the channel again. It is noted that in this scheme, the Polling operation is centralized controlled by the LC; while in GMAC [60], the sequential transmission at intra-group tier is scheduled by the group leader, where the group leader is required to have more advanced computing capability. Therefore, our scheme is more suitable for the use case of SMN, because the group leader in SMN is just the normal SM with simple infrastructure. The operation of this scheme is outlined in Fig.3.6.

3.2.5 Group Division and Management for DCFT Scheme

On the contrary to the TDCF scheme, in order to reduce the hidden node events of the random access at inter-group tier, we have to select $\lceil \frac{N}{n_2} \rceil$ SMs located close to the LC to act as the group leaders, among which there is no hidden node problem. After that, all other SMs may be randomly picked to associate to each group leader and form the group with group size n_2. The details of the group division algorithm are described in the Fig.3.7, along with the association and disassociation procedure. After division, as shown in the

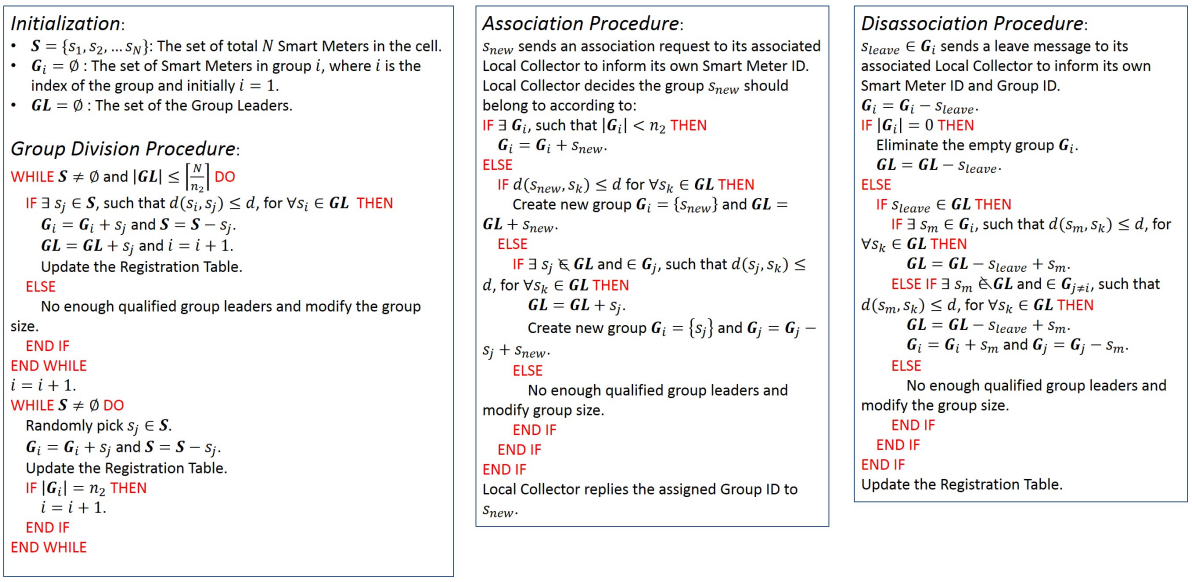

Figure 3.7: Group Division and Management Algorithms for DCFT Scheme

Fig.3.3, the grouping status is also recorded in the Registration Table.

Furthermore, from the calculation in Section 3.6, the approximate value of d is $1600m$. If we model it as a disk with radius $800m$, the number of SMs within this area is about 2000. That means, as long as the group size for TDCF scheme and the number of group leaders for DCFT scheme is smaller than 2000, it is believable to assume that there is few hidden nodes in these two grouping based schemes.

3.3 Analysis Model

3.3.1 Unsaturated Traffic Analysis for EV Charging Data

Due to the random generation of EV charging data, the SMN usually works under unsaturated condition. Therefore, in order to capture this important traffic feature, we model it from the following two aspects. First, because the EV charging data is event-driven, thus, from the perspective of entire network, only part of all the SMs are active and involved concurrently in the contention during a certain interval [9], whose percentage is denoted as q_o. It is noted that the value of q_o is largely dependent on the selected interval. For

example, from 7:00pm to 9:00pm, the number of charging vehicle is much larger than that at noon, which leads to higher q_o. The accurate numerical estimation of q_o counts on the detailed analysis of power data and customer behaviors, which is beyond our scope in this paper. Therefore, for simplicity and without loss of generality, we may assume q_o to be constant in this paper.

On the other hand, even though a SM is active to transmit data within a short interval, it is still not reasonable to assume that the buffer of this active SM is always filled up if the packet arrival rate λ, representing the rate at which the packet reaches the buffer from the upper layers, is not large enough [16]. In order to model the unsaturated traffic caused by this case, for the TDMA at intra-group tier in DCFT scheme, we use the parameter q' to denote the probability that any SM has a packet to transmit in the time slot it is polled, which is a function of λ as derived in Section 3.4. For the random access scheme, we refer to [16] and make modifications on the two-dimensional Markov Process model in [18] to take the unsaturated traffic condition into consideration, which will be discussed in following subsection.

3.3.2 Markov Process Model

Because all these three MAC protocols include random access regardless of inter-group or intra-group tier, we adopt the two-dimensional Markov process model presented in [18], but make some modifications by considering channel busy probability [15] and unsaturated traffic conditions [16] so as to match the unique features of SMN closely. Similar to [18], our model is also based on the following two assumptions:

- The probability that any transmission attempt experiences a collision is constant regardless of the number of retransmissions suffered.

- The probability that a SM will attempt to transmit in a generic time slot is constant across all time slots.

These two assumptions become more accurate as the number of nodes involved in the contention gets larger, which exactly matches the condition of SMN. In order to present our

analysis more concisely, we list the parameters involved in this Chapter as:

- N: Total number of SMs in one cell.
- n_1, n_2: Number of SMs in each group for TDCF scheme and DCFT scheme respectively.
- n_{g1}, n_{g2}: Number of groups for TDCF scheme ($n_{g1} = \lceil \frac{N}{n_1} \rceil$) and DCFT scheme ($n_{g2} = \lceil \frac{N}{n_2} \rceil$) respectively.
- n: Since the group size for different schemes may be different, for simplicity of the analysis, we use n to denote the general number of SMs concurrently involved in the random access regardless of scheme.
- $\bar{C}$: Average PHY transmission rate.
- σ: Duration of unit time slot.
- δ: One-way propagation delay between SM and LC.
- p: Probability that any transmission experiences a collision regardless of the number of retransmissions suffered.
- p_b: Probability that the channel is busy and SM freezes its back-off counter during the back-off phase.
- q: Probability that any active SM gets a packet from upper layer to transmit in a generic time slot during the random access contention.
- τ: Probability that any SM attempts to transmit a packet in a generic time slot.
- W: Smallest contention window size $CW_{min} = W$.
- W_m: Largest contention window size $CW_{max} = W_m = 2^m W$.

- $W_i = 2^i W$: The i^{th} stage contention window size in the back-off phase, where $i \in [0, m]$.

- $E[X]$: Expected payload in one transmission. We may assume that each packet shares the same payload length, therefore $E[X] = X$.

- $s(t) = i, i \in [0, m]$: Stochastic process representing the back-off stage at time slot t.

- $b(t) = k, k \in [0, W_i - 1]$: Stochastic process representing the back-off time in a specific stage at time slot t.

According to [16], in order to describe the unsaturated traffic condition in random access, we introduce a new state I to represent the temporary idle state that the active SM's buffer is empty and waiting for the new packet from upper layer. Furthermore, the probability q_{DCF} and q_{TDCF} involved in the SM random access for traditional DCF scheme and TDCF scheme depend on λ, which may not always be saturated. On the contrary, for the DCFT scheme, because the group leaders are always trying to capture the channel for its group, the parameter q_{DCFT} could be assumed to be 1 constantly. In sum, the Markov process model is shown in Fig.3.8, which is governed by the following transition probabilities[1]:

- The back-off counter decrements by one when the SM senses the channel idle.

$$P_{i,k|i,k+1} = 1 - p_b, \text{ where } k \in [0, W_i - 2], i \in [0, m]. \tag{3.1}$$

- The back-off counter freezes when the SM senses the channel busy.

$$P_{i,k|i,k} = p_b, \text{ where } k \in [1, W_i - 1], i \in [0, m]. \tag{3.2}$$

- The SM enters back-off stage 0 after a successful transmission and it has a packet to transmit in its buffer.

$$P_{0,k|i,0} = q(1-p)/W_0, \text{ where } k \in [0, W_0 - 1], i \in [0, m]. \tag{3.3}$$

[1] $P_{i,k|j,n}$ is short for $P[s(t+1) = i, b(t+1) = k | s(t) = j, b(t) = n]$.

- The back-off counter increments by one after an unsuccessful transmission.

$$P_{i,k|i-1,0} = p/W_i, \text{ where } k \in [0, W_i - 1], i \in [1, m]. \tag{3.4}$$

- The back-off counter has reached the maximal stage and remains at this stage after an unsuccessful transmission.

$$P_{m,k|m,0} = p/W_m, \text{ where } k \in [0, W_m - 1]. \tag{3.5}$$

- The SM enters idle state I after a successful transmission and it has no packet to transmit in its buffer.

$$P_{I|i,0} = (1-q)(1-p), \text{ where } i \in [0, m]. \tag{3.6}$$

- The SM enters stage 0 from idle state I when a new packet reaches its buffer.

$$P_{0,k|I} = q/W_0, \text{ where } k \in [0, W_0 - 1]. \tag{3.7}$$

- The SM remains in idle state I with empty buffer and waits for the new packet.

$$P_{I|I} = 1 - q. \tag{3.8}$$

After that, we use

$$b_{i,k} = \lim_{t \to \infty} P[s(t) = i, b(t) = k], \text{where } k \in [0, W_i - 1], i \in [0, m] \tag{3.9}$$

to denote the stationary distribution that any SM occupies a given state.

First, we note the following relations:

$$b_{i,0} = p^i b_{0,0}, \text{where } i \in [0, m-1], \tag{3.10}$$

$$b_{m,0} = \frac{p^m}{1-p} b_{0,0}, \text{where } i = m. \tag{3.11}$$

Then deriving from the equations (3.10) and (3.11), we obtain

$$\begin{aligned} b_I &= (1-q)(1-p)\sum_{i=0}^{m} b_{i,0} + (1-q)b_I \\ &= \frac{1-q}{q} b_{0,0}. \end{aligned} \tag{3.12}$$

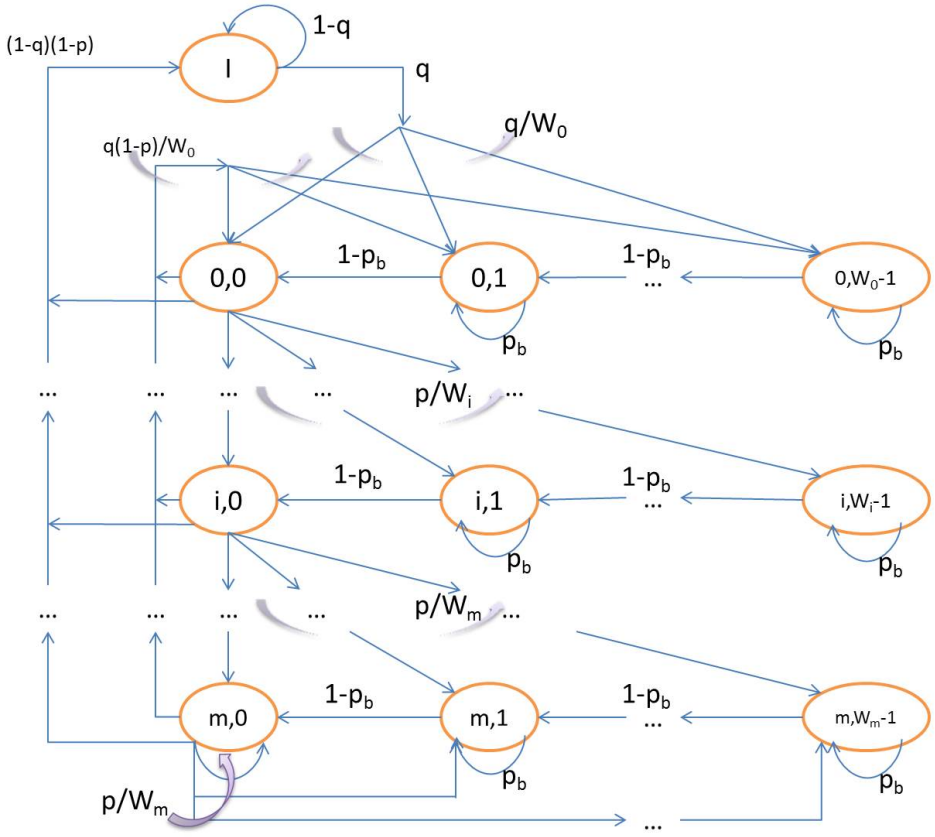

Figure 3.8: Markov Process Model for Random Access under Unsaturated Traffic Conditions

On the other hand, the stationary distribution from the vertical dimension of the Markov process can be given as:

$$b_{i,k} = \frac{W_i - k}{W_i(1-p_b)} \begin{cases} q(1-p)\sum_{j=0}^{m} b_{j,0} + (1-q)b_I & i = 0, \\ pb_{i-1,0} & i \in [1, m-1], \\ p(b_{m-1,0} + b_{m,0}) & i = m. \end{cases} \tag{3.13}$$

According to the equations (3.10), (3.11) and (3.12), we could simplify the relation in (3.13) as:

$$b_{i,k} = \frac{W_i - k}{W_i} \frac{1}{1-p_b} b_{i,0}, \text{where } k \in [1, W_i - 1], i \in [0, m]. \tag{3.14}$$

Employing the normalization condition, we could obtain:

$$\begin{aligned} 1 &= \sum_{i=0}^{m} \sum_{k=0}^{W_i-1} b_{i,k} + b_I \qquad (3.15) \\ &= \sum_{i=0}^{m} \sum_{k=1}^{W_i-1} \frac{W_i - k}{W_i} \frac{1}{1-p_b} b_{i,0} + \sum_{i=0}^{m} b_{i,0} + b_I \\ &= \frac{b_{0,0}}{2} \left[\frac{W}{1-p_b} \left(\frac{1-(2p)^m}{1-2p} + \frac{(2p)^m}{1-p} \right) + \frac{1-2p_b}{(1-p)(1-p_b)} + \frac{2(1-q)}{q} \right]. \end{aligned}$$

After solving the equation (3.15), we obtain the closed form for $b_{0,0}$, which is given in (3.16). Then we may compute the probability τ by summing $b_{i,0}$ over all the back-off stages, which is given in (3.17).

$$b_{0,0} = \frac{2q(1-p)(1-2p)(1-p_b)}{q\left[Wp(1-(2p)^m) + (W+1-2p_b)(1-2p)\right] + 2(1-q)(1-p)(1-2p)(1-p_b)} \tag{3.16}$$

$$\begin{aligned} \tau &= \sum_{i=0}^{m} b_{i,0} \qquad (3.17) \\ &= \frac{b_{0,0}}{1-p} = \frac{2q(1-2p)(1-p_b)}{q\left[Wp(1-(2p)^m) + (W+1-2p_b)(1-2p)\right] + 2(1-q)(1-p)(1-2p)(1-p_b)} \end{aligned}$$

As a result, we can determine the following probability parameters and specify them with respect to different schemes:

- The probability p_b is given as:

$$p_b = 1 - (1-\tau)^n, \tag{3.18}$$

$$p_b^{DCF} = 1 - (1-\tau)^{q_o N},$$

$$p_b^{TDCF} = 1 - (1-\tau)^{q_o n_1},$$

$$p_b^{DCFT} = 1 - (1-\tau)^{n_{g2}}.$$

- The probability p is given as:

$$p = 1 - (1-\tau)^{n-1}, \tag{3.19}$$

$$p^{DCF} = 1 - (1-\tau)^{q_o N - 1},$$

$$p^{TDCF} = 1 - (1-\tau)^{q_o n_1 - 1},$$

$$p^{DCFT} = 1 - (1-\tau)^{n_{g2} - 1}.$$

- The probability p_s that only one transmission exists in the channel conditioned on the fact that at least one SM transmits is given as:

$$p_s = \frac{n\tau(1-\tau)^{n-1}}{1-(1-\tau)^n}, \tag{3.20}$$

$$p_s^{DCF} = \frac{q_o N \tau (1-\tau)^{q_o N - 1}}{1-(1-\tau)^{q_o N}},$$

$$p_s^{TDCF} = \frac{q_o n_1 \tau (1-\tau)^{q_o n_1 - 1}}{1-(1-\tau)^{q_o n_1}},$$

$$p_s^{DCFT} = \frac{n_{g2} \tau (1-\tau)^{n_{g2} - 1}}{1-(1-\tau)^{n_{g2}}}.$$

In order to present the analysis more concisely, we do not use the superscript to differentiate these probability parameters with respect to different schemes in the following sections. However, it is noted that these parameters have to be modified and adapted to their associated schemes with different probability q and number n.

3.3.3 Analysis Model Update with Hidden Node Events

In order to update our analysis model by including the hidden node problem, we make some modifications on the parameters according to [37], which are listed as:

- The probability p is modified as:

$$p = 1 - (1-\tau)^{n(1-h)-1}(1-\tau)^{nhT_v}, \text{ where} \tag{3.21}$$

- The number of time slots of vulnerable frame T_v based on RTS/CTS mechanism is given as:

$$T_v = \lceil \frac{2(RTS + \delta + SIFS)}{\sigma} \rceil. \tag{3.22}$$

- The probability p_s is modified accordingly as:

$$p_s = \frac{n\tau(1-\tau)^{n(1-h)-1+nhT_v}}{1-(1-\tau)^n}. \tag{3.23}$$

After that, we may use the updated p and p_s in the performance analysis for the traditional DCF scheme.

3.4 Throughput Analysis

In [18], the author assumes any transmission in the random access contention, whether it is successful or not, is a renewal process cycle. However, in order to calculate the throughput for the grouping based schemes, we have to specify different renewal process cycle for different schemes. After that, the closed form equation for normalized throughput of the considered renewal process cycle is expressed as:

$$\begin{aligned} S &= \frac{E[\text{payload transmitted in one renewal cycle}]/\bar{C}}{E[\text{length of one renewal cycle}]} \\ &= \frac{E[P]/\bar{C}}{E[L]}. \end{aligned} \tag{3.24}$$

3.4.1 Traditional DCF

In this scheme, because of no group division, the number of SMs concurrently involved in a generic period of contention phase $n = q_o N$. According to [18], the normalized throughput for traditional DCF S_{DCF} is given as:

$$S_{DCF} = \frac{p_b p_s E[X]/\bar{C}}{(1-p_b)\sigma + p_b p_s T_s^{DCF} + p_b(1-p_s)T_c^{DCF}}, \tag{3.25}$$

- The average time slots of a successful transmission for the traditional DCF scheme T_s^{DCF} is given as:

$$\begin{aligned} T_s^{DCF} &= (RTS+\delta) + SIFS + (CTS+\delta) + SIFS + (\frac{H+E[X]}{\bar{C}} + \delta) \\ &+ SIFS + (ACK+\delta) + DIFS. \end{aligned} \tag{3.26}$$

- The average time slots of an unsuccessful transmission for the traditional DCF scheme T_c^{DCF} is given as:

$$T_c^{DCF} = (RTS+\delta) + DIFS. \tag{3.27}$$

- The probability q for traditional DCF scheme is given as:

$$q_{DCF} = 1 - e^{-\lambda E[T]_{DCF}}, \text{ where} \tag{3.28}$$

$$E[T]_{DCF} = (1-p_b)\sigma + p_b p_s T_s^{DCF} + p_b(1-p_s)T_c^{DCF}. \tag{3.29}$$

3.4.2 TDMA-DCF Scheme

In this scheme, we consider any transmission attempt within the random access at intra-group tier, including the preceding idle interval, as a renewal process cycle. Therefore, the number of SMs concurrently involved in the random access $n = q_o n_1$. During the renewal process cycle, as long as there exists packet to be transmitted (with probability $1-(1-p_b)^{T_I}$) and without collision (with probability p_s), the payload is $E[X]$. Therefore, $E[P]_{TDCF}$ is given as:

$$E[P]_{TDCF} = E[X](1-(1-p_b)^{T_I})p_s. \tag{3.30}$$

On the other hand, the length L of the renewal process cycle with respect to the transmission starting time j is given as:

$$L_{TDCF} = \begin{cases} j\sigma + p_s T_s^{TDCF} + (1-p_s) T_c^{TDCF} & j \leq T_I - 1 \\ \text{with probability } (1-p_b)^j p_b, & \\ T_I \sigma & j = T_I \\ \text{with probability } (1-p_b)^{T_I}, & \end{cases} \tag{3.31}$$

where $T_s^{TDCF} = T_s^{DCF}$ and $T_c^{TDCF} = T_c^{DCF}$.

The probability q for TDCF scheme is given as:

$$q_{TDCF} = 1 - e^{-\lambda E[T]_{TDCF}}, \text{ where} \tag{3.32}$$

$$E[T]_{TDCF} \approx (n_{g1} - 1) T_G. \tag{3.33}$$

The number of time slots for T_I is given as [59]:

$$T_I = \frac{DIFS}{\sigma} + 2^m W. \tag{3.34}$$

Therefore, the $E[L]_{TDCF}$ can be calculated as:

$$E[L]_{TDCF} = (1-p_b)^{T_I} T_I \sigma + \sum_{j=0}^{T_I - 1} (1-p_b)^j p_b \left[j\sigma + p_s T_s^{TDCF} (1-p_s) T_c^{TDCF} \right]. \tag{3.35}$$

Then we may get the normalized throughput for a generic group according to equation (3.24):

$$S_{TDCF}(G_i) = \frac{E[P]_{TDCF} / \bar{C}}{E[L]_{TDCF}}. \tag{3.36}$$

It is noted that as $T_I \to \infty$ and $n_1 = N$, then $S_{TDCF} = S_{DCF}$. This is reasonable because, TDCF scheme with these two assumptions - there only exists one group and its own subframe is infinite - is exactly equivalent to the traditional DCF scheme. Since different groups may contain various number of SMs, we average the normalized throughput with respect to all the groups, which is given as:

$$S_{TDCF} = \frac{\sum_{i=0}^{n_{g1}} S_{TDCF}(G_i)}{n_{g1}}. \tag{3.37}$$

3.4.3 Group Leader DCF-TDMA Scheme

In this scheme, we consider any transmission attempt within the random access among all the group leaders as a renewal process cycle. Then the number of SMs concurrently involved in the random access is $n = n_{g2}$ and the average group size is $\bar{n}_2 = n/n_{g2}$. Similar to (3.25), the normalized throughput for this scheme is given as:

$$\begin{aligned} S_{DCFT} &= \frac{E[P]_{DCFT}/\bar{C}}{E[L]_{DCFT}} \\ &= \frac{p_b p_s \bar{n}_2 q_o q' E[X]/\bar{C}}{(1-p_b)\sigma + p_b p_s T_s^{DCFT} + p_b(1-p_s)T_c^{DCFT}}, \end{aligned} \tag{3.38}$$

- The average time slots of a successful group leader request and the following intra-group tier transmission T_s^{DCFT} is given as:

$$T_s^{DCFT} = (RTS+\delta)+SIFS+(CTS+\delta)+SIFS+E[I]+(END+\delta)+DIFS. \tag{3.39}$$

- The average time slots of an unsuccessful group leader request with collision T_c^{DCFT} is given as:

$$T_c^{DCFT} = (RTS+\delta)+DIFS. \tag{3.40}$$

- The probability q' is given as:

$$q' = 1 - e^{-\lambda E[T]_{DCFT}}, \text{ where} \tag{3.41}$$

$$E[T]_{DCFT} \approx n_{g2} T_s^{DCFT} + n_{g2}\frac{(1-p_s)}{p_s} T_c^{DCFT}, \tag{3.42}$$

- The average time slots consumed by the intra-group tier transmission within the 'winner' group $E[I]$ is given as:

$$E[I] = \bar{n}_2(q_o q'(\frac{H+E[X]}{\bar{C}} + ACK + SIFS + 2\delta) + Poll + \delta + 2SIFS). \tag{3.43}$$

3.5 Delay Analysis

3.5.1 Traditional DCF

Delay is defined as the duration starting from the generation of the packet to its successful reception. If a generic packet experiences the first successful transmission at its $i+1^{th}$

attempt (with probability $(1-p)p^i$), the delay D_i^{DCF} is given as:

$$D_i^{DCF} = B_i^{DCF} + T_s^{DCF} + iT_c^{DCF} + E[F]_{DCF}, \text{ where} \tag{3.44}$$

- The back-off time B_i^{DCF} is given as:

$$B_i^{DCF} = \begin{cases} \sum_{j=0}^{i} \left(\frac{W_j-1}{2}\right)\sigma & i < m, \\ \sum_{j=0}^{m} \left(\frac{W_j-1}{2}\right)\sigma + \sum_{j=m+1}^{i} \left(\frac{W_m-1}{2}\right)\sigma & i \geq m. \end{cases} \tag{3.45}$$

- The back-off counter freeze time $E[F]_{DCF}$ is given as:

$$E[F]_{DCF} = E[N_F]_{DCF}(p_s T_s^{DCF} + (1-p_s)T_c^{DCF}). \tag{3.46}$$

- The average times of back-off counter freeze $E[N_F]_{DCF}$ is given as [15]:

$$E[N_F]_{DCF} = \frac{B_i^{DCF}}{max(\frac{1-p_b}{p_b}, 1)} - 1. \tag{3.47}$$

In sum, the mean packet delay for the traditional DCF scheme can be calculated as:

$$E[D]_{DCF} = \sum_{i=0}^{\infty} (1-p)p^i D_i^{DCF}. \tag{3.48}$$

3.5.2 TDMA-DCF Scheme

Similarly, if a generic packet is not transmitted successfully until the $i+1^{th}$ transmission attempt within the random access during its assigned sub-frame, the delay term D_i^{TDCF} is basically similar to that for traditional DCF scheme D_i^{DCF}, except changing some parameters, such as T_s, T_c, p, p_s and p_b to adapt to the TDCF scheme.

Furthermore, if $D_i^{TDCF} - T_s^{TDCF} > T_G$, the packet may not be transmitted in the current sub-frame and has to wait until the next allocated sub-frame. The waiting latency is given as:

$$Z_i^{TDCF} = \lfloor \frac{D_i^{TDCF} - T_s^{TDCF}}{T_G} \rfloor \times T_G \times (n_{g1} - 1). \tag{3.49}$$

On the other hand, if the packet is generated outside its own sub-frame, then it has to wait until the next associated sub-frame comes. Therefore, if the packet arrival follows the

Poisson Process with packet arrival rate λ, this waiting time is calculated as:

$$\begin{aligned} E[Y] &= \int_0^{T_G(n_{g1}-1)} (T_G(n_{g1}-1)-y)\lambda e^{-\lambda y} dy \\ &= (T_G(n_{g1}-1)+\frac{1}{\lambda}) - (2T_G(n_{g1}-1)+\frac{1}{\lambda})e^{-\lambda T_G(n_{g1}-1)}. \end{aligned} \tag{3.50}$$

Combining these three terms mentioned above, the mean packet delay for a SM s_j within a generic group can be calculated as:

$$E[D]_{TDCF}(s_j) = \sum_{i=0}^{\infty} (1-p)p^i (D_i^{TDCF} + Z_i^{TDCF}) + E[Y]. \tag{3.51}$$

Similar to the throughput calculation, we average the mean delay with respect to all the SMs that belong to different groups, which is given as:

$$E[D]_{TDCF} = \frac{\sum_{j=0}^{q_o N} E[D]_{TDCF}(s_j)}{q_o N}. \tag{3.52}$$

3.5.3 Group Leader DCF-TDMA Scheme

Similar to the throughput analysis before, we focus on the random access at inter-group tier and assume a generic group leader first captures the channel at its $i+1^{th}$ attempt, the mean packet delay D_i^{DCFT} for any SM inside this group is given as:

$$D_i^{DCFT} = B_i^{DCFT} + iT_c^{DCFT} + E[F]_{DCFT} + (T_s^{DCFT} - \frac{E[I]}{2} - (END + \delta + DIFS)), \tag{3.53}$$

where B_i^{DCFT} and $E[F]_{DCFT}$ are basically similar to those in the traditional DCF scheme except some parameters, such as T_s, T_c, need to be updated and adapted to the DCFT scheme. The successful transmission time slot is modified because the considered packet is uniformly distributed within the intra-group TDMA sequence.

In sum, the mean packet delay for the Group Leader DCF-TDMA scheme can be calculated as:

$$E[D]_{DCFT} = \sum_{i=0}^{\infty} (1-p)p^i D_i^{DCFT}. \tag{3.54}$$

Parameter	Value	Parameter	Value
CW_{min} W	32	Max. Back-off Stage m	5
Unit Slot Time σ	9 μs	One – way Propagation Delay δ	1 μs
DIFS	34 μs	SIFS	16 μs
MAC Header	24 byte / $\dot{C}$ s	PHY Header	16 byte / $\dot{C}$ s
Poll	(14 byte + PHY Header) / $\dot{C}$ s	END	(14 byte + PHY Header) / $\dot{C}$ s
Packet Payload	1024 byte	ACK	(14 byte + PHY Header) / $\dot{C}$ s
RTS	(20 byte + PHY Header) / $\dot{C}$ s	CTS	(14 byte + PHY Header) / $\dot{C}$ s
Cell Radius R	975 m	Sub-frame for TDCF Scheme T_G	35 ms
Default Average PHY Tran. Rate $\dot{C}$	1 $Mbps$	Default Num. of SM per Cell N	4000
Default Group Size for TDCF Scheme n_1	500	Default Group Size for DCFT Scheme n_2	10
Default Hidden Node Ratio h	0.04	Default Probability q_o	0.7
Default Packet Arrival Rate λ	25 pkt/s		

Figure 3.9: Parameter List for Numerical Results and Discussions

3.6 Numerical Results and Discussions

In this section, we show the throughput and delay performance of the three MAC protocols on the application of EV charging data transmission based on the equations derived in the Section 3.4 and 3.5. The default values of the parameters used to obtain the numerical results are summarized in Fig.3.9, when they are not regarded as the variables in X-axis. Furthermore, the reasonability of these default parameters has been verified in the previous sections.

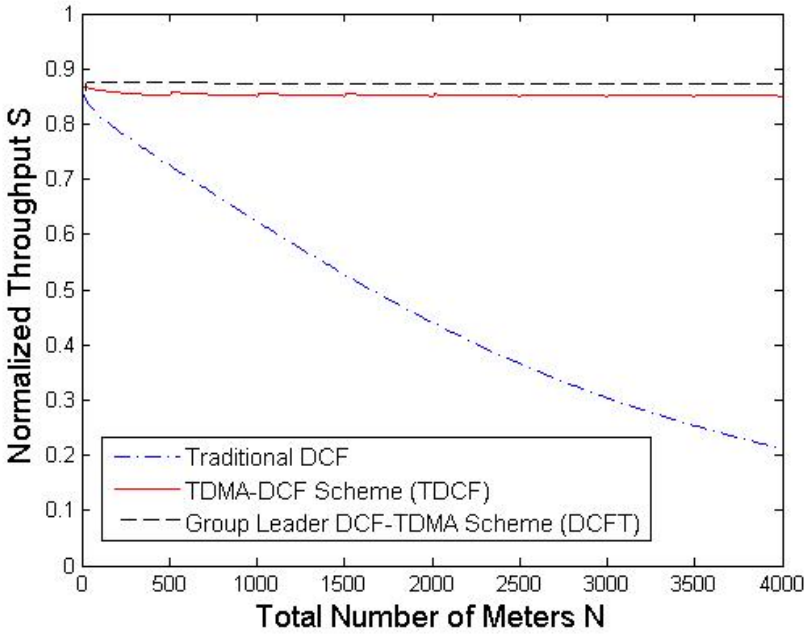

Figure 3.10: Throughput with respect to the Total Number of SMs N

3.6.1 Performance with respect to the Total Number of SMs N

As shown in the Fig.3.10 and Fig.3.11, both the performance of throughput and delay for the two grouping based schemes are better than that of traditional DCF as we expected, because regulating the medium access of SMs group by group can decrease both the hidden node events and the collision rate dramatically, which leads to fewer retransmissions and better performance. This benefit is especially obvious when N grows, which means the grouping based scheme is a good solution to the scalability issue. It is noted that the throughput of DCFT scheme is a little bit better because the TDMA at intra-group tier makes better use of time resource to transmit data. However, the random access at intra-group tier for TDCF scheme may experience some collisions and waste the allocated sub-frame. On the other hand, the bounded delay thanks to the TDMA mechanism for both grouping based schemes gives them lower average delay.

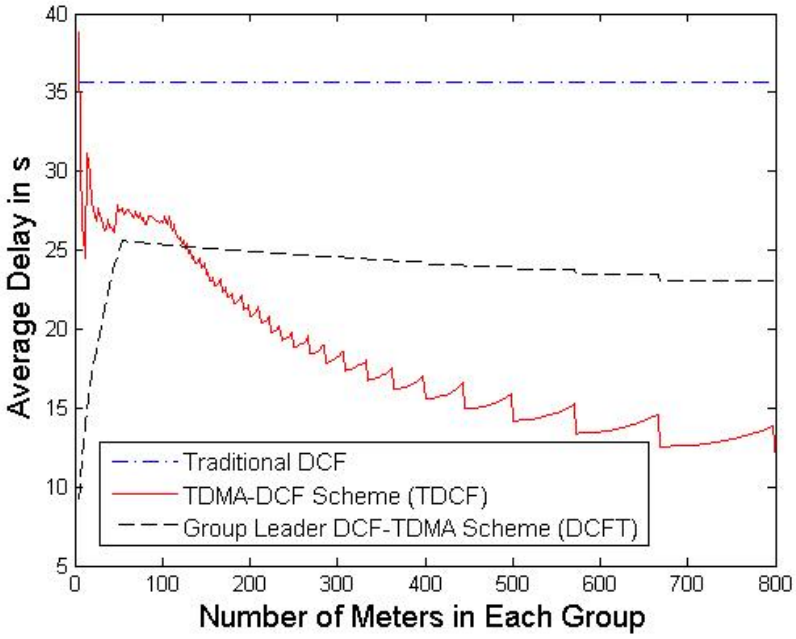

Figure 3.11: Delay with respect to the Total Number of SMs N

3.6.2 Performance with respect to the Average PHY Transmission Rate $\bar{C}$

As shown in the Fig.3.12 and Fig.3.13, we can see that the performance, from the aspects of both throughput and delay of the traditional DCF scheme is getting much worse at lower $\bar{C}$, while the two grouping based schemes are largely insensitive to the different PHY transmission rates. This is because, under the case with significant hidden nodes, the lower transmission rate may prolong the vulnerable duration and increase the possibility for the hidden nodes to interrupt the ongoing transmission especially in the dense populated network. Therefore, we conclude that the applications of grouping based schemes are more necessary and beneficial at the low transmission rate environment. This exactly matches the feature of SMN, because the IEEE 802.11ah TG only allocates 1 MHz as the channel bandwidth for SMN and set low transmission rate requirement given the low traffic load of SM [4]. Based on the discussions in these two subsections, we may suggest adjusting the cell radius R or hardware specifications to change the capacity of one LC according to different

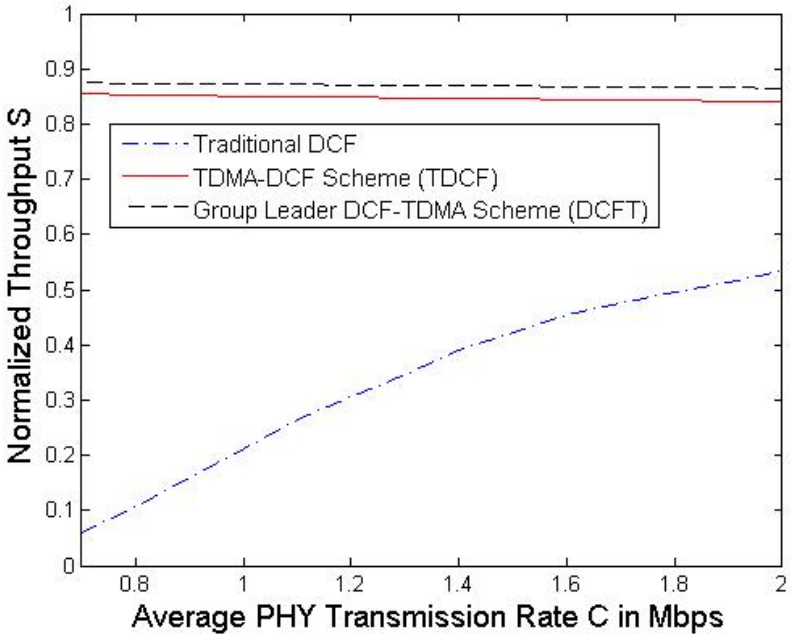

Figure 3.12: Throughput with respect to the Average PHY Transmission Rate $\bar{C}$

SM population density ρ. For example, in the sub-urban environment with sparse density of SM, we may increase the cell radius R and improve the sensitivity threshold $P_{X,dB,th}$ to enable the LC to cover more SMs at the cost of sacrificing the PHY transmission rate.

3.6.3 Performance with respect to the Groups Size

We set the range of group size from 4 to 800, within which we may guarantee that there is no hidden node for both grouping based schemes, as verified by the calculations in the Section 3.2. As shown in the Fig.3.14 and Fig.3.15, the throughput, for DCFT scheme, may get saturated after the group size n_2 exceeds 20. This is because smaller group size and resulting larger number of groups may lead to stronger contention and more collisions on the inter-group tier, and then affect the throughput. On the other hand, we can see that the delay is low when group size is small, which is reasonable because the TDMA at intra-group tier may perform well when small number of SMs are involved. The decreasing trend of delay as n_2 is beyond 60 results from the fewer groups and less contention on the random

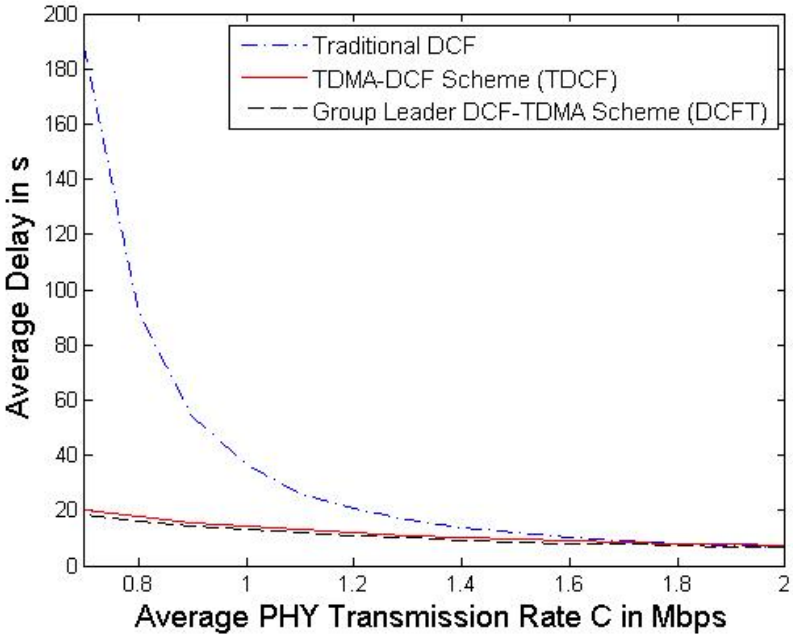

Figure 3.13: Delay with respect to the Average PHY Transmission Rate $\bar{C}$

access among the group leaders. Therefore, considering the aspects, the optimal group size for DCFT scheme is suggested from 10 to 30. On the other hand, the throughput and delay for TDCF scheme both drop down as the group size grows, because the increasing group size may lead to fewer groups and decrease part of the waiting time in delay, and however increases random access contention inside the group. Therefore, the optimal operating point for this scheme is from 400 to 600. After knowing the optimal of group size, we may estimate the area coverage of one group according to the various SM population density ρ. Then, we may further lower the $P_{RX,dB,th}$ or $P_{X,dB,th}$ to relax the requirements of the hardware given the higher ρ and the resulting smaller group coverage.

3.6.4 Performance with respect to the Hidden Nodes Ratio h

As shown in the Fig.3.16 and Fig.3.17, we can see that both the throughput and delay performance of grouping based schemes remain stable with respect to varying hidden nodes ratio. This is reasonable because the group division of the SMs according to their physical

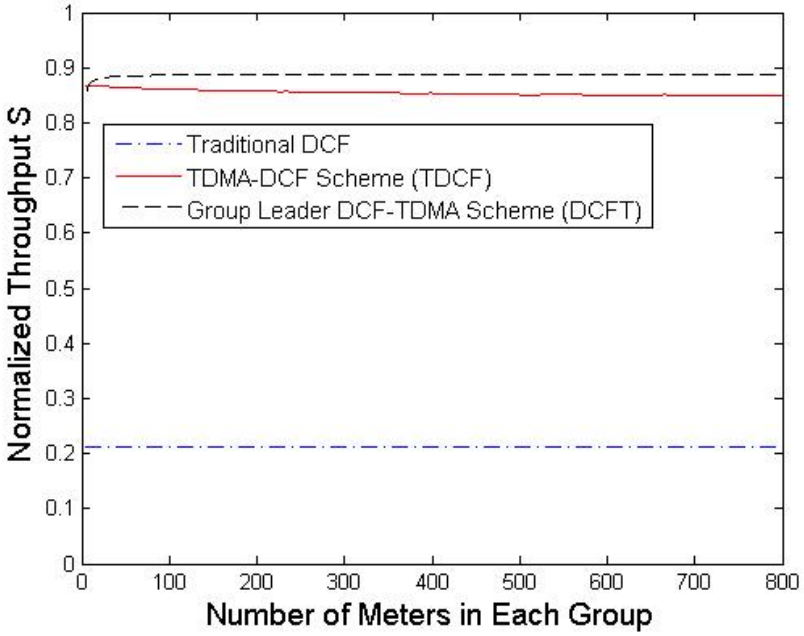

Figure 3.14: Throughput with respect to the Group Size

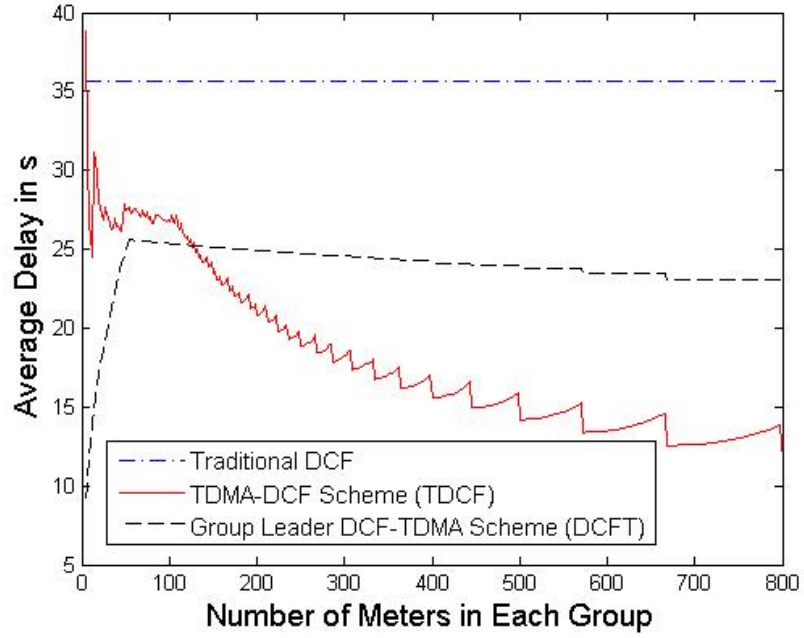

Figure 3.15: Delay with respect to the Group Size

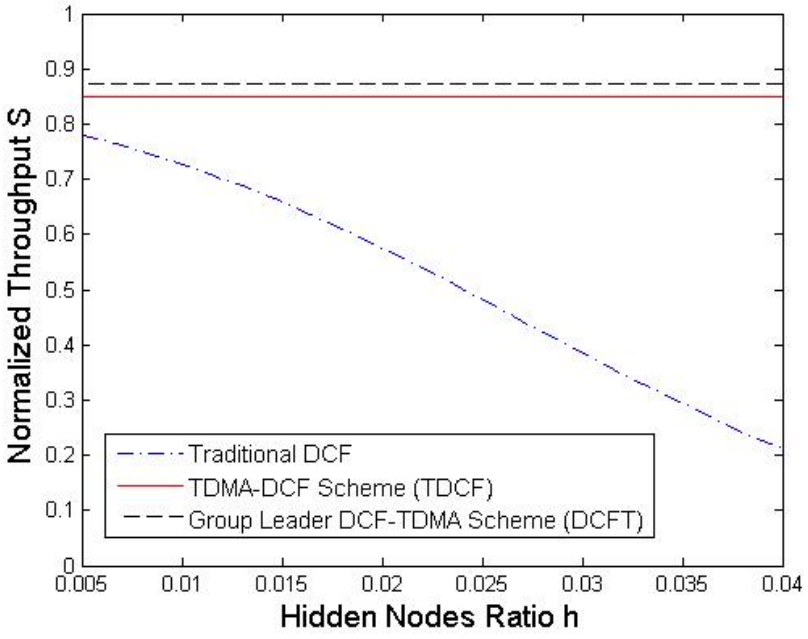

Figure 3.16: Throughput with respect to the Hidden Nodes Ratio h

location can mitigate the impact of hidden nodes effectively as we expected. On the contrary, the traditional DCF scheme is influenced dramatically by the increasing hidden nodes due to the resulting collisions. Therefore, it is more necessary and beneficial to employ the grouping based schemes under the condition of higher hidden nodes ratio and larger coverage area. Furthermore, the grouping based schemes also give the designer a flexibility to relax the requirements of hardware. For example, if the designer wishes to relax the $P_{X,dB,th}$ to reduce the power consumption and simplify the SM communication chips, which will increase the hidden nodes ratio even with smaller network coverage, then the grouping based schemes may be employed to compensate the effect of hidden nodes on the performance.

3.6.5 Performance with respect to the Probability q_o

As shown in the Fig.3.18 and Fig.3.19, from the aspect of throughput, we may see the DCFT scheme does not get saturated at the range of low q_o because the frequent polling to many inactive SMs at the intra-group tier wastes the transmission resource. The delay

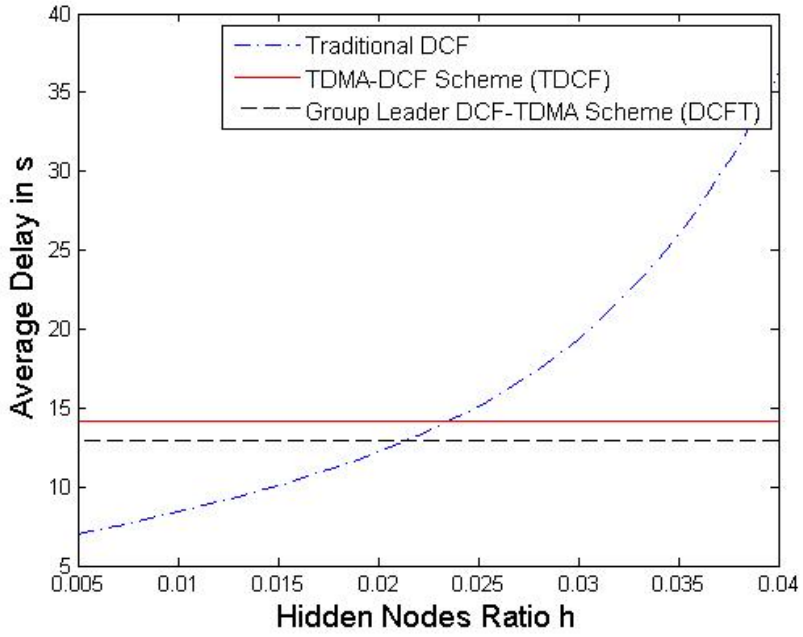

Figure 3.17: Delay with respect to the Hidden Nodes Ratio h

of this scheme increases approximately linearly because the main part of its delay, payload transmission, is proportional to q_o. The performance of TDCF scheme is less sensitive to q_o because the limited group size attenuates the effect of this kind of unsaturated traffic case. On the other hand, the performance aggravation for traditional DCF when q_o is increased is because there are more active SMs getting involved in the random access and resulting higher collision rate. It is also noted that both of the two grouping based schemes have better performance regardless of the value of q_o. The benefit is more obvious especially at the range of large q_o, which means these two schemes are more necessary and beneficial at the power consumption peak hours, e.g. from 7:00pm to 9:00pm when more EVs are charging at home.

3.6.6 Performance with respect to the Arrival Packet Rate λ

As shown in the Fig.3.20 and Fig.3.21, all of the three schemes are not sensitive to the packet arrival rate except at the range of small λ, which matches the results shown in the

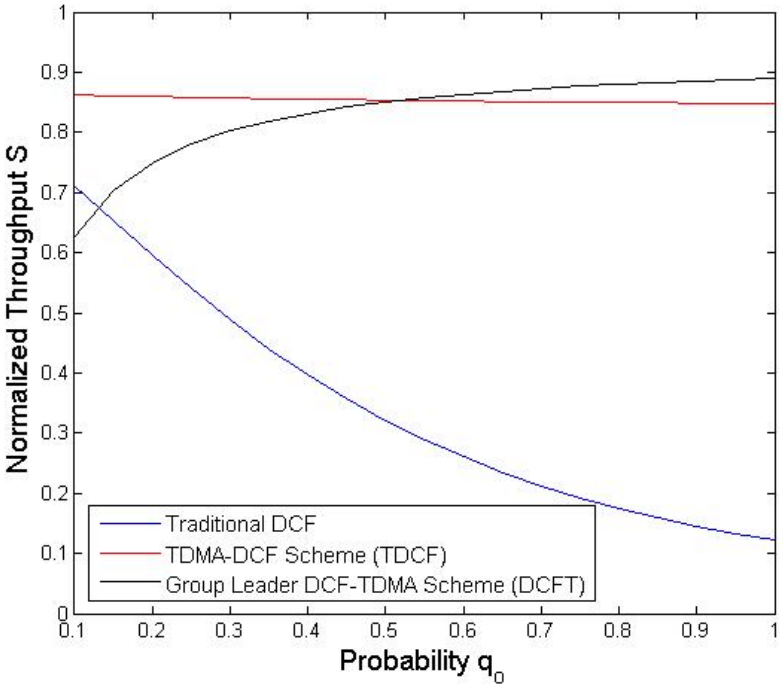

Figure 3.18: Throughput with respect to the Probability q_o

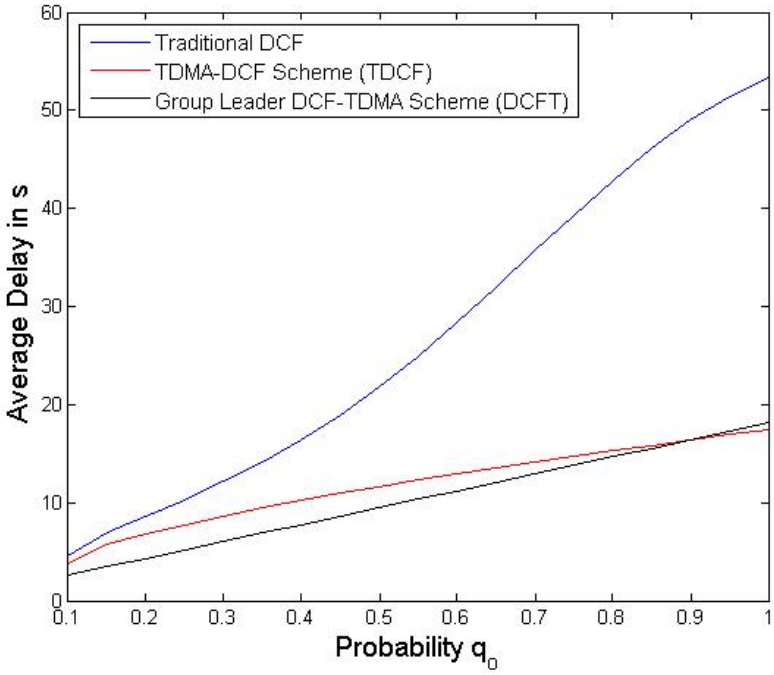

Figure 3.19: Delay with respect to the Probability q_o

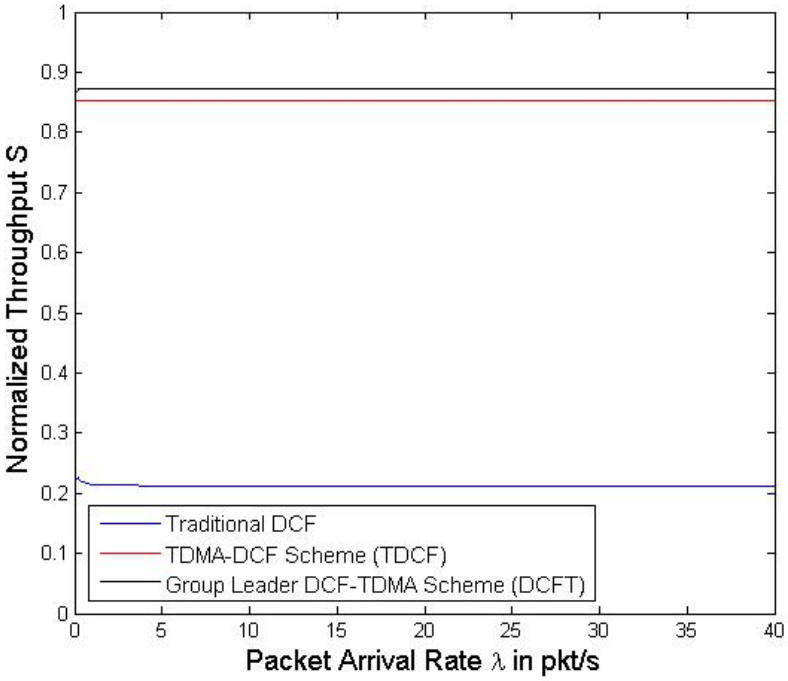

Figure 3.20: Throughput with respect to the Arrival Packet Rate λ

[16]. This is because the frequent retransmissions in traditional DCF and the long waiting time due to the TDMA mechanisms in both grouping based schemes get the buffers of the SMs filled up easily especially in the dense populated network.

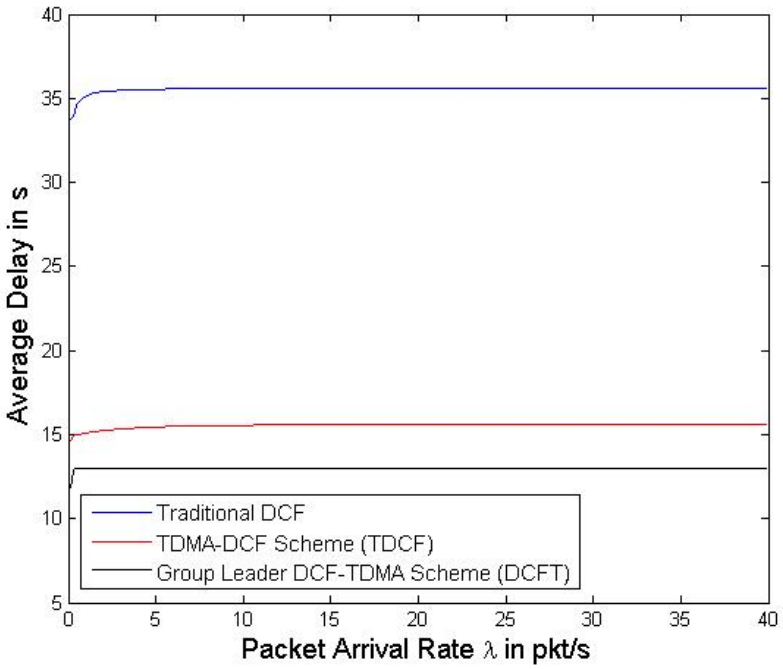

Figure 3.21: Delay with respect to the Arrival Packet Rate λ

3.7 Conclusions

In this Chapter, we proposed two grouping based MAC protocols: TDMA-DCF scheme and Group Leader DCF-TDMA scheme to support the EV charging data transmission and solve the scalability issue in SMN. We also conduct comprehensive throughput and delay analysis on these two schemes with the consideration of unsaturated traffic conditions and hidden node events. The numerical results and following discussions verify the benefit and better performance of these two schemes than that of traditional random access MAC protocol.

Chapter 4

MAC PROTOCOL DESIGN WITH COGNITIVE RADIO FOR PERIODIC DATA TRANSMISSION IN SMART METERING NETWORK

4.1 Introduction

As an important part of the demand response and load management applications, every Smart Meter needs to report the energy consumptions and other related parameters to the utility once every interval, such as 15 mins [50]. Furthermore, the detailed data format of the periodic energy consumptions report is also defined in the Decade 3 of Standard ANSI C12.19 [8]. After that, according to [55], the utilities would exploit these periodic data to analyze the power consumption situation over the entire grid and conduct the load management when necessary. Since the energy consumption data reporting is periodic, it is a straightforward mechanism to use the centralized control and taking-turns MAC protocol to support the communication of such data, with the advantage of guaranteeing a certain rate for every Smart Meter [50]. For instance, the Point Coordination Function (PCF) defined in WiFi is such a suitable MAC protocol, in which the Access Point (AP) polls each station one by one and schedule their transmissions without any contention. Furthermore, the PCF based MAC protocol is also accepted by the IEEE 802.11ah TG when considering the collection of periodic data from Smart Meters at Local Collector. However, the traditional PCF protocol does not work well in SMN due to the scalability issue. As the number of communication nodes is increased, the throughput will get saturated. As a result, the total time for the Local Collector to receive all the periodic data from the Smart Meters will be linearly increased. Although the grouping based MAC protocols have been proved to improve the throughput and delay effectively for event-driven (random access) data transportation, it still has room of performance improvement by designing a suitable MAC protocol in the intra-group tier for periodic data communications. Therefore, in this work, we comply with the grouping concept and design a PCF based MAC protocol for

this periodic traffic in SMN, such as energy consumption report, and against the impact of scalability.

Fortunately, the concept of Cognitive Radio (CR) gives us an option to solve this problem. Currently, it has been more and more attractive that the CR is included in the Smart Grid Communication, especially in SMN. In brief, the communication node implemented with cognitive radio is able to scan and identify some available channels which are not occupied by the Primary Users (PUs). After that, they can switch their transceivers to the identified available channels and communicate with other nodes through these channels. Exploiting this special function of CR, we propose a modified PCF MAC protocol combined with CR, in which the Local Collector with multiple antennas is able to scan and identify all the available channels. Then in each sub-frame allocated to a generic group, the collector will allocate all those identified channels to the Smart Meters belonging to this group and poll them by broadcasting one piece of control message. Then all the polled Smart Meters will reply the message and send their energy consumption data to the Local Collector simultaneously. Because all the channels are mutually independent and the collector is implemented with multiple antennas, the parallel transmissions of reporting data are able to be received by the collector at the same time and without any contention. In sum, we summarize four main benefits obtained from the combination of CR and PCF:

- The inclusion of cognitive radio helps the system to achieve spectrum efficiency and mitigate spectrum scarcity [6]. According to [4], the IEEE 802.11ah standard defines several schemes of channelization. With the aid of CR, we may employ the channelization with small bandwidth and thus support larger capacity without any sacrifice of performance.

- With the aid of CR, we may employ more channels and achieve parallel transmissions, which reduce the overall time to finish all the transmissions in the report period.

- The usage of CR can strengthen the robustness of the SMN. As mentioned in [5][17], more available channels provide Smart Meters with backup channels to communicate

with the Local Collector when the performance of dedicated channel is not good enough.

- According to [43][40], the generated energy-related uplink data from Smart Meters will be up to tens of thousands of terabytes per year per utility. This poses a significant challenge for any existing communication network to collect, transmit, and store such large-scale data, especially for SMN with low data rate. The usage of CR potentially improves spectrum utilization and communication capacity to support large-scale data transmissions.

In the rest of the Chapter, we give an overview of the traditional PCF scheme in Section 4.2. After that, we give a detailed description of the modified PCF MAC protocol with CR (CR-PCF) in the Section 4.3. The numerical analysis on the performance of traditional PCF and CR-PCF is presented in the Section 4.4. In Section 4.5, we compare the performance between these two schemes through both numerical results and simulation results (NS-3). We conclude this chapter in 4.6.

4.2 Overview of Traditional PCF

Point Coordination Function (PCF) is defined in the legacy 802.11 Standards to support the time-bound and periodic communication services. For example, applying the PCF with grouping concept on the energy consumption reporting in NAN, the LC broadcasts a beacon at the beginning of each sub-frame allocated to a generic group. After that, the LC polls the SMs in this associated group and asks for their packet transmissions. Upon receiving the poll message, the polled SM acknowledges it and sends back a pending packet. After LC receives this packet and checks its correctness, it acknowledges the successful data reception and piggybacks a piece of poll message to another SM. On the other hand, if the LC receives no response from the polled SM after waiting for a PCF Interframe Space (PIFS), it ignores the current SM and polls the next one. As shown in the Fig.4.1, the duration to finish one Poll-ACK message and payload transmission is defined as one Periodic Duration. After finishing all the transmissions in one group, the LC allocates the sub-frame to the

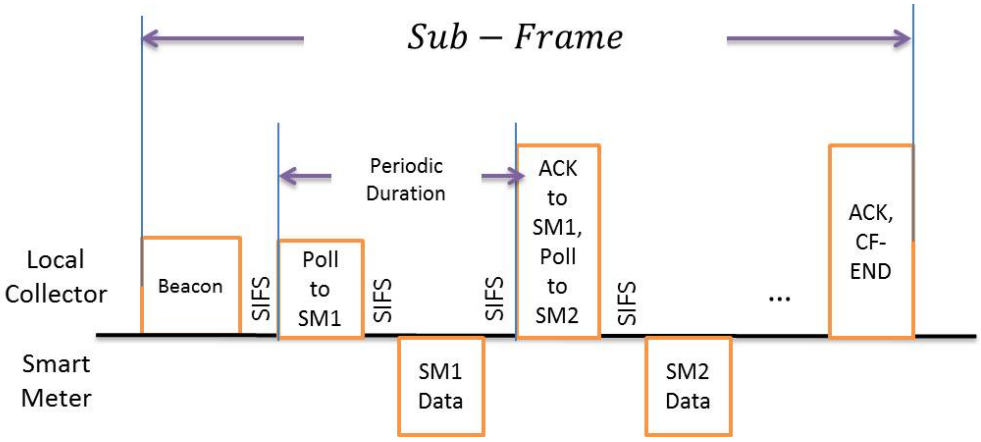

Figure 4.1: Traditional PCF Scheme Operation Example

next group. This operation continues until all the energy consumption report packets are received at the LC side. PCF seems to work fine in this application when the number of SMs is limited. However, as shown in the Section V, the throughput of traditional PCF gets saturated as the number of the SMs increases. As a result, the total time to collect all the reporting packets at LC will be increased. In order to solve this problem, we combine the PCF scheme and cognitive radio technology to solve the scalability issue, which is presented in detail in the following section.

4.3 Modified PCF Scheme with Cognitive Radio

4.3.1 System Model and Assumptions

Based on the network topology, we make the following assumptions and define the following notations to formulate the system model in this Chapter.

- There are M SMs, which are randomly distributed over the coverage of one LC and divided into several groups; each of them comprises M_g SMs.
- Since the uplink report data has a fixed format, as shown in ANSI C12.19 [8], the LC is able to know the number of packets to be transmitted from each SM, L, and the identical length of each packet X.

- In the NAN, there is one dedicated channel H_0, in which the LC and SM conduct reliable communications of payload packets or control message without the interference of PU.

- Besides the dedicated channel H_0, there are other N potential available channels $\{H_i | i = 1, 2, ..., N\}$, in which the LC and SM work as the secondary users. It is noted that those N channels are mutually independent and interference-free.

- The LC is implemented with $N + 1$ antennas, so that it is able to receive the packets from the $N + 1$ individual channels or sense these $N + 1$ channels simultaneously. However, the LC is not able to sense and communicate at the same channel at the same time.

- Each SM only needs to be implemented with one antenna, which can be switched among the $N + 1$ channels.

- We model the traffic behavior of PU on each of the N supplementary channels as an ON-OFF state alternation, i.e. the PU communicates for a time T^1_{ON}, and then turns off and remains off for a time T^1_{OFF}. After that, it turns on for T^2_{ON} and off for T^2_{OFF} and so on. Furthermore, we assume that the T_{ON} and T_{OFF} follows the exponential distribution:

$$T_{ON} \sim exp(Z_{ON}) \text{ and } T_{OFF} \sim exp(Z_{OFF}). \tag{4.1}$$

  Therefore, the long-run proportion of channel off is:

$$\gamma = \frac{Z_{OFF}}{Z_{OFF} + Z_{ON}}. \tag{4.2}$$

- For simplicity, we consider the packet error only results from the collision between secondary user transmissions and primary user transmissions in this paper.

4.3.2 Initialization

Based on the assumptions mentioned above, the LC, similar to the traditional PCF, broadcasts a beacon to initiate the sub-frame. After that, it initializes the first channel allocation

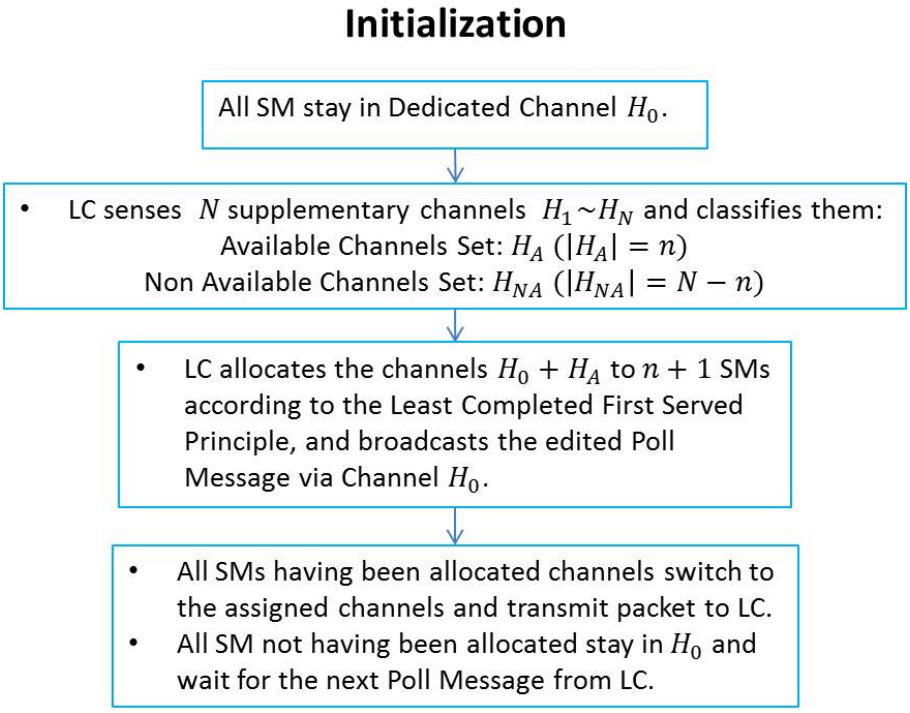

Figure 4.2: Initialization of CR-PCF Scheme

and transmission according to the algorithm shown in the Fig.4.2.

Compared to the Poll frame in the traditional PCF, the modification of that in our proposed protocol is quite limited. We only need to enclose the ACK and channel allocation information for all the SMs in the frame body. On the other hand, the fairness among all the SMs is also quite important in the protocol design. For example, the LC first serves the specific $n + 1$ SMs in a generic group and does not allocate channels to the rest of the SMs until the first $n + 1$ SMs finish their transmission of all L packets. After that, the LC focuses on serving another $n + 1$ SMs until they finish their L-packet transmissions. As a consequence, there may exist a situation that the number of SMs which still need to be served is smaller than the number of available channels when approaching the end of sub-frame. It is obvious that this case is a waste of channel resource, which will also lead to increasing the duration to finish the entire reporting transmission. In order to avoid this situation, we propose a Least Completed First Served Principle as shown in the Fig.4.3.

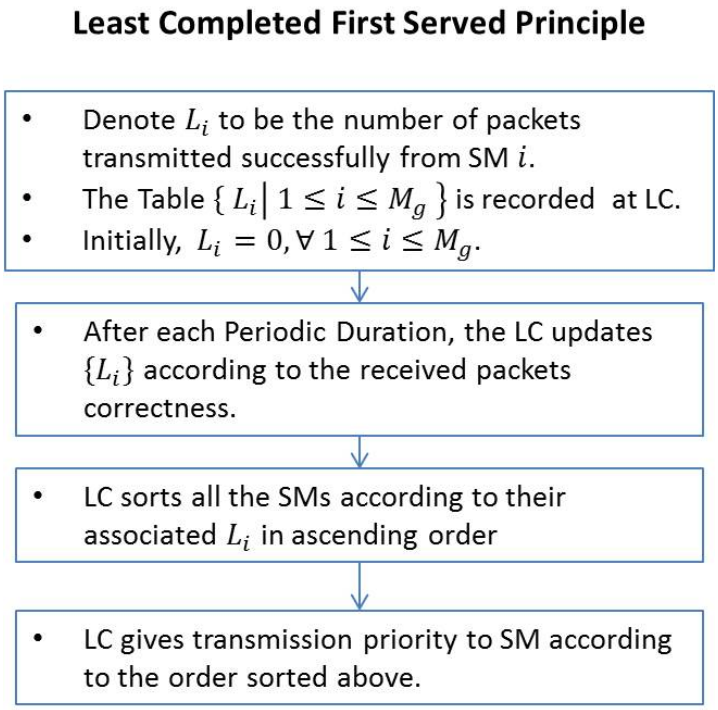

Figure 4.3: Least Completed First Served Principle

In brief, at each round of channel sensing and allocation, the LC prefers to allocate the channels to the SMs with the least completed transmissions so as to try to guarantee the fairness among all the SMs.

4.3.3 Stepwise Algorithm

After the initial channel allocation and payload transmission, we design the stepwise algorithm according to which the LC and SM will work during each Periodic Duration. In this algorithm, only the LC is required to sense all the channels while the SMs only need to follow the scheduling and control message from LC. The details and operation example are shown in the Fig.4.4 and Fig.4.5 respectively. From the example, it is easy to find out that the gain of the throughput performance comes from the parallel utilization of available channels. However, the cost is that we have to extend the SIFS ahead of Poll-ACK Message to τ_{Sense} so as to guarantee the LC is able to sense all the available channels correctly enough.

Furthermore, the SIFS right behind Poll-ACK Message is also required to be extended to τ_{Switch} so that the SMs having been allocated the available channels have enough time to switch to those channels. It is also noted that because $\tau_{Sense} > \tau_{Switch}$, all the SMs are able to switch back to H_0 as the LC is sensing the channels.

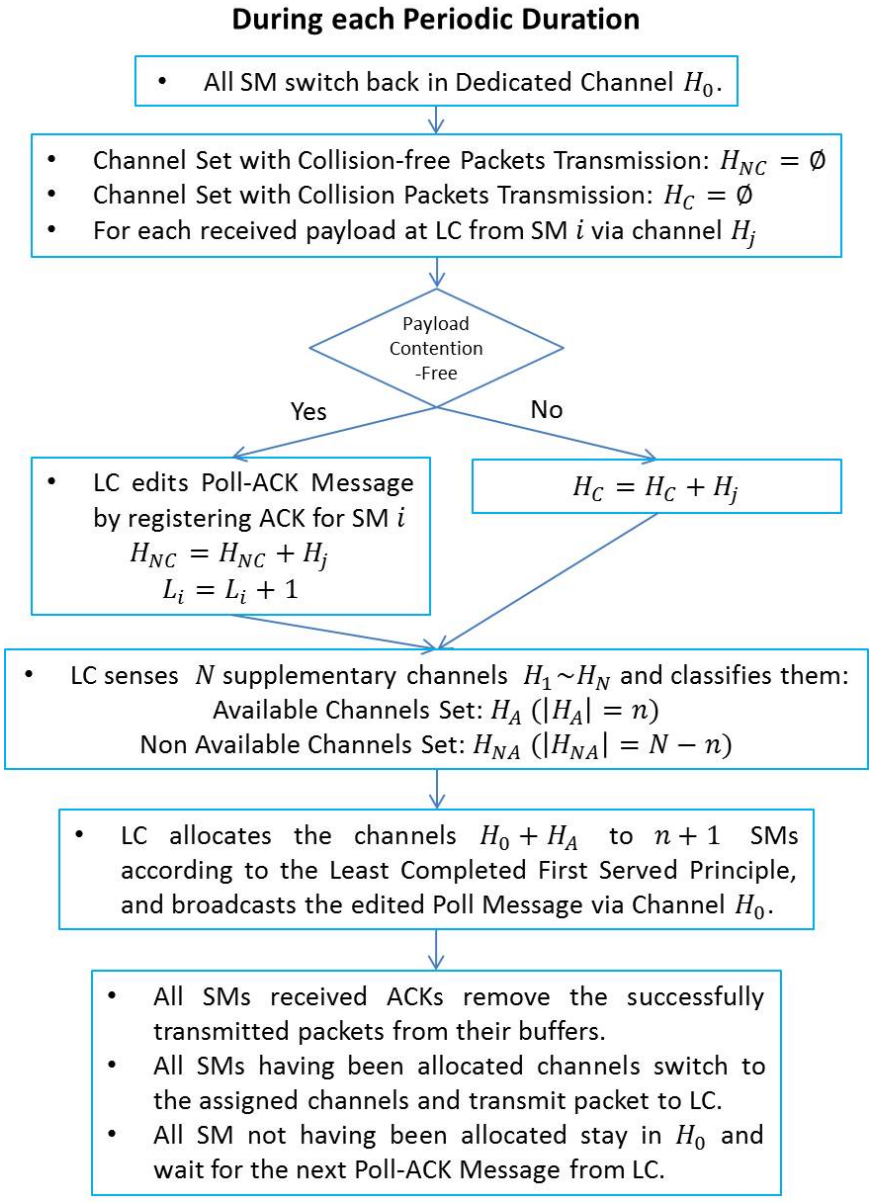

Figure 4.4: Stepwise Algorithm of CR-PCF Scheme

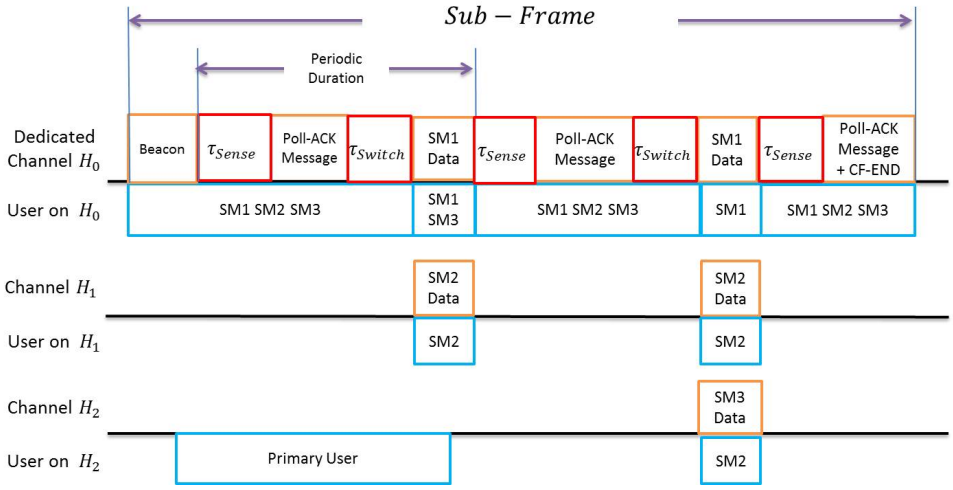

Figure 4.5: CR-PCF Scheme Operation Example

4.4 Performance Analysis

4.4.1 Traditional PCF

In the traditional PCF scheme, all the packets have to be transmitted to LC through the dedicated channel H_0 one by one. The length of one Periodic Duration is:

$$T_{PCF} = SIFS + \frac{Poll}{C} + \delta + SIFS + \frac{X + Header}{C} + \delta, \tag{4.3}$$

where C and δ denote the transmission rate and propagation delay respectively. If each of the M SMs needs to report L packets to the LC, then the time used for the payload transmission is given as:

$$T^1_{PCF} = LM\frac{X}{C}. \tag{4.4}$$

On the other hand, the total time spent on finishing the entire reporting transmission is given as:

$$T^2_{PCF} = \lceil \frac{M}{M_g} \rceil \left(\frac{Beacon}{C} + SIFS + LM_g \cdot T_{PCF} + \frac{Poll}{C} \right). \tag{4.5}$$

Therefore, the throughput for the traditional PCF follows:

$$S_{PCF} = \frac{T^1_{PCF}}{T^2_{PCF}}. \tag{4.6}$$

4.4.2 PCF with Cognitive Radio (CR-PCF)

As we mentioned above, the SIFS interval in the traditional PCF is replaced with τ_{Sense} and τ_{Switch} so as to guarantee the channel sensing and channel switch successfully. Therefore, the length of the Periodic Duration is modified as:

$$T_{CRPCF} = \tau_{Sense} + \frac{Poll}{C} + \delta + \tau_{Switch} + \frac{X + Header}{C} + \delta, \tag{4.7}$$

Since all the channels are mutually independent, thus whenever the LC senses the channels, there are average $n = N\gamma$ channels which are not occupied by PUs and able to be used for LC-SM communication. For each of the n channels, due to the memoryless property of exponential distribution, the probability that LC-SM communication will not be interrupted by the PU during the Periodic Duration is given as:

$$p = Pr(T_{OFF} < y) = 1 - e^{-\lambda y}, \tag{4.8}$$

where $y = T_{CRPCF} - \tau_{Sense}$ and $\lambda = \frac{1}{Z_{OFF}}$. Therefore, the expected number of available channels per Periodic Duration is $ne^{-\lambda y}$ and accordingly, the number of total Periodic Durations is approximately $\frac{LM_g}{ne^{-\lambda y}+1}$. Since in each Periodic Duration, there are n SMs switching channels twice, thus the total number of channel switches is given as:

$$O = \frac{LM_g}{ne^{-\lambda y} + 1} 2n. \tag{4.9}$$

Then the total time for the entire transmission is given as:

$$T^2_{CRPCF} = \lceil \frac{M}{M_g} \rceil \left(\frac{Beacon}{C} + \tau_{Sense} + \frac{LM_g}{ne^{-\lambda y} + 1} T_{CRPCF} + \frac{Poll}{C} \right). \tag{4.10}$$

As a result, the throughput for the CR-PCF follows:

$$S_{CRPCF} = \frac{T^1_{CRPCF}}{T^2_{CRPCF}} = \frac{LMX}{CT^2_{CRPCF}}. \tag{4.11}$$

Furthermore, it is noted that extending the length of payload X will both increase the good throughput and make its transmission more vulnerable to the interruption of PUs, which will decrease the throughput. Therefore, given the traffic behavior of PUs, it is valuable to calculate the optimal $\bar{X}$ so as to maximize the throughput S, which is derived as:

$$\bar{X} := \frac{dS_{CRPCF}}{dX} = 0. \tag{4.12}$$

4.5 Numerical and Simulation Results

In this section, we evaluate the throughput of traditional PCF scheme and CR-PCF based on equation (4.6) and (4.11) respectively. The number of channel switches for CR-PCF is evaluated based on equation (4.9). Furthermore, all the results are also verified by running the simulation with NS-3. The NS-3 is an open-source and discrete-event network simulator for Internet systems, LTE, WiFi and so on. In this work, we referred and modified the following modules in the NS-3:

- *Core Models-Simulator*: The core part of the simulator that schedules the discrete-event timeline.
- *WiFi Models-YansWifiPhy*: The fundamental models that includes the WiFi MAC and WiFi Phy models.
- *Application Models*: We used it to control the packets generation of Smart Meters and Primay Users.

In addition, in order to implement our own MAC protocol design, we create two new models:

- *groupwifi Model*: We created it to implement the grouping concept in the WiFi.
- *crpcf Model*: We created it to implement PCF Protocol with CR.

The default values of the parameters used in the section are summarized in the Fig.4.6. when they are not regarded as the variables in X-axis.

4.5.1 Performance with respect to Number of SM M and Number of Packets per SM L

As investigating the impact of the total number of SM M on the performance, we fix the number of groups to be 4 and thus $M_g = \frac{M}{4}$ (increasing as M). On the other hand, when we evaluate the impact of the parameter L, we set $M = 600$ and $M_g = 150$ as default. As shown in the Fig.4.7 and Fig.4.8, the throughput of both schemes are almost constant, which is because the throughput is easily get saturated in the scenario of NAN where L and

Parameter	Value	Parameter	Value
Beacon	100 byte	Poll-ACK Message	50 byte
Payload X	1024 byte	Header	50 byte
SIFS	16 μs	δ	1 μs
τ_{Sense}	300 μs	τ_{Switch}	120 μs
Z_{ON}	8000 μs	Z_{OFF}	25000 μs
Transmission Rate C	1 $Mbps$	Default Num. of Packets per SM L	15
Default Num. of SMs M	600	Default Num. of SMs in each group M_g	150
Default Num. of Channel N	15		

Figure 4.6: Parameter List for Numerical and Simulation Analysis

M_g are large enough. We may see that the throughput of the CR-PCF is much better than that of traditional PCF. This gain comes from the parallel transmissions over the available channels without the interference of PUs. On the other hand, the overall number of channel switches is linearly increased as we expected based on the equation (4.9). It is also noted that, the simulation results are quite accurate compared to the numerical results especially as L and M_g are large enough, which exactly matches the communication scenario in NAN.

4.5.2 Performance with respect to Number of Channels N

As shown in the Fig.4.9, the throughput of the CR-PCF is approximately linearly increased as we give more available channels to the network. It is quite reasonable that more available channels will lead to more parallel pipes to be used for transmissions. On the other hand, the number of channel switches rises dramatically at first because there are more SMs have chance to switch to non-dedicated channels. After that, it gets saturated when the number of channels is large enough. This is because the rounds of Periodic Duration is decreased as more channels are available.

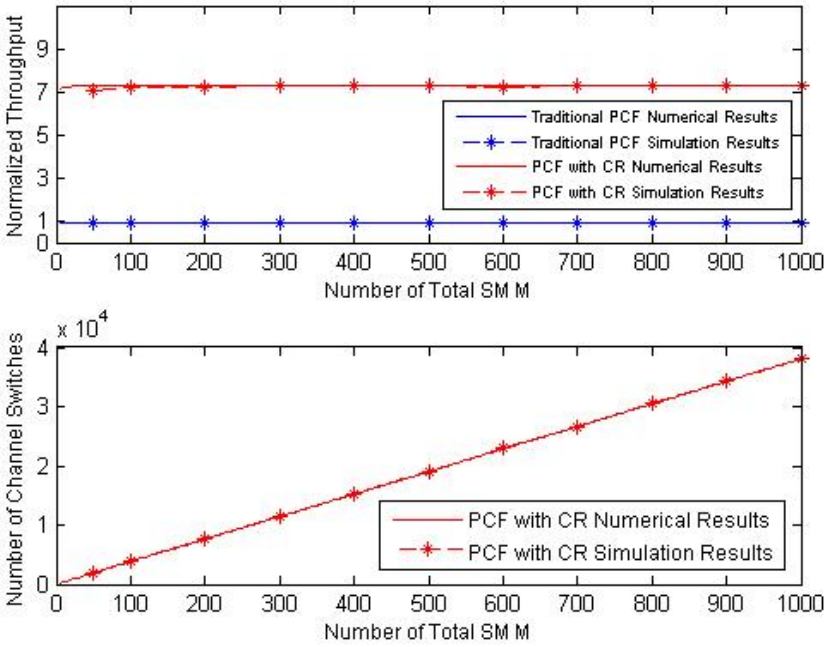

Figure 4.7: Performance Vs. Number of Total SM M

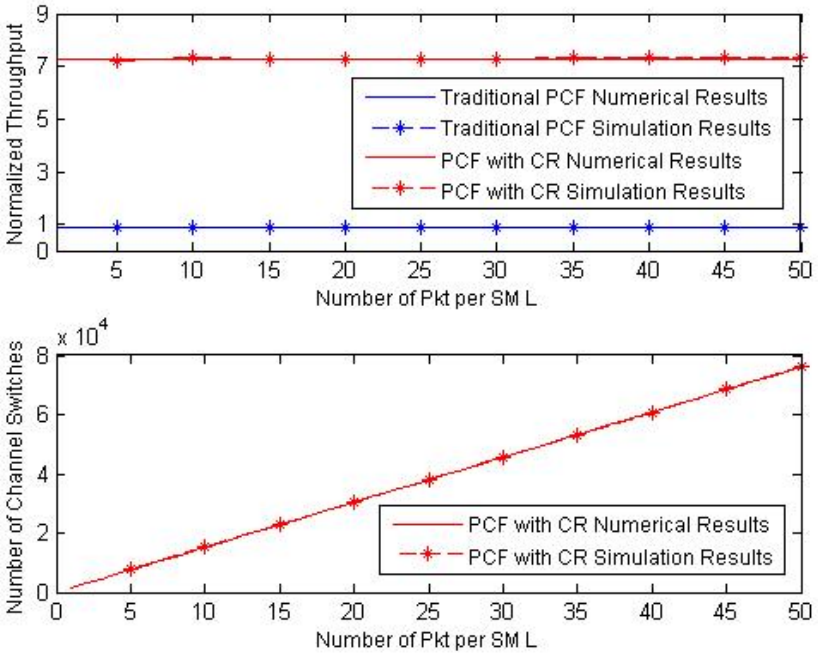

Figure 4.8: Performance Vs. Number of Packets per SM L

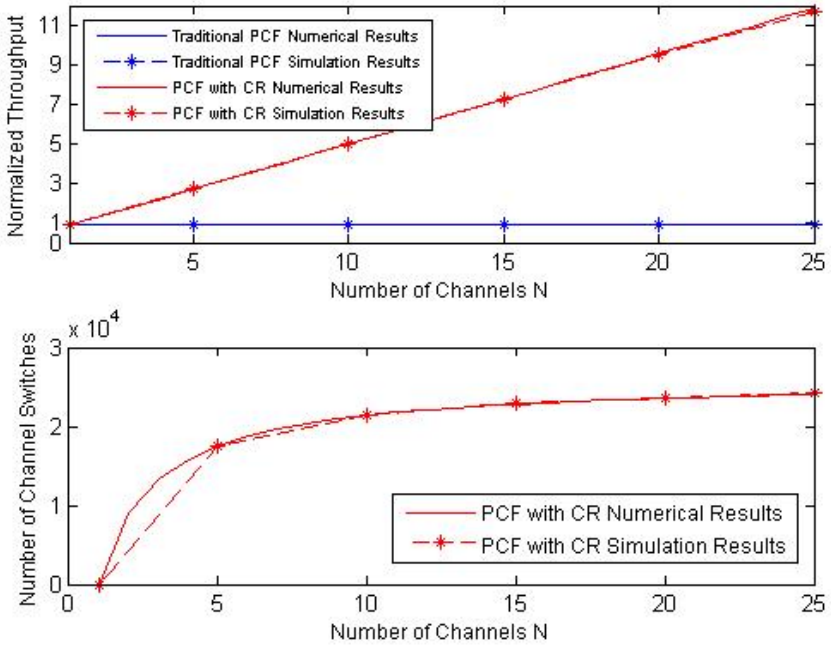

Figure 4.9: Performance Vs. Number of Channels N

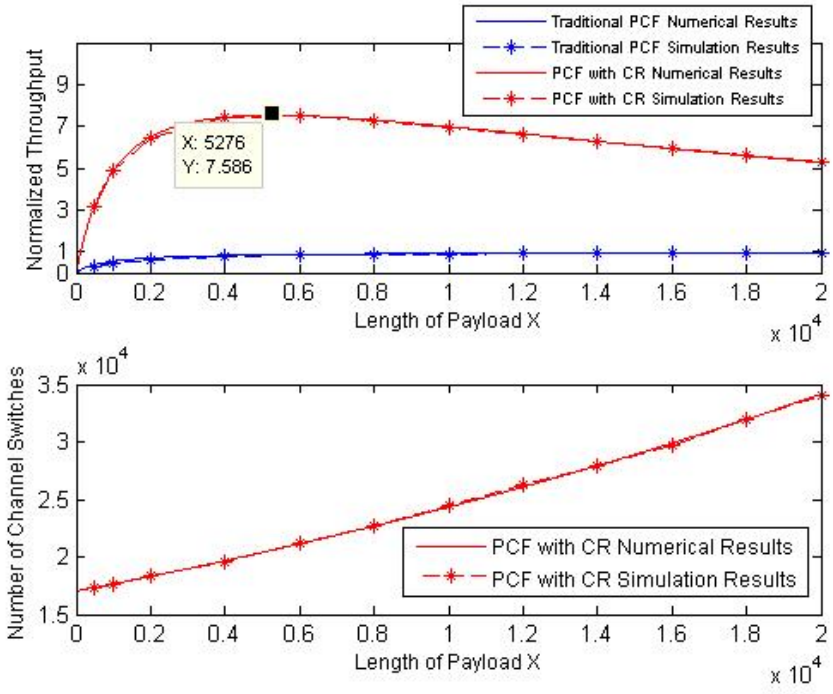

Figure 4.10: Performance Vs. Length of Payload X

4.5.3 Performance with respect to Length of Payload X

As shown in the Fig.4.10, the throughput of traditional PCF scheme is getting saturated as length of packets X becomes large enough, which is because the ratio between Payload and Header is getting larger and the time portion wasted on the Header transmission also shrinks. Similarly, the throughput of the CR-PCF rises at first stage. However, it starts to drop after the optimal length of Payload because the longer payload will make its transmission more vulnerable to the interruption of PU. Then it will lead to more retransmissions and decrease the throughput. As a result, there will be more rounds of Periodic Duration required, which also increases the overall number of channel switches as shown in the Fig.4.10.

4.5.4 Performance with respect to the long-run proportion of channel off γ

As shown in the Fig.4.11, the throughput of the CR-PCF is increasing as γ becomes large. This is because the less the PUs occupy the channels, the more chances that the SMs can

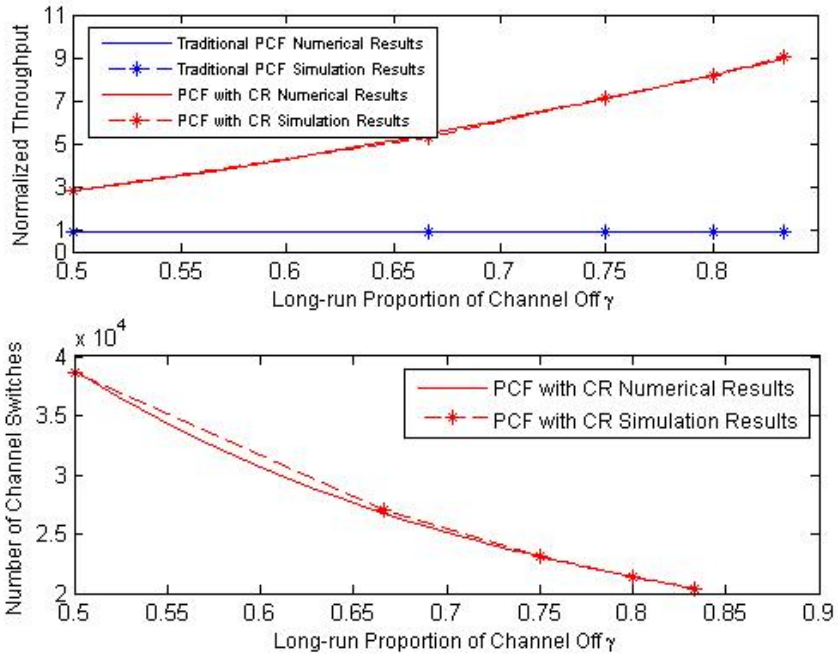

Figure 4.11: Performance Vs. Long-run Proportion of Channel Off γ

use the available channels to transmit their data. As a consequence, both of the rounds of Periodic Duration required and resulting overall number of channel switches decrease.

4.6 Conclusions

In this Chapter, in order to support the periodic energy consumption report in a densely populated network like SMN, we propose a modified PCF MAC protocol with the combination of Cognitive Radio technology, in which the Smart Meters and Local Collector may communicate with each other through the white space when Primary Users are not present. We conduct the throughput analysis for this proposed scheme. Furthermore, the numerical and simulation results through NS-3 show that the PCF scheme with CR significantly outperforms the traditional one.

Chapter 5

MAC PROTOCOL DESIGN WITH COMPRESSIVE SENSING FOR PERIODIC POWER FACTOR MEASUREMENT TRANSMISSION IN SMART METERING NETWORK

The power factor measurement is essential to the entire grid security and stability, which thus needs to be reported to Local Collector periodically. Furthermore, when we investigate the overall power factor measurement in a large building which consists of many units, we may observe its value is time invariant over a duration of hours. Therefore, in this chapter, we focus on this periodic and infrequently changing measurement report and aim to choose a suitable Multiple Access Control (MAC) protocol carefully to support its transmission.

However, the traditional contention-free MAC protocols, such as PCF in IEEE 802.11 [23], do not work well on this periodic data transmission in SMN due to the scalability issue. As shown in [58], both the coverage of network and the number of Smart Meters involved in SMN significantly exceed those in indoor WLAN networks for which application the PCF were originally designed. For example, IEEE 802.11ah TG requires one data collector to support a network with upto 6000 Smart Meters as a benchmark [2], while the average number of the communication nodes served by a single WiFi BSSID is on the order of 20-30. In such a densely populated network, the total delay for all the Smart Meters to complete their own reports sequentially using the traditional PCF may become prohibitively large, e.g. minutes for about 2000 nodes.

The traditional random access MAC protocols, such as DCF [23], would suffer longer delay from the scalability issue due to the extremely competitive channel contentions and the resulting retransmissions. Therefore, the grouping idea has been adopted by IEEE 802.11ah TG for the future SMN implementation to relieve these strong competitions [48]. In that scheme, all the Smart Meters are divided into several groups and the network channel access is accordingly separated into two two-tiers: inter-group and intra-group tier. Then the coordinating AP distributes to each group a non-overlapping interval (sub-frame) and allows

the Smart Meters in each group to try to communicate only within their allocated interval. Although the grouping based MAC protocols have been proved to improve the throughput and transmission delay effectively for event-driven (random access) data transportation in [58], it still has room of performance improvement by designing a suitable MAC protocol in the intra-group tier specially for the periodic and infrequently changing measurement data transmission.

Therefore, complying with the grouping concept in IEEE 802.11ah Standards and inspired by the idea in [20], [11] and [12], we employ the time-invariant nature of power factor measurement and propose a MAC protocol by using Compressive Sensing (CS), a famous and popular signal processing technique, to solve the scalability issue in the intra-group tier of SMN. In this method, whenever a generic group has been allocated the sub-frame, instead of reporting the absolute value, all Smart Meters within this group repeatedly send the changing value of the power factor measurements simultaneously with a prior-distributed pseudo-random gain for several times. We note that the changing value could be approximately zero due to the measurement stability, which leads to the sparsity of transmitted data vector. Then at the receiver side, the compressive sensing technique is applied to reconstruct the sparse transmitted data vector. Therefore, we can observe that the transmission delay is bounded and the transmission overhead in the traditional PCF and DCF, such as Poll message and DIFS, can be avoided to decrease the total delay further. Furthermore, we also discuss the implementation of this new protocol on the scenario that Smart Meters may have different reporting periods.

The primary contributions of this work can be summarized as follows:

- We develop a new MAC protocol by employing the Compressive Sensing technology to decrease the transmission delay of the periodic and nearly time-invariant measurement reporting effectively.

- We evaluate and compare the performance of proposed MAC protocols by using real power factor measurement data accessed from the Pacific Northwest Smart Grid Demonstration Project [46], in which the University of Washington installed Smart

Meters in 216 buildings to collect energy related measurements and analyze the energy usage for research purpose.

The remainder of the chapter is organized as follows: we present the MAC protocol with compressive sensing in details and compare it with some other optional protocols in Section 5.1. The implementations of these protocols on the non-identical scenario are discussed in Section 5.2. The simulation results and performance analysis will be discussed in Section 5.3. The paper concludes with Section 5.4.

5.1 MAC Protocol Design for Periodic Power Factor Measurement Report

In this section, we assume all the Smart Meters share identical reporting period. Before describing the following MAC protocols, we define the related parameters and terms next:

- Reporting Period: The interval between two successive power factor measurement reports. According to the grouping idea, the reporting period generally comprises multiple non-overlapping intervals, defined as *Sub-Frame*, allocated to each group, as shown in Fig.5.1.

- N: The number of Smart Meters, whose physical layer transmission rate is identical and defined as C.

- N_g: The number of Smart Meters in each group.

- $pf_i(t)$: The power factor measurement from Smart Meter i $(1 \leq i \leq N)$ during the t^{th} reporting period. Furthermore, we also define $\Delta pf_i(t) = pf_i(t) - pf_i(t-1)$.

- $x_i(t)$: The actual transmitted data from Smart Meter i during the t^{th} reporting period.

- $y_i(t)$: At the local collector, the received or recovered data for Smart Meter i during the t^{th} reporting period.

- $e_i(t)$: The data error for Smart Meter i during the t^{th} reporting period, which is defined as $e_i(t) = |y_i(t) - \Delta pf_i(t)|$.

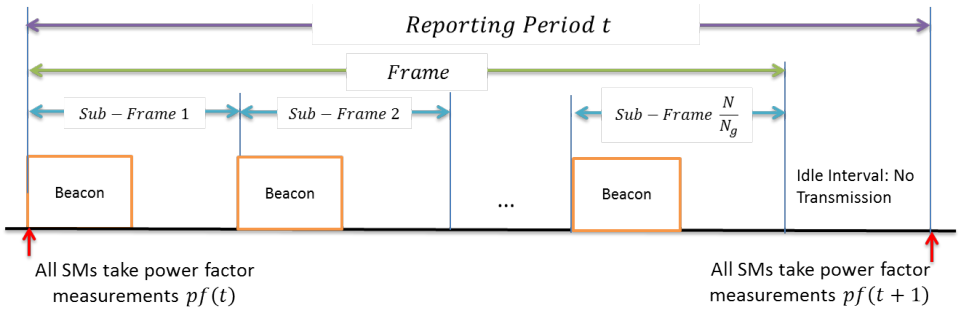

Figure 5.1: Example of Reporting Period and Sub-Frames

- $D(t)$: The delay spent on finishing the power factor measurement report for all Smart Meters during the t^{th} reporting period. Furthermore, $D = \frac{\sum_{t=1}^{T} D(t)}{T}$ is defined as the average delay.

- Since we focus on the MAC protocol design in this paper, we assume that the communication noise is negligible and thus do not consider it in our system model.

5.1.1 Baseline: Traditional PCF

As shown in Fig.5.2, during the allocated sub-frame in t^{th} reporting period, every Smart Meter i just reports $\Delta pf_i(t)$ sequentially as the reply to the Poll message from Local Collector, which means $y_i(t) = x_i(t) = \Delta pf_i(t)$. This baseline method leads to perfect accuracy (without consideration of transmission noise), i.e. $e_i(t) = 0\ \forall i$ and $\forall t$ and its delay D is given as:

$$\begin{aligned} D_{PCF} &= D_{PCF}(t) \\ &= N\left(\frac{Poll}{C} + SIFS + \frac{Payload}{C} + SIFS\right) + \lceil \frac{N}{N_g} \rceil \left(\frac{Beacon}{C} + SIFS\right). \end{aligned} \tag{5.1}$$

Since D is linear in N, thus the traditional PCF may experience high delay especially when N is large.

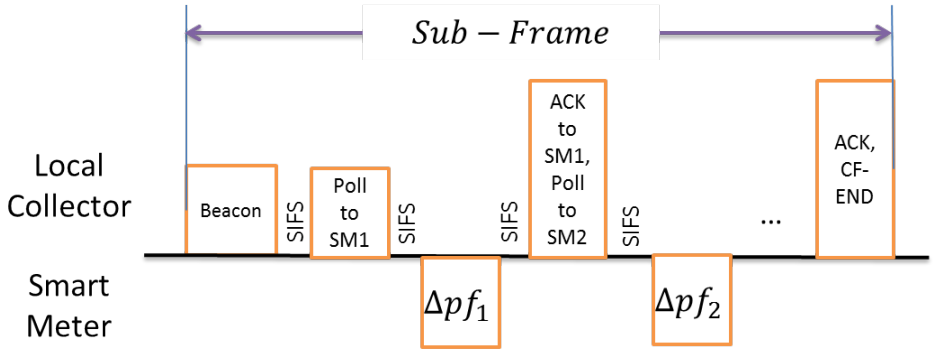

Figure 5.2: Transmission Example for Traditional PCF

5.1.2 PCF with Transmission Threshold (PCF-TT)

Since the power factor measurement value is usually time-invariant, thus for most of the reporting period t, $\Delta pf_i(t) \simeq 0$. By employing this feature, we may set a transmission threshold δ and modify the traditional PCF as follows:

- If $|\Delta pf_i(t)| > \delta$: Smart Meter i just reports the $\Delta pf_i(t)$ to the Local Collector within its allocated sub-frame in response to the Poll message, which means $y_i(t) = x_i(t) = \Delta pf_i(t)$ and $e_i(t) = 0$.

- If $|\Delta pf_i(t)| \leq \delta$: Smart Meter i keeps silent with respect to the Poll message. After waiting for PIFS, the Local Collector assumes no change on the power factor of the current Smart Meter and starts to poll the next one. Therefore, $y_i(t) = x_i(t) = 0$ and $e_i(t) = |\Delta pf_i(t)|$.

The transmission example is displayed in the Fig.5.3. We can observe that this method may lead to imperfect data accuracy during each reporting period and the accumulated error $\sum_{t=1}^{T} e_i(t)$ may become a large mismatch. In order to compensate, we require each Smart Meter to report an accurate measurement $pf_i(t)$ after every T reporting periods.

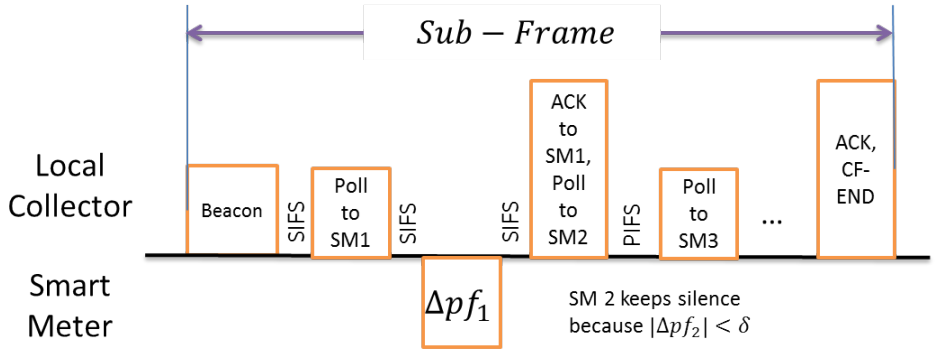

Figure 5.3: Transmission Example for PCF with Transmission Threshold

This method may lead to lower delay $D(t)$, which is given as:

$$\begin{aligned} D_{PCF-TT}(t) &= N_{tran}(t)\left(\frac{Poll}{C}+SIFS+\frac{Payload}{C}+SIFS\right) \\ &+ (N-N_{tran}(t))\left(\frac{Poll}{C}+PIFS\right)+\lceil\frac{N}{N_g}\rceil\left(\frac{Beacon}{C}+SIFS\right), \end{aligned} \tag{5.2}$$

where $N_{tran}(t)$ is the number of Smart Meters whose data $|\Delta pf(t)| > \delta$ at the t^{th} reporting period and $\frac{\sum_{t=1}^{T} N_{tran}(t)}{T} = \alpha_{tran} N$ $(0 < \alpha_{tran} < 1)$.

5.1.3 DCF with Transmission Threshold (DCF-TT)

In this method, we still employ the transmission threshold δ and modify the traditional DCF as follows:

- If $|\Delta pf_i(t)| > \delta$: Smart Meter i joins the channel contention within its allocated sub-frame via traditional DCF and tries to report $\Delta pf_i(t)$ after the beacon broadcast from Local Collector, which means $y_i(t) = x_i(t) = \Delta pf_i(t)$ and $e_i(t) = 0$.

- If $|\Delta pf_i(t)| \leq \delta$: Smart Meter i does not join the channel contention during the entire t^{th} reporting period. Therefore, $y_i(t) = x_i(t) = 0$ and $e_i(t) = |\Delta pf_i(t)|$.

The transmission example is displayed in the Fig.5.4. Similarly, the accumulated error can also be compensated by running one accurate measurement $pf_i(t)$ report in every T

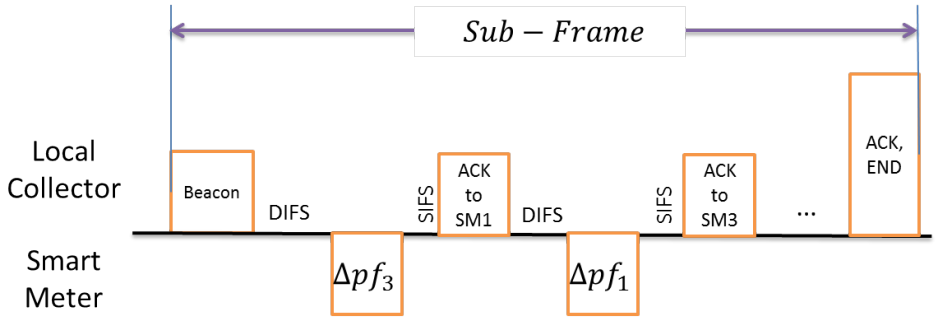

Figure 5.4: Transmission Example for DCF with Transmission Threshold

reporting periods.

5.1.4 MAC Protocol with Compressive Sensing (CS)

In this method, we set $x_i(t) = \Delta pf_i(t)$ for each Smart Meter i. Then the transmitted data in each sub-frame during the t^{th} reporting period can be represented as a vector [1]:

$$\mathbf{X}_{N_g \times 1} = \mathbf{\Delta PF}_{N_g \times 1} = [\Delta pf_1, \Delta pf_2, ..., \Delta pf_{N_g}]^T, \tag{5.3}$$

which could be quite sparse due the infrequent changes of power factor measurement. Therefore, inspired by the theory of compressive sensing [20],[14], we require that all the Smart Meters repeatedly transmit their own data $\Delta pf_i(t)$ simultaneously for L times during their allocated sub-frame. Then the received data vector $\mathbf{R}$ at the Local Collector is given as:

$$\begin{aligned} \mathbf{R} &= \mathbf{A} \times \mathbf{X} \\ &= \begin{bmatrix} s_1(1)h_1(1) & \cdots & s_{N_g}(1)h_{N_g}(1) \\ s_1(2)h_1(2) & \cdots & s_{N_g}(2)h_{N_g}(2) \\ \cdots & \cdots & \cdots \\ s_1(L)h_1(L) & \cdots & s_{N_g}(L)h_{N_g}(L) \end{bmatrix} \begin{bmatrix} \Delta pf_1(t) \\ \Delta pf_2(t) \\ \cdots \\ \Delta pf_{N_g}(t) \end{bmatrix}, \end{aligned} \tag{5.4}$$

where

$$\mathbf{R}_{L \times 1} = [r(1), r(2), ..., r(L)]^T, \tag{5.5}$$

[1] we skip the time index t for simplicity here

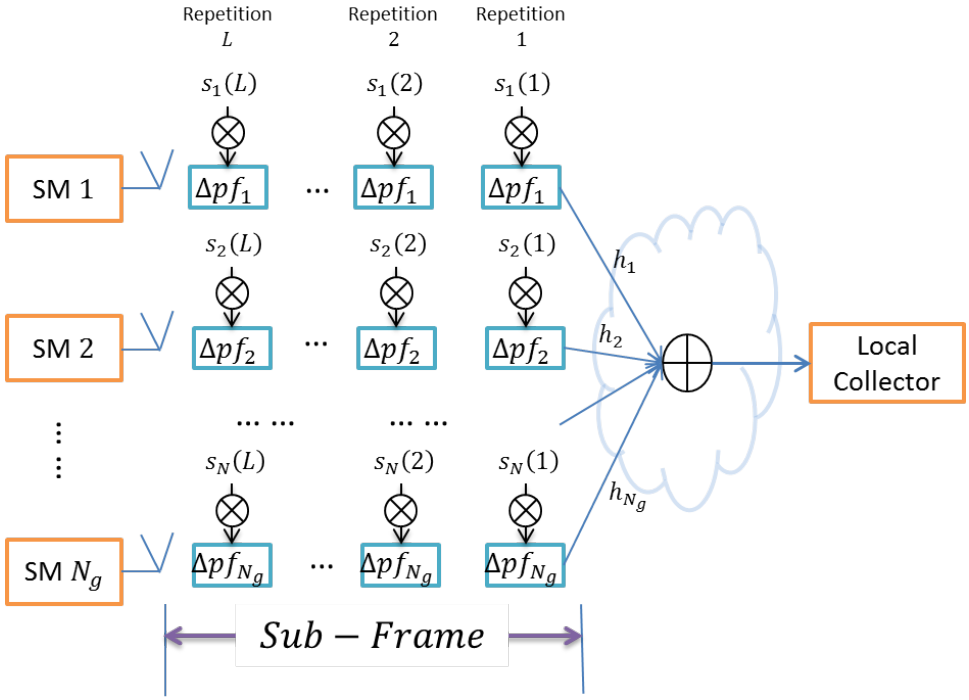

Figure 5.5: Transmission Example for MAC Protocol with Compressive Sensing

and $h_i(l)$ is the channel gain between Smart Meter i and Local Collector at $l^{th}(1 \leq l \leq L)$ transmission repetition. We assume that $h_i(l)$ is a random variable which is independent of i and l, and known to both Local Collector and Smart Meter via channel estimation technology. On the other hand, $s_i(l)$ represents the pseudo-random operating gain for Smart Meter i in the l^{th} transmission repetition. It can be generated from a key that has been distributed to the Smart Meter before the operation, which thus makes it also known to both Local Collector and Smart Meter. The transmission example is displayed in the Fig.5.5.

Due the near-sparsity of vector $\mathbf{\Delta PF}$, we may set $L = \alpha_L N_g$ and $\alpha_{tran} < \alpha_L < 1$. Then the average delay is given as:

$$\begin{aligned} D_{CS} &= D_{CS}(t) \\ &= \alpha_L N \left(\frac{Payload}{C} + SIFS \right) + \lceil \frac{N}{N_g} \rceil \left(\frac{Beacon}{C} + SIFS \right). \end{aligned} \tag{5.6}$$

Referring to [13] and [45], we may recover the transmitted measurement data $\mathbf{Y}$ by solving

the following optimization equation:

$$min||\mathbf{Y}||_1 \tag{5.7}$$

$$s.t.||\mathbf{r} - \mathbf{A} \times \mathbf{Y}||_2 < \epsilon$$

where

$$\mathbf{Y} = [y_1(t), y_2(t), ..., y_{N_g}(t)]^T, \tag{5.8}$$

and ϵ is the predetermined threshold. We can observe that this optimization problem is convex and can be efficiently solved by linear programming. Similarly, reporting one accurate measurement $pf_i(t)$ in every T reporting periods can also reduce the accumulated error.

5.2 Implementations on Non-Identical Reporting Period Scenario

As mentioned above, if all the Smart Meters share the same reporting period, then, during each reporting period, the number of Smart Meters reporting their power factor measurements is constant. On the other hand, due to the variety of implementation, the Smart Meters may be classified into different categories; each of them may have different reporting periods. Therefore, the Local Collector has to keep track the reporting period information of all the Smart Meters and then determine the exact number of Smart Meters that will have measurement data to transmit in any reporting period. Furthermore, the MAC protocols mentioned above may also need some modifications. In order to make the following descriptions more concise, we define the related parameters next:

- M: The total number of Smart Meters classes.
- N_m: The number of Smart Meters that belong to Class m.
- t_m: The length of reporting period for Class m Smart Meters.

5.2.1 Grouping Scheme Modifications

First, in order to maintain the effectiveness and benefits of the grouping scheme, in the group division step, we need to guarantee that all the Smart Meters in the same group

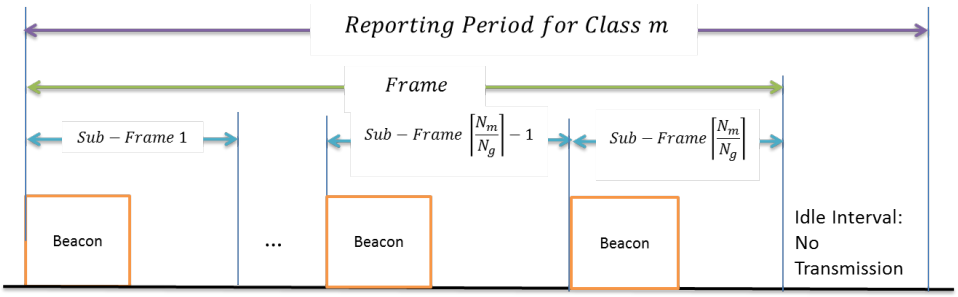

Figure 5.6: Example of Reporting Period and Sub-Frames for Class M

have to share the same reporting period. Otherwise, during a generic reporting period for Class m, the Smart Meters not belonging to Class m will have no data to transmit and give no response to Poll message. In return, more groups will be allocated sub-frames in this reporting period to cover all the Class m Smart Meters, which leads to more unnecessary Beacon messages. Therefore, the communication resources allocated to the sub-frames and associated groups may not be fully utilized, which may lead to the inefficiency of the MAC protocols.

For Class m Smart Meters, they may be divided into $\lceil \frac{N_m}{N_g} \rceil$ groups. Among them, $\lfloor \frac{N_m}{N_g} \rfloor$ groups have N_g Smart Meters, and the rest $N_m - \lfloor \frac{N_m}{N_g} \rfloor \times N_g$ Smart Meters are in the last group if any. After that, in a generic reporting period, the Local Collector only needs to allocate the sub-frames to the groups whose Smart Meters have measurements to transmit so as to increase the efficiency of MAC protocols, as shown in the Fig.5.6.

5.2.2 MAC Protocols Design Modifications

Since the PCF and DCF based schemes are either fully centralized or fully distributed MAC protocols, thus the operations in the intra-group tier of all those three schemes may not need to be modified as long as the Local Collector keeps track all the reporting period information and allocate sub-frames to correct groups appropriately according to the modified grouping division scheme. Accordingly, the transmission delay in one reporting period for Class m Smart Meters is modified and given as:

For Traditional PCF

$$\begin{aligned} D^m_{PCF} &= N_m \left(\frac{Poll}{C} + SIFS + \frac{Payload}{C} + SIFS \right) \\ &+ \lceil \frac{N_m}{N_g} \rceil \left(\frac{Beacon}{C} + SIFS \right). \end{aligned} \tag{5.9}$$

For PCF with Transmission Threshold

$$\begin{aligned} D^m_{PCF-TT}(t) &= N^m_{tran}(t) \left(\frac{Poll}{C} + SIFS + \frac{Payload}{C} + SIFS \right) \\ &+ (N_m - N^m_{tran}(t)) \left(\frac{Poll}{C} + PIFS \right) + \lceil \frac{N_m}{N_g} \rceil \times \left(\frac{Beacon}{C} + SIFS \right). \end{aligned} \tag{5.10}$$

For the MAC protocol with Compressive Sensing, since the Smart Meters in a generic group has to know the transmission repetition length L, which depends on the group size N_g, thus, in each sub-frame, the Local Collector understanding the global information is required to broadcast the transmission repetition length L to all the Smart Meters in the associated group. Then the transmission delay in this scheme is also modified as:

$$D^m_{CS} = \alpha_L N_m \left(SIFS + \frac{Payload}{C} \right) + \lceil \frac{N_m}{N_g} \rceil \times \frac{Beacon}{C}. \tag{5.11}$$

In sum, we average the transmission delay over all the classes to obtain the average delay D as

$$D = \frac{\sum_{m=1}^{M} D_m \frac{\prod_{n=1}^{M} t_n}{t_m}}{\sum_{m=1}^{M} N_m \frac{\prod_{n=1}^{M} t_n}{t_m}} N \tag{5.12}$$

5.3 Simulation Results

We used real power factor measurement data from the Pacific Northwest Smart Grid Demonstration Project [46] to evaluate and compare the performance of our proposed MAC protocols. In order to quantify the performance, in addition to average delay D, we also define the average received/recovered data error as follows:

$$E = \frac{\sum_{t=1}^{T} \sum_{i=1}^{N} e_i(t)}{NT} = \frac{\sum_{t=1}^{T} \sum_{i=1}^{N} |y_i(t) - \Delta p f_i(t)|}{NT}. \tag{5.13}$$

In this section, we created a new model, *cspcf Model*, to implement and test the PCF Protocol with CS in the NS-3 simulator. The default parameters used in the simulation are listed in the Table 5.1.

Parameter	Value
SIFS	16 μs
DIFS	34 μs
PIFS	25 μs
Congestion Window Slot Time	9 μs
Congestion Window Size	32
Max Congestion Window Stage	5
ACK Size	30 byte
Poll Message Size	36 byte
Beacon Size	50 byte
Default Payload Size	34 byte
Physical Layer Transmission Rate C	100 kbps
Default Number of Smart Meters N	2800
Default Number of Smart Meters in each Group N_g	700
Default Number of Transmission Repetition Ratio α_L	90%
Default Transmission Threshold Value δ	0.01
Default Number of Classes M	1

Table 5.1: Parameters List

5.3.1 Performance with respect to Number of Smart Meters N

In this subsection, we fix the number of groups to be 4 and thus $N_g = \frac{N}{4}$. As shown in the Fig.5.7, the average data error of MAC protocol with CS is lowest among all the protocols because the transmitted data vector $\mathbf{\Delta PF}$ is sparse enough ($\alpha_{tran} < \alpha_L$) so that the data can be recovered accurately at the Local Collector. As shown in the Fig.5.8, the average delay for DCF with transmission threshold increases significantly as N_g goes up, due to the intense channel contention in the intra-group tier and the resulting retransmissions. On the contrary, the average delay for other three MAC protocols increases linearly as the number of Smart Meters. The slopes of these three lines are given as:

- Traditional PCF:

$$\begin{aligned} \frac{dD_{PCF}}{dN} &= \left(\frac{Poll}{C} + SIFS + \frac{Payload}{C} + SIFS\right) \\ &+ \left(\frac{Beacon}{C} + SIFS\right)/N_g \end{aligned} \tag{5.14}$$

- PCF with transmission threshold:

$$\begin{aligned} \frac{dD_{PCF-TT}}{dN} &= \alpha_{tran}\left(\frac{Poll}{C} + SIFS + \frac{Payload}{C} + SIFS\right) \\ &+ (1-\alpha_{tran})\left(\frac{Poll}{C} + SIFS\right) + \left(\frac{Beacon}{C} + SIFS\right)/N_g \end{aligned} \tag{5.15}$$

- MAC protocol with CS:

$$\frac{dD_{CS}}{dN} = \alpha_L\left(\frac{Payload}{C} + SIFS\right) + \left(\frac{Beacon}{C} + SIFS\right)/N_g \tag{5.16}$$

We can observe that the MAC protocol with CS has the smallest slope and the lowest delay. This is because, in that method, the Local Collector does not need to send any Poll Message, which thus reduces the transmission overhead.

5.3.2 Performance with respect to Transmission Threshold δ

As shown in the Fig.5.9 and Fig.5.10, the performance of traditional PCF and MAC protocol with CS do not change because they are independent of the transmission threshold δ. On the

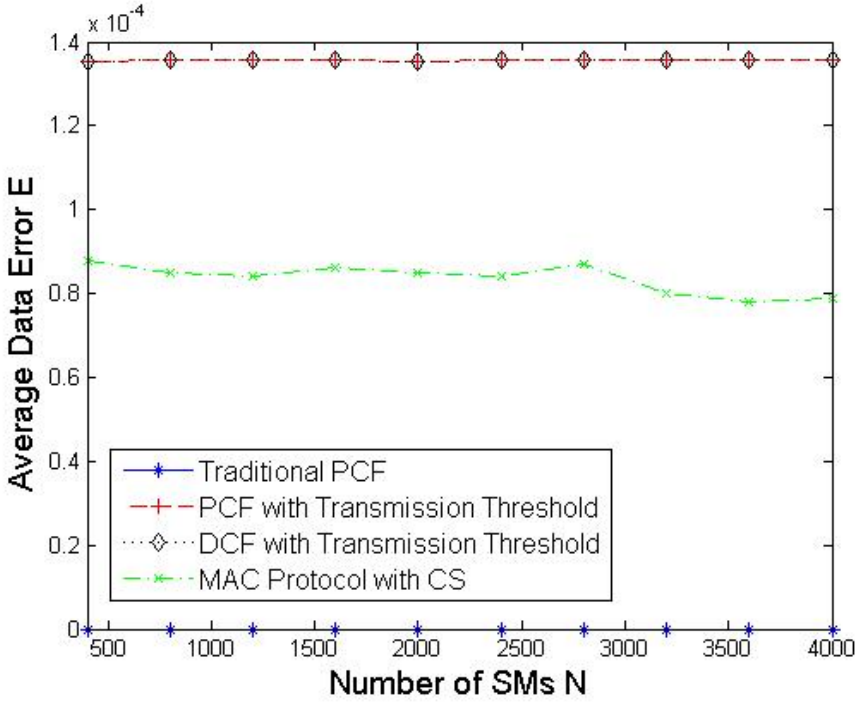

Figure 5.7: Average Data Error E Vs Number of Smart Meters N

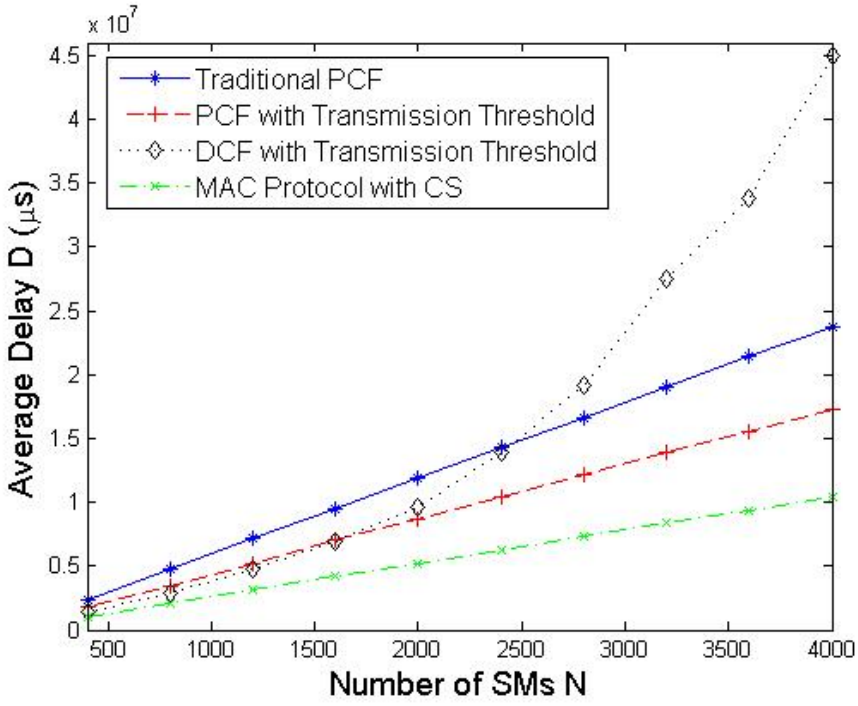

Figure 5.8: Average Delay D Vs Number of Smart Meters N

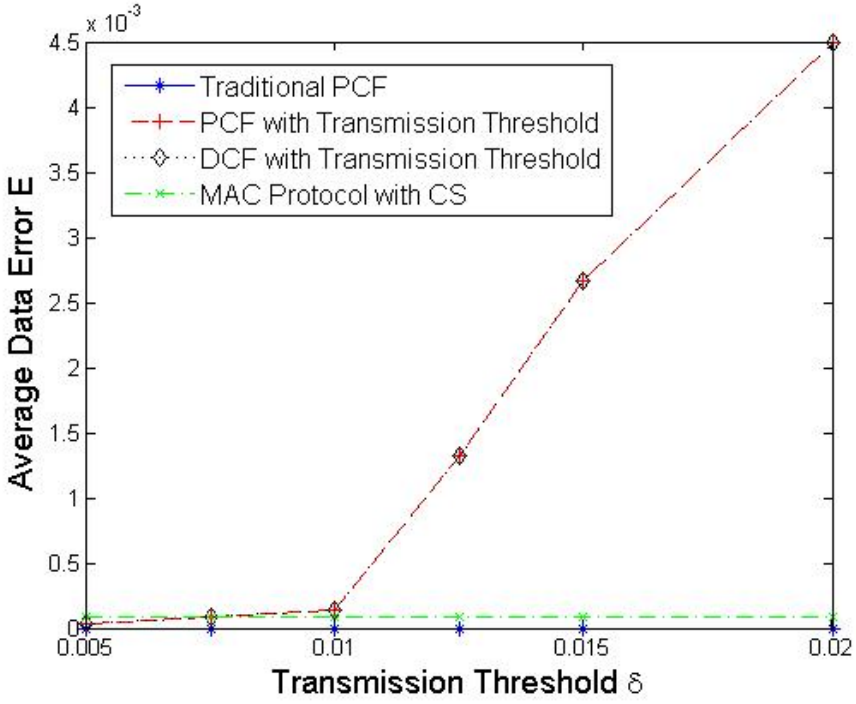

Figure 5.9: Average Data Error E Vs Transmission Threshold δ

other hand, the average delay for both PCF and DCF with transmission threshold decreases as δ becomes large. This is because, with looser threshold δ, more Smart Meters keep silent during the reporting period, which reduces the transmission delay D but deteriorates the average data error E as the cost. Therefore, the transmission threshold δ needs to be selected carefully to balance the tradeoff between average delay and data error.

5.3.3 Performance with respect to Transmission Repetition Length Ratio α_L

As shown in the Fig.5.11 and Fig.5.12, the delay of MAC protocol with CS increases linearly as the repetition length ratio α_L according to the equation (5.7). However, we can observe that the delay of MAC protocol with CS with $\alpha_L = 1$ is still smaller than those of other protocols, which is because the MAC protocol with CS suffers less from the transmission overhead, such as Poll Message. As shown in the Fig.5.11, when α_L is not large enough, the average data error of MAC protocol with CS goes up significantly because the Local

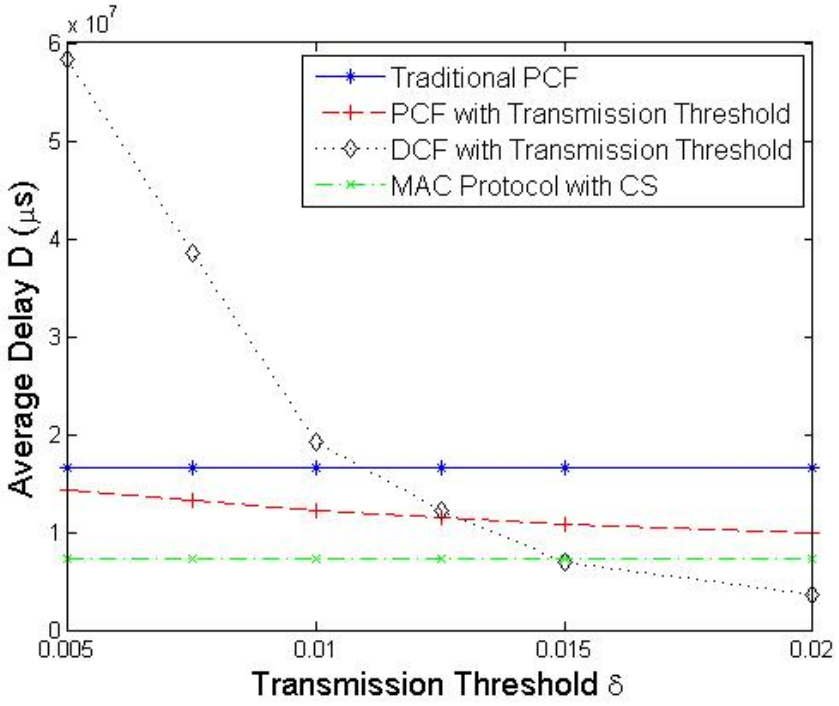

Figure 5.10: Average Delay D Vs Transmission Threshold δ

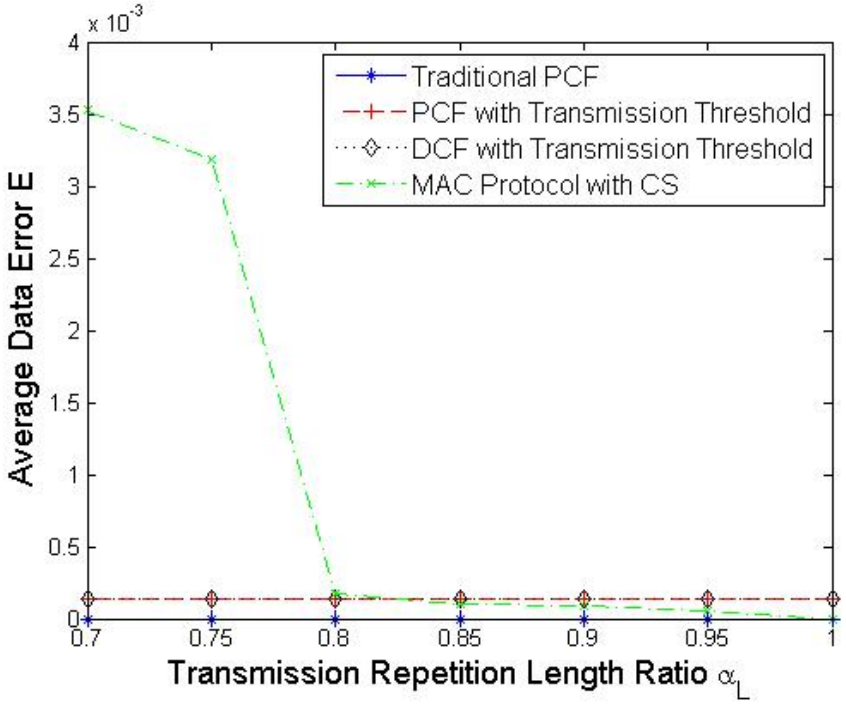

Figure 5.11: Average Data Error E Vs Transmission Repetition Length Ratio α_L

Collector cannot recover the data accurately when $\alpha_L < \alpha_{tran}$.

5.3.4 Performance with respect to Payload Length

Since the average data error is independent of the payload length, we only investigate the delay here. As shown in the Fig.5.13, the average delay D for all the MAC protocols increase linearly as the payload length. The slope of these four lines are given as:

- Traditional PCF and DCF with transmission threshold:

$$\frac{dD_{PCF}}{dPayload} = \frac{dD_{MDCF}}{dPayload} = \frac{N}{C}. \tag{5.17}$$

- PCF with transmission threshold:

$$\frac{dD_{PCF-TT}}{dPayload} = \frac{\alpha_{tran} N}{C} \tag{5.18}$$

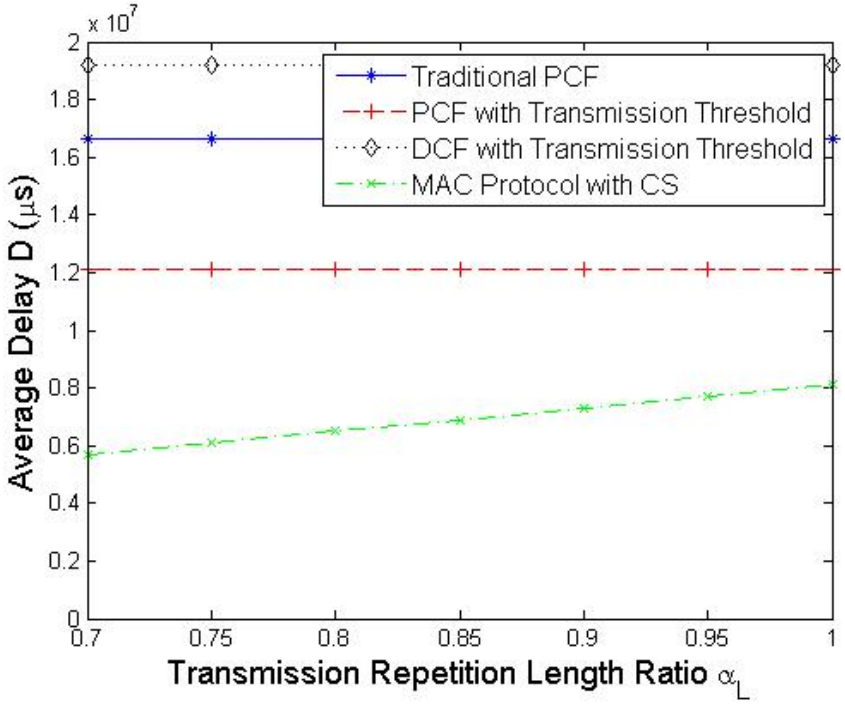

Figure 5.12: Average Delay D Vs Transmission Repetition Length Ratio α_L

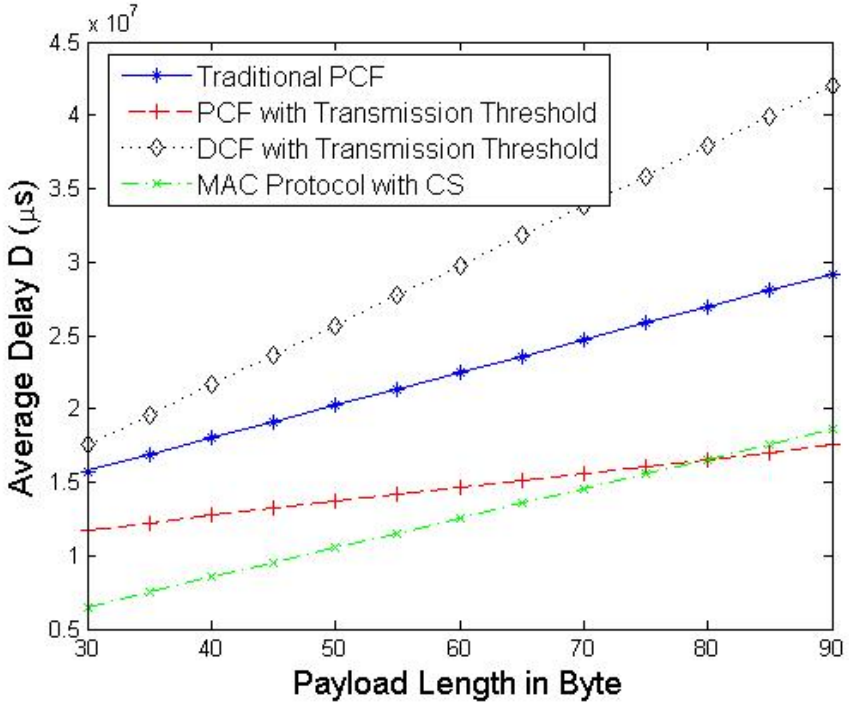

Figure 5.13: Average Delay D Vs Payload Length in byte

- MAC protocol with CS:

$$\frac{dD_{CS}}{dPayload} = \frac{\alpha_L N}{C} \tag{5.19}$$

Among them, we can observe that the slope of PCF scheme with transmission threshold is smallest. Furthermore, if we set equation (5.2)=(5.7), we can obtain

$$Payload^* = \frac{\frac{Poll}{C} + (1-\alpha_{tran})PIFS + (2\alpha_{tran} - \alpha_L)}{\alpha_L - \alpha_{tran}} C \tag{5.20}$$

Therefore, when the payload length is large than $Payload^*$, the MAC protocol with CS may experience longer transmission delay than the PCF with transmission threshold. This is because $\alpha_L > \alpha_{tran}$ and the time spent on these additional payload transmission exceeds the time saved by less transmission overhead. Fortunately, the power factor measurement transmission may only need lower payload length, which benefits the performance of MAC protocol with CS.

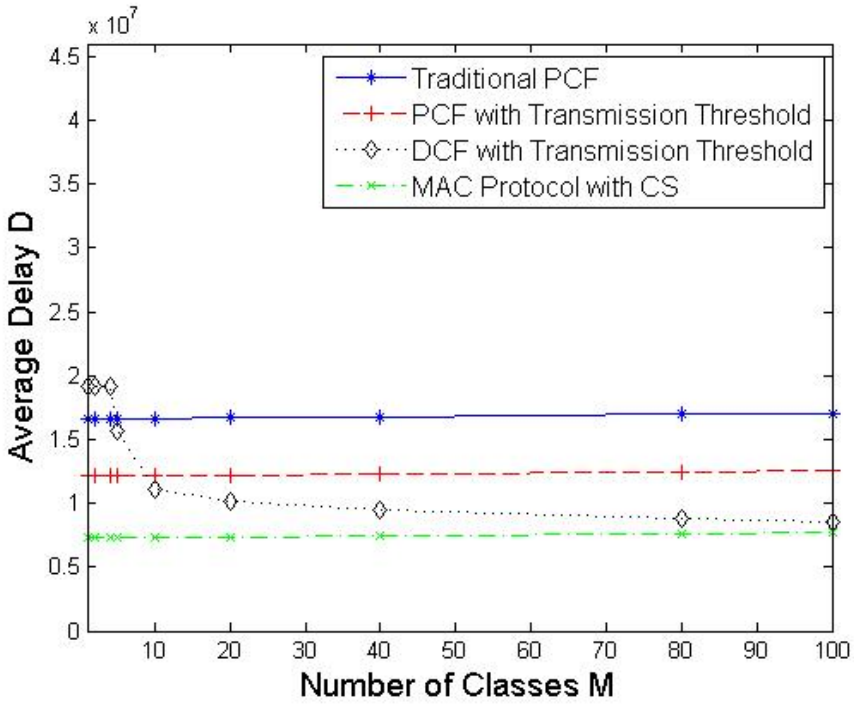

Figure 5.14: Average Delay D Vs Number of Classes

5.3.5 Performance with respect to Number of Classes M

Similarly, we only focus on the average delay D in this subsection because the average data error E is not affected by the number of various classes M. Without loss of generality, we assume that the number of Smart Meters in each class is identical, i.e. $N_m = \frac{N}{M}$ $(\forall m)$. As shown in the Fig.5.14, the average delay of PCF based schemes and MAC protocol with CS are slightly increased. This is because as M becomes larger, the number of groups and sub-frames is also increased, which leads to the additional beacon transmissions and larger transmission delay. On the other hand, since we fix the total number of Smart Meters N, thus with the larger number of classes and groups, the actual number of Smart Meters in each group decreases. Then, by using the DCF with transmission threshold, the intra-group tier channel contention becomes less competitive and transmission delay D drops accordingly as shown in the Fig.5.14.

5.4 Conclusions

In this chapter, by exploiting the time-invariant nature of measurement and complying with the grouping idea, we proposed the MAC protocol with compressive sensing to solve the scalability issue for power factor measurement reporting in the Smart Metering Network. The implementation of this protocol on the scenario that Smart Meters may have different reporting periods is also discussed. As shown in Section 5.3, our proposed protocol significantly outperforms the traditional MAC protocols to support such periodic and time-invariant measurement reporting.

Chapter 6

REAL-TIME DISAGGREGATION OF USER POWER CONSUMPTION USING THE VITERBI ALGORITHM

6.1 Introduction

The data driven algorithm that enables the consumers to access to disaggregated power consumption status at individual appliance level would be critical to the future demand response implementation in AMI. Traditionally, field surveys have been used to summarize customer's energy usage behavior [38]. However the accuracy of this method is quite limited because it basically relies on self-reporting, with resulting data sparsity and biases. At some future point, direct distributed measurement of power consumption at each individual appliance may be feasible. However, it entails costly installation and associated maintenance issues [25] and consequently the preferred solution architecture is the one proposed below.

Our disaggregation algorithm in this Chapter is based on the class of *single-point sensing and analysis* following the pioneering work on Non-Intrusive Load Monitoring (NILM) first introduced in [19]. Advanced single-point sensing techniques are being developed to disaggregate the observed power consumption data. In this approach, the key features (power, voltage, current, etc.) of each class of electrical appliances are assumed to be available from an authoritative database. Then, given a series of aggregate energy consumption feature measurements, the energy use for individual electrical appliances can be obtained. Most NILM algorithms rely on real/reactive/apparent power signature pattern matching [30],[31],[36], in which multiple electrical appliances are classified into different groups according to their average power consumption. However, these algorithms are usually limited to *large loads*; in typical building scenarios, the differences among different home/office appliances in terms of average power may not be significant enough for classification. In order to improve feature selection, [7], [44] and [25] use start-up current and voltage signature instead of the power signature. However, all these methods suffer higher expense

and complexity of implementation and maintenance as the cost of disaggregation accuracy improvement. On the other hand, the authors in [47] proposed to use electromagnetic interference (EMI) as signature for appliance identification; [34] subsequently undertook an in-depth study into the reliability and feasibility of EMI sensing and its modeling. Although EMI sensing based schemes are promising due to their universality, its disaggregation performance is still heavily impacted by background noise as well as EMI filters integrated into specific appliances. Instead of selecting one generic energy related parameter, [56] proposed using a Factor Graph (FG) - a graphical model involving a function of multiple parameters, including power, frequency, voltage and phase angle, for improved disaggregation accuracy at the cost of increased implementation complexity. Another approach pioneered by [27] uses signal separation techniques for disaggregation of power consumption. The approach - termed *Discriminative Disaggregation Sparse Coding* formulates it as a single-channel source separation problem. While this approach is promising because it can be applied on almost any type of appliances without load magnitude limitation, it may sometimes lead to poor disaggregation when multiple devices have similar power consumption behavior within a generic interval.

It is fair to say that existing algorithms based on average power consumption patterns *cannot* achieve real-time disaggregation as they must use consumption measurements over several hours. For example, the dictionary dimension used in [27] is on the order of a week, which means that this algorithm disaggregates the power consumption measurements in a block of weeks; such long disaggregation delay cannot satisfy the timing requirements of real-time price generation and demand response. Our work presumes that aggregated power consumption measurements is available at the rates offered by new Smart Meters to which we apply a new Markov Chain model as described next. First, the (continuous valued) power consumption data over one minute intervals for each electrical appliance is discretized into a set of suitable levels. Then, a straightforward way to disaggregate the observed aggregate power consumption at any time instant is to a) select one representative level for each appliance and b) find the optimal combination that most closely approximates the observed measurements. However, these may yield poor performance if some appliances share similar minute-resolution power consumption signatures or multiple candidate combinations with

similar sum values are obtained. Fortunately, according to [35], the power consumption of generic electrical appliance have strong correlation over one minute time intervals. Furthermore, there also exist mutual correlations among the power consumption behaviors of some specific electrical appliances. Therefore, we may generate a temporal Markov Chain for each electrical appliance's power consumption pattern as well as an inter-device power consumption mapping table so as to capture such two dimensional correlations. Subsequently, we implement the Viterbi Algorithm (VA) - a version of dynamic programming - widely used in many applications in networking and signal processing [51],[42], to determine the most likely disaggregated power consumption profile among the multiple candidates.

The primary contributions of this work can be summarized as follows:

- Develops a new Markov Chain based model for device level power consumption that captures temporal and inter-class correlations.

- Implements the Viterbi Algorithm to determine disaggregated power consumption; the proposed method is capable of near real-time operation with desired prediction accuracy.

- Validates the approach by evaluating performance using *real minute-resolution power consumption data* from Pecan Street's Dataport [39], the world's largest source of energy consumption data at minute resolution from residential and industrial customers, widely used for performance benchmarking.

The proposed real-time disaggregation framework is developed in Section 6.2. We then introduce the algorithm testing methods and discuss its performance in Section 6.3. This chapter concludes with Section 6.4.

6.2 Real-time Disaggregation Algorithm based on Markov Chain Model and Viterbi Algorithm

We represent the disaggregation problem via the block diagram in Fig.6.1. The minute-resolution aggregated power consumption measurements $R(T) = [r(1), r(2), ..., r(T)]$ are fed into the disaggregation block sequentially. After running the disaggregation algorithm,

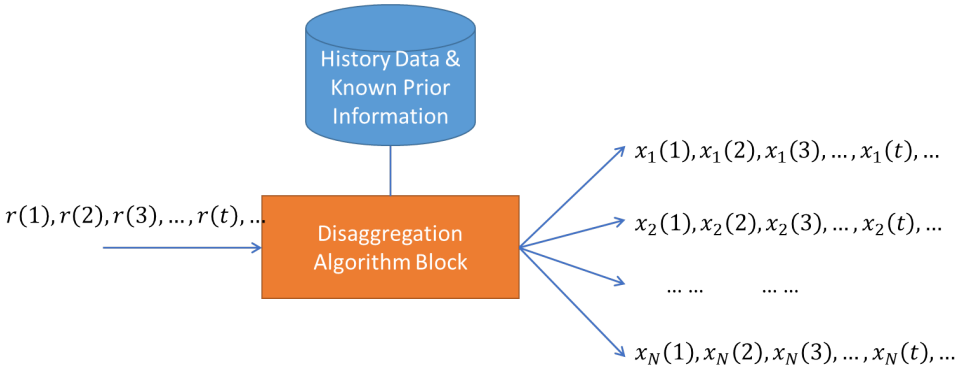

Figure 6.1: Real-Time Disaggregation Block Diagram

the disaggregated power consumption status of N individual electrical appliances at any minute interval t $(1 \leq t \leq T)$, denoted by the vector $X(t) = [x_1(t), x_2(t), ..., x_N(t)]$, can be determined, where the element $x_i(t)$ denotes the power consumption of appliance i $(1 \leq i \leq N)$ at minute instant t.

First, we discretize the continuous minute-resolution power consumption values of appliance i into a finite number of levels, denoted as $U_i = \{u_i^{(j)}\}$, where $1 \leq i \leq N$, $1 \leq j \leq |U_i|$. Subsequently, a traditional way to disaggregate $R(t)$ $(1 \leq t \leq T)$ is to find the optimal combination of discrete power consumption levels of each individual appliance $X^*(t) = [x_1^*(t), x_2^*(t), ..., x_N^*(t)]$ respectively, such that the mismatch $|r(t) - \sum_{i=1}^{N} x_i^*(t)|$ is minimized, where $x_i^*(t) \in U_i$. However, this class of approaches has several limitations - including estimation accuracy as shown in the Section 5.3 and in some cases, the lack of a unique solution.

Therefore, we propose an innovative, real-time disaggregation algorithm for the measurement sequence $R(T)$. According to [35], the power consumption of a generic electrical appliance shows a strong correlation over several minute durations. We may thus generate a Markov Chain of the minute-resolution power consumption levels for each electrical appliance to describe such temporal correlation. In addition, there also exist inter-device correlations among the power consumption behaviors of some specific appliances, which can be captured by a power consumption level mapping table of these devices. Therefore, by employing the generated Markov Chains and mapping table, we can implement Viter-

bi Algorithm to determine the unique and optimal combination of disaggregated power consumption profile at any instant, with only a short (and controllable) decoding delay.

6.2.1 Class of Electrical Appliances

We may classify the ordinary electrical appliances into two categories. The power consumption behaviors of the first class devices have little relation to the customer behaviors. Once the electrical appliance is turned on, it would keep operating according to the inherent and quite obvious power consumption pattern until a pre-determined duration passes or it completes some specific missions without manual interruption. Therefore, the temporal correlations of these devices, e.g. clothes washer, dishwasher, air conditioner, furnace and kettle, are easily captured and employed to identify their individual power consumption statuses from the aggregated measurements. Our proposed real-time disaggregation algorithm works better on this class of electrical appliances but does not fit the other class, whose power consumption behaviors are not very determined and largely depend on the customer behaviors, such as light, TV, computer and other plug-in devices. Since it is quite complicated to use Markov Chain to statistically investigate the customer behaviors, thus the temporal correlations of the second class devices cannot be easily summarized and we do not take them into consideration in our work.

6.2.2 Temporal Correlations

In order to demonstrate the inherent temporal correlation of individual appliance and generate the associated Markov Chain, we select two representative electrical appliances from a specific family in the Pecan Street's Dataport: clothes washer and dishwasher. As the first step, we discretize their continuous minute-resolution power consumption values into several discrete levels. For example (in unit of kW),

- Dishwasher: $U_1 = \{0, 0.2, 0.4, 0.5, 0.7, 0.9, 1.1, 1.31\}$

- Clothes washer: $U_2 = \{0, 0.1, 0.3, 0.5\}$

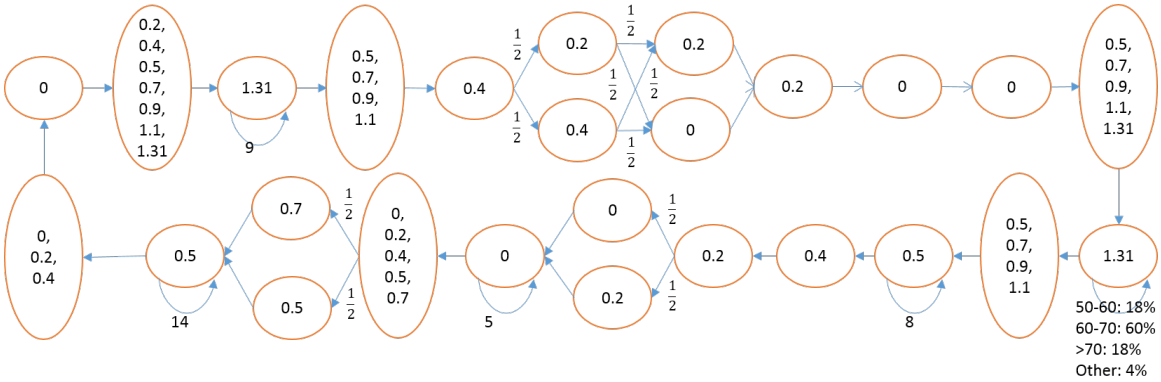

Figure 6.2: Markov Chain of Dishwasher Minute-Resolution Power Consumption Level

It is noted that the step size and level value have been carefully selected through many rounds of testing so as to optimize the disaggregation accuracy and computation complexity, which will be explained in details through a simulation scenario in the Section 6.3. Next, taking the minute-resolution power consumption data of these two electrical appliances during a period of two years from Pecan Street's Dataport as the training data, we infer the transition probabilities between their discrete power consumption levels based on Maximum Likelihood Estimation Algorithm for Naive Bayes Model [32]. Then using these transition probabilities, we generate Markov Chain for dishwasher and clothes washer respectively, as shown in the Fig.6.2 and Fig.6.3.

- The circles represent different states, composed of minute-resolution discretized power consumption level, $u_i^{(j)} \in U_i$;

- The state transitions are represented by a directional arrow from one state to another with probability 1 by default or probability p otherwise;

- According to the power consumption behavior, the electrical appliance may change their steady levels of power consumption in some specific minute slots during the

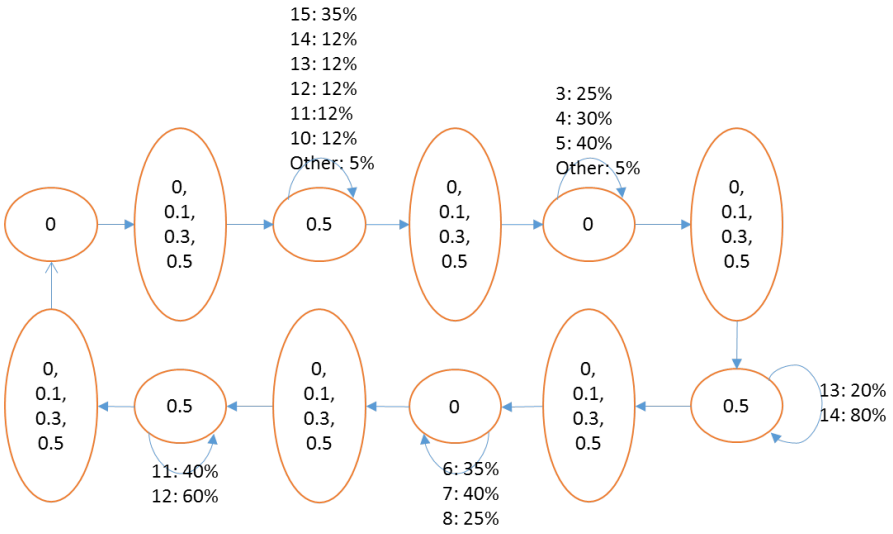

Figure 6.3: Markov Chain of Clothes Washer Minute-Resolution Power Consumption Level

operation, such as start-up, operating mode change and finish stage. These "steady level jumps" may happen at any second within these specific minutes. Therefore the value of "average power" (minute-resolution data) for these slots with "jumps" could be a continuous variable between those two steady levels with uniform probability. After discretization, we may capture and describe this feature by listing K discrete levels in one circle (minute slot), e.g. $u_i^{(j_1)}, u_i^{(j_2)}, ..., u_i^{(j_K)}$. Accordingly, the transition probability from the previous state to any one of these K levels is given as $\frac{1}{K}$ or $\frac{p}{K}$ as appropriate. It is noted that $K \leq |U_i|$ so that the modeling inaccuracy is quite limited;

- A self-transition within the same state with k implies that the appliance keeps operating at this discrete power consumption level for k minute slots before transition to the next state. The probability of this occurring is described by a probability mass function (p.m.f) shown besides the arrow.

6.2.3 Inter-Device Correlations

In addition to the temporal correlations, the power consumptions of some specific electrical appliances show mutual correlations between each other as can be expected. For example, the power consumption behavior of a furnace is synchronized with that of the air conditioner and their respective discrete minute-resolution power consumption levels can be mapped with each other. Therefore, we establish the joint discrete power consumption levels set for air conditioner and furnace, given as (in unit of kW):

- Air Conditioner: $U_3 = \{0, 0.1, 0.3, ..., 2.1, 2.2, ..., 2.9\}$

- Furnace: $U_4 = \{0, 0.12, 0.22, 0.32, 0.42\}$

Subsequently, we generate the Markov Chain for these two devices to capture both their inherent temporal correlations (Fig.6.4) and their discrete power consumption levels mapping table to represent the inter-device correlations, shown in the Table 6.1. Note that in Fig.6.4, the states with notation "$< v$" inside means that the power consumption of this appliance in this minute slot could be any discrete level $u_i^{(j)} \in U_i$ as long as $u_i^{(j)} < v$. On the other hand, if $u_3^{(k)} \in U_3$ is not included in the row with $u_4^{(l)} \in U_4$, then the joint event (air conditioner is consuming power level $u_3^{(k)}$ and furnace is at the power consumption level $u_4^{(l)}$ in the same minute) never happens.

6.2.4 Obtaining Candidate Power Consumption Combinations

Given the discretized power consumption levels of all the appliances, $U_i (1 \leq i \leq N)$, and a measurement of aggregated power consumption $r(t)$ at time t, we may obtain a set of candidate combinations of the disaggregated power consumption levels by enumerative searching, defined as $G(t)$:

$$G(t) = \left[X^1(t), X^2(t), ..., X^{|G(t)|}(t)\right]^T, \tag{6.1}$$

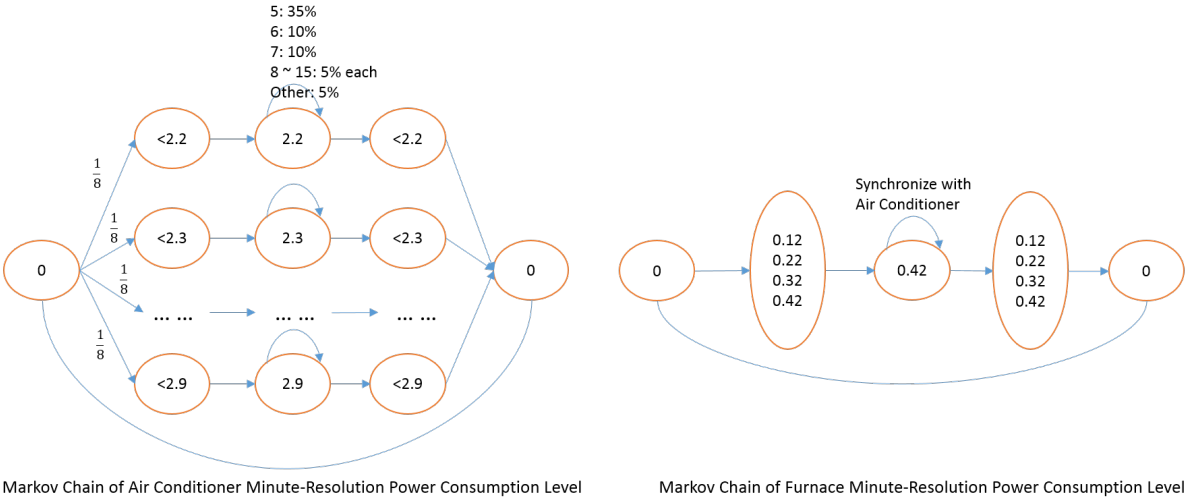

Figure 6.4: Markov Chain of Air Conditioner and Furnace Minute-Resolution Power Consumption Level

Furnace Level	Possible Air Conditioner Level in the same minute
0	0, 0.1, 0.3
0.12	0.1, 0.3, 0.5, 0.7, 0.9
0.22	0.7, 0.9, 1.1, 1.3, 1.5
0.32	1.3, 1.5, 1.7, 1.9
0.42	1.7, 1.9, 2.1, 2.2, 2.3, 2.4, 2.5, 2.6, 2.7, 2.8, 2.9

Table 6.1: Furnace and Air Conditioner Minute-Resolution Power Consumption Levels Mapping Table

where

$$X^g(t) = \left[x_1^g(t), x_2^g(t), ..., x_N^g(t)\right] \quad (1 \leq g \leq |G(t)|), \tag{6.2}$$

and $\forall X^g(t)$, such that

$$|r(t) - \sum_{i=1}^{N} x_i^g(t)| \leq \epsilon, \text{ and } e(x_3^g(t), x_4^g(t)) = 1 \tag{6.3}$$

The element $x_i^g(t) \in U_i$ $(1 \leq i \leq N)$ in the vector $X^g(t)$ denotes the discrete power consumption level of electrical appliance i in the g^{th} combination at minute t, and $e(x_3^g(t), x_4^g(t))$ is defined as

$$e(x_3^g(t), x_4^g(t)) = \begin{cases} 1 & \text{if } x_3^g(t) \text{ and } x_4^g(t) \text{ are in the same row of mapping Table 6.1,} \\ 0 & \text{otherwise.} \end{cases} \tag{6.4}$$

Example 1: with four electrical appliances (dishwasher, clothes washer, air conditioner and furnace), if we choose $\epsilon = 0.02$ and obtain the measurements $r(1) = 0.1, r(2) = 0.5, r(3) = 0.3$, then the groups of possible combinations $G(1), G(2)$ and $G(3)$ are given as:

$$G(1) = \begin{bmatrix} X^1(1) = [0, 0.1, 0, 0] \\ X^2(1) = [0, 0, 0.1, 0] \end{bmatrix} \tag{6.5}$$

$$G(2) = \begin{bmatrix} X^1(2) = [0, 0.5, 0, 0] \\ X^2(2) = [0, 0.1, 0.3, 0.12] \\ X^3(2) = [0, 0.3, 0.1, 0.12] \\ X^4(2) = [0.2, 0, 0.3, 0] \\ X^5(2) = [0.2, 0.1, 0.1, 0.12] \\ X^6(2) = [0.2, 0.3, 0, 0] \\ X^7(2) = [0.4, 0, 0.1, 0] \\ X^8(2) = [0.4, 0.1, 0, 0] \end{bmatrix} \tag{6.6}$$

$$G(3) = \begin{bmatrix} X^1(3) = [0, 0.3, 0, 0] \\ X^2(3) = [0, 0, 0.3, 0] \\ X^3(3) = [0, 0.1, 0.1, 0.12] \\ X^4(3) = [0.2, 0.1, 0, 0] \\ X^5(3) = [0.2, 0, 0.1, 0] \end{bmatrix} \tag{6.7}$$

6.2.5 *Disaggregation Decision based on Markov Chain and Implementation of Viterbi Algorithm*

Per development in the last subsection, we obtain multiple candidate combinations of the disaggregated power consumption levels at any time slot t; therefore we collect consecutive measurements and employ the Markov Chain and mapping table to help determine the *most likely* solution among the candidates. The aggregated power consumption measurements are fed into the disaggregation block continuously for an interval of T minutes to yield $R(T) = [r(1), r(2), ..., r(T)]$ with the corresponding group of candidate combinations $G(1), G(2), ..., G(T)$. If we aim to determine the most likely sequence of disaggregated power consumption over this period, i.e. $[X^*(1) \Rightarrow X^*(2) \Rightarrow \cdots \Rightarrow X^*(T)]$, we have to search among the $\prod_{t=1}^{T} |G(t)|$ possible sequences, implying that the computation complexity increases exponentially.

The Viterbi Algorithm [51] is a widely used decoding algorithm for Markov chains; we tailor it to our model to determine the optimal sequence. First, we group L consecutive disaggregated power consumption statuses into one state $s(t) = [X(t-L+1), X(t-L+2), ..., X(t)]$[1], where L is called *Memory Length*. At any t, there are $M(t) = \prod_{\tau=t-L+1}^{t} |G(\tau)|$ different candidate states $s_i(t)$ $(1 \leq i \leq M(t))$. Note that in contrast to the classical Viterbi Algorithm, the number of states per minute $M(t)$ is *not* time invariant in our model, because $|G(t)|$ is dependent on the current measurement $r(t)$ and is thus time varying, as shown in the *Example 1*. Furthermore, we define the *Branch Metric* $\lambda(s(t) \Rightarrow s(t+1))$ to evaluate the likelihood of the transition from state $s(t)$ to state $s(t+1)$, given as:

$$\begin{aligned} & \lambda(s(t) \Rightarrow s(t+1)) \\ = \; & P[X(t-L+1) \Rightarrow \cdots \Rightarrow X(t) \Rightarrow X(t+1)] \\ = \; & \prod_{i=1}^{N} P[x_i(t-L+1) \Rightarrow \cdots \Rightarrow x_i(t) \Rightarrow x_i(t+1)], \end{aligned}$$

where $P[x_i(t-L+1) \Rightarrow \cdots \Rightarrow x_i(t) \Rightarrow x_i(t+1)]$ is the path probability in the generated Markov Chain for appliance i. The disaggregation procedure is exemplified in the trellis diagram in Fig.6.5 with $L = 2$ and based on *Example 1*. With this model, we aim to find

[1]Without loss of generality, we ignore the superscript index here for simplicity.

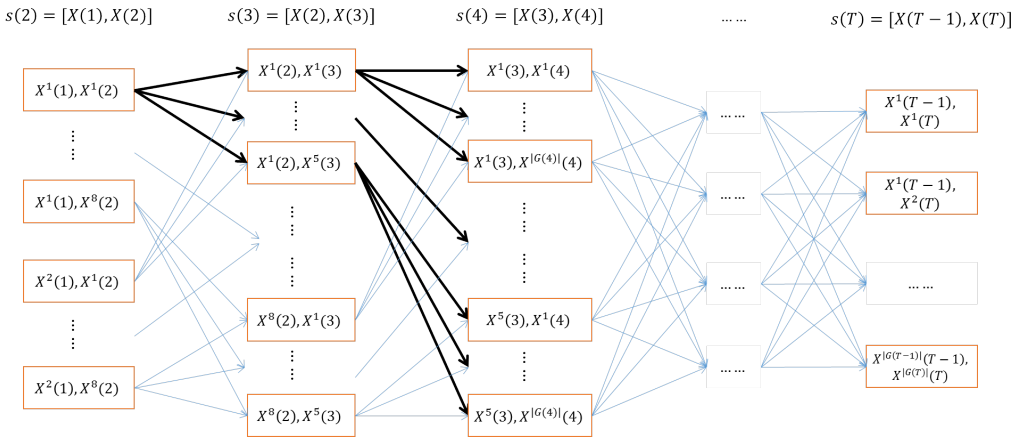

Figure 6.5: Trellis Diagram of Disaggregation Procedure based on Viterbi Algorithm

the optimal state sequence $[s^*(L) \Rightarrow s^*(L+1) \Rightarrow \cdots \Rightarrow s^*(T)]$ such that the corresponding branch metric $\Lambda(T) = \prod_{t=L}^{T-1} \lambda(s(t) \Rightarrow s(t+1))$ is maximized; in turn, this determines the optimal disaggregated solution $[X^*(1) \Rightarrow X^*(2) \Rightarrow \cdots \Rightarrow X^*(T)]$.

According to the Principle of Optimality in Viterbi Algorithm [51], at any given state $s_i(t)$ $(1 \leq i \leq M(t))$, we may select one unique path with the largest accumulated branch metric up to the current minute t, i.e. $\Lambda(t) = \prod_{\tau=L}^{t-1} \lambda(s(\tau) \Rightarrow s(\tau+1))$, among the $|G(t-L)|$ entering paths as the *Survivor*. After that, all these $M(t)$ states extend their survivors in all admissible ways and generate $|G(t+1)| \times M(t)$ candidate paths, which then enables the next-minute states $s(t+1)$ to select their own survivors and merge all these candidate paths into $M(t+1)$ paths (one for each state), as shown in Fig.6.6 and Fig.6.7.

The above "Extend-Merge" is iteratively run along the trellis until the very last state $s(T)$. Hence, at any given minute t, we only need to track $M(t)$ states and associated survivor paths. Therefore, the computation complexity C to check and determine the survivors per minute step is

$$\begin{aligned} C &= \sum_{t=L+1}^{T} |G(t-L)| \times M(t) \\ &= \sum_{t=L+1}^{T} \left(\prod_{\tau=t-L}^{t} |G(\tau)| \right), \end{aligned}$$

which is linear with number of measurements T and exponential with memory size L.

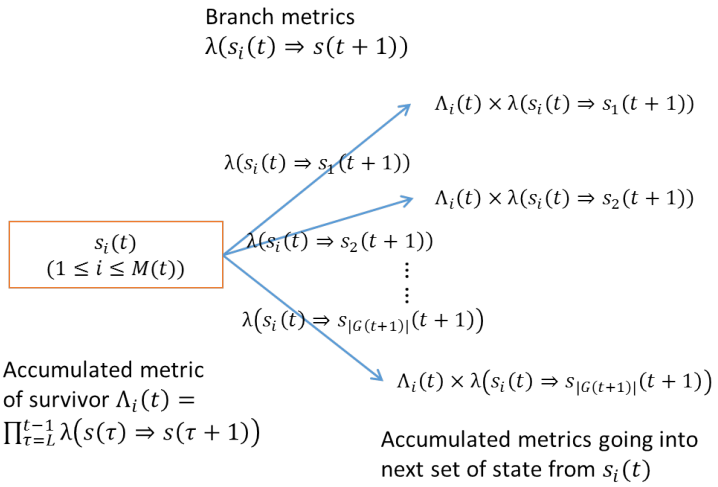

Figure 6.6: The Extend Step of Disaggregation Procedure based on Viterbi Algorithm

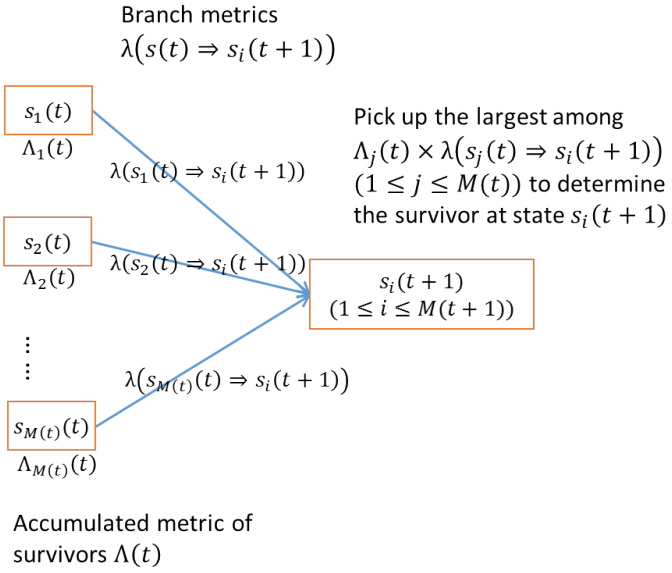

Figure 6.7: The Merge Step of Disaggregation Procedure based on Viterbi Algorithm

In the standard Viterbi Algorithm, as we move forward along the trellis, we may observe that all survivor paths at minute $T' < T$ have already merged at some point in the past and shared a sub-branch, e.g. $s^*(t_1) \Rightarrow s^*(t_2) \Rightarrow \cdots \Rightarrow s^*(t_K)$. Then we make the decision that this common sub-branch must be part of the optimal path and $X^*(t_1 - L + 1) \Rightarrow X^*(t_1 - L + 2) \Rightarrow \cdots \Rightarrow X^*(t_K)$ will be the associated optimal disaggregation solution. For example, as shown in the Fig.6.5, at minute 4, all the survivors have merged at state $s^*(2) = \left[X^1(1), X^1(2)\right]$, which means that the disaggregation solutions to measurements $r(1)$ and $r(2)$ are $X^1(1)$ and $X^1(2)$ respectively. After that, we remove all the states at minute $t_1, t_2, ..., t_K$, (i.e. $s(t_1), s(t_2), ..., s(t_K)$), and process new measurements to continue the Viterbi Algorithm. Then $d(t) = T' - t$, $(t = t_1 - L + 1, ...t_K)$, is the *Decoding Delay* for the measurement $r(t)$.

Although the standard Viterbi Algorithm can achieve high disaggregation accuracy, it may sometimes incur long and unbounded decoding delay. Therefore, we may run a simplified Viterbi Algorithm by imposing a hard constraint on the decoding delay. In this way, in order to disaggregate measurement $r(t)$, at the minute $t + d$, we may choose the optimal state sequence with the highest accumulated branch metrics among the current $M(t + d)$ survivors and obtain the associated optimal disaggregated power consumption statuses $X^*(t)$. After that, we similarly remove all the states at minute $t + L - 1$ from the trellis and feed new measurement, $r(t + d + 1)$, to continue the simplified Viterbi Algorithm and estimate the disaggregated power consumption statuses minute by minute. As a result, a bounded decoding delay $d(t) \leq d$ is achieved for all t.

6.3 Disaggregation Algorithm Tests and Performance Discussions

In order to quantify the performance, we define the disaggregation accuracy, normalized absolute error and average disaggregation delay.

1. Disaggregation Accuracy

To compare the disaggregation solution $X^*(t)$ with the true disaggregated power consumption statuses $Z(t) = [z_1(t), z_2(t), ..., z_N(t)]$, we define the correctness of disaggregation

at minute t, $I(t)$, as

$$I(t) = \prod_{i=1}^{N} I_i(t), \tag{6.8}$$

where

$$I_i(t) = \begin{cases} 1, & \text{if } \exists u_i^{(j)} \in U_i, \text{ such that } |u_i^{(j)} - z_i(t)| \leq \epsilon_i, \text{ and } u_i^{(j)} = x_i^*(t), \\ 0, & \text{otherwise.} \end{cases} \tag{6.9}$$

After feeding the aggregated power consumption measurements for duration T into the disaggregation block and obtaining the associated solutions, we obtain the disaggregation accuracy as $\frac{\sum_{t=1}^{T} I(t)}{T}$.

2. Normalized Absolute Error

In addition to the disaggregation accuracy, we define the normalized absolute error so as to evaluate the numerical mismatch between the disaggregation solution and true disaggregated power consumption status:

$$V(t) = \frac{\sum_{i=1}^{N} |x_i^*(t) - z_i(t)| + |r(t) - \sum_{i=1}^{N} z_i(t)|}{r(t)} \tag{6.10}$$

Hence, the numerical error for a duration T is also given as $\frac{\sum_{t=1}^{T} V(t)}{T}$.

3. Average Disaggregation Delay

We define the average disaggregation delay as

$$D = D_{decode} + D_{proc}, \tag{6.11}$$

where

$$D_{decode} = \frac{\sum_{t=1}^{T} d(t)}{T}, \tag{6.12}$$

and D_{proc} denotes the average processing delay per one minute measurement, which mainly depends on computational complexity C. In order to obtain the average D_{proc}, our algorithm is run on a data set spanning a year's (2013) worth of measurements, i.e. $T = 525600$, from Pecan Street Dataport. The parameters used in the disaggregation algorithm are listed in Table 6.2.

Parameter	Value
Number of Appliances N	4
Default Aggregated Resolution Tolerance ϵ	0.15
Resolution Tolerance for Dishwasher ϵ_1	0.1
Resolution Tolerance for Clothes Washer ϵ_2	0.1
Resolution Tolerance for Air Conditioner ϵ_3	0.1
Resolution Tolerance for Furnace ϵ_4	0.1
Measurement Duration T	1 Year
Default Hard Decoding Delay Bound d	3
Default Memory Length L	2

Table 6.2: Parameters List

Disagg. Accuracy	Norm. Abs. Err.	D_{decode}	D_{proc}	D
58.97%	46.88%	60s	0.057s	60.057s

Table 6.3: Disaggregation Performance of Traditional Real-time Disaggregation Algorithm based on Power Signature Matching

6.3.1 Performance of Traditional Real-time Disaggregation based on Power Signature Matching

As shown in the Table 6.3, the traditional algorithm exhibits poor performance with low disaggregation accuracy and high normalized absolute error due to the fact that it does not use temporal or inter-device correlation information.

6.3.2 Performance of Disaggregation based on Standard Viterbi Algorithm

As shown in the Table 6.4, both the disaggregation accuracy and normalized absolute error is significantly improved compared to the traditional method, due to incorporation of two dimensional correlations captured by the Markov Chain and mapping table. However, there also exist some instances in which the disaggregation algorithm fails. For example, when

Disagg. Accuracy	Norm. Abs. Err.	D_{decode}	D_{proc}	D
98.41%	2.63%	376.2s	2.86s	379.06s

Table 6.4: Disaggregation Performance of Disaggregation based on Standard Viterbi Algorithm

two or more electrical devices start/finish operations within the same minute (very highly transient), it is not possible to identify the accurate power consumption value for each device. During such transient stages, the power consumption value of one device could be any possible discrete level with uniform probability and is independent of the power consumption behavior in the adjacent minutes. Fortunately, in practice, we care more about the power consumption behaviors in the *non-transient* scenarios which comprise the majority cases of interest. On the other hand, the average decoding delay D_{decode} is (stochastically) longer than that of traditional method because with the Standard Viterbi Algorithm, as we have to wait for the convergence of all survivors for a decision.

6.3.3 Performance of Disaggregation based on Simplified Viterbi Algorithm with Hard Constraint on Decoding Delay

As shown in the Table 6.5, the decoding delay D_{decode} is bounded and much improved by using this simplified Viterbi Algorithm. Furthermore, the processing delay D_{proc} also decreases slightly since it only needs to check shorter paths (requiring less computation) when tracing back the state sequence to find the shared sub-branches. However, the disaggregation accuracy and normalized absolute error deteriorate slightly. This is because the simplified Viterbi Algorithm with a hard constraint on decoding delay may lose some temporal correlation information and lead to some unsolvable situations. For example, we observe that the Markov Chains for dishwasher and clothes washer both have a sequential series of states, like $0.5 \Rightarrow 0.5 \Rightarrow \cdots \Rightarrow 0.5$. Therefore, if the aggregated power consumption measurements include such series lasting for more than 6 minutes, this method cannot distinguish between dishwasher and clothes washer.

Disagg. Accuracy	Norm. Abs. Err.	D_{decode}	D_{proc}	D
97.7%	3.94%	180s	0.593s	180.593s

Table 6.5: Disaggregation Performance of Disaggregation based on Simplified Viterbi Algorithm

Disagg. Accuracy	Norm. Abs. Err.	D_{decode}	D_{proc}	D
97.8%	3.82%	240s	11.148s	251.148s

Table 6.6: Disaggregation Performance of Disaggregation based on Simplified Viterbi Algorithm with Larger Memory Length

6.3.4 Impact of Viterbi Algorithm Memory Length L on Performance

In this subsection, we increase the Viterbi Algorithm memory length to $L = 3$ and rerun the simplified Viterbi Algorithm with hard decoding delay bound $d = 4$, whose performance is shown in Table 6.6. The disaggregation accuracy and normalized absolute error are as good as those in Table 6.4. This is because $L = 3$ and $d = 4$ are still not long enough to capture most of the parts of the Markov Chain that can distinguish, for example, between dishwasher and clothes washer when a series of measurements such as $0.5 \Rightarrow 0.5 \Rightarrow \cdots \Rightarrow 0.5$ occurs. On the other hand, the processing delay D_{proc} when $L = 3$ goes up greatly because the computational complexity C increases exponentially with the memory length. However, it is also noted that D_{proc} is still very small compared to the value of D_{decode} and the entire delay D is still on the order of a minute, which satisfies the timing requirements for real-time disaggregation.

6.3.5 Impact of Discretization Step Size on Performance

In this subsection, we shrink the step size to 0.1 kW for air conditioner minute-resolution power consumption discretization and briefly explore its impact on the performance. Then, we set $\bar{U}_3 = \{0, 0.1, 0.2, ..., 2.9\}$ and modify the air conditioner Markov Chain Fig.6.4 and Mapping Table 6.1 accordingly, which is not shown here for conciseness. After that, we

Disagg. Accuracy	Norm. Abs. Err.	D_{decode}	D_{proc}	D
97.74%	3.8%	180s	3.194s	183.194s

Table 6.7: Disaggregation Performance of Disaggregation based on Simplified Viterbi Algorithm with Narrower Step Size

rerun the simplified Viterbi Algorithm with hard decoding delay bound $d = 3$ and obtain the disaggregation performance as shown in Table 6.7. We can observe the disaggregation accuracy is basically the same with that in Table 6.5 and normalized absolute error is improved slightly. This is because shrinking the discretization step size for air conditioner may improve the disaggregation precision even though it cannot work out the unsolvable scenario mentioned above. On the other hand, the processing delay goes up greatly when we set narrower step size. This is because the codebook size $M(t)$ is increased as $|\bar{U}_3| > |U_3|$, which leads to more paths having to be checked in the "Extend-Merge" operation and more computation workloads as a result. Therefore, the step size and discrete level number need to be well designed through many rounds of simulations so as to balance the tradeoff between the disaggregation accuracy and the computation complexity.

6.3.6 Robustness Discussions: Impact of Measurement Noise on Performance

In this subsection, we introduce a bounded and uniformly distributed measurement noise into the aggregated power consumption data, i.e. $r(t) = \sum_{i=1}^{N=4} z_i(t) + w(t)$, $w(t) \sim U(-0.05, +0.05)$. Accordingly, we reset the aggregated resolution tolerance $\epsilon = 0.15+0.05 = 0.2$ to avoid missing correct solutions due to the measurement noise and rerun the simplified Viterbi Algorithm with hard decoding delay bound $d = 3$. As shown in the Table 6.8, both the disaggregation accuracy and normalized absolute error deteriorate slightly because the power consumption of some devices are misestimated due to the measurement noise. However, we can observe that the performance is still more than acceptable because the variance of the measurement noise is quite limited and bounded. On the other hand, the processing delay is increased because loosing the aggregated resolution tolerance ϵ may lead to larger $M(t)$ and heavier computation workloads as a result.

Disagg. Accuracy	Norm. Abs. Err.	D_{decode}	D_{proc}	D
97.0%	5.33%	180s	1.581s	181.581s

Table 6.8: Disaggregation Performance of Disaggregation based on Simplified Viterbi Algorithm with Bounded Measurement Noise

Disagg. Accuracy	Norm. Abs. Err.	D_{decode}	D_{proc}	D
92.01%	20.7%	180s	32.41s	212.41s

Table 6.9: Disaggregation Performance of Disaggregation based on Simplified Viterbi Algorithm with One Unknown Device

6.3.7 Robustness Discussions: Impact of the Inclusion of Unknown Devices on Performance

In this subsection, we include the energy use of a new electrical device, natural gas-powered dryer, in the aggregated measurement data and disaggregation block, whose two-dimensional correlations have not been studied and only the maximal minute-resolution power consumption value 0.45 kW is known. Therefore, we rest $\epsilon = 0.15+0.45 = 0.6$ and rerun the simplified Viterbi Algorithm with hard decoding delay bound $d = 3$. As shown in the Table 6.9, both the disaggregation accuracy and normalized absolute error deteriorate. This is because the power consumption behavior information of natural gas-powered dryer is blind to our disaggregation algorithm, then thus the energy consumed by this newly added device may be easily mislabeled by other appliances, especially when they are not consuming any energy at all. Moreover, the processing delay is increased greatly due to the much looser ϵ and the resulting huge codebook size $M(t)$.

After that, we consider the case that in addition to the four already-analyzed devices, there also exist multiple electrical appliances whose total minute-resolution power consumption pattern $W(t)$ is unknown other than its maximal value W_{max}, i.e. $r(t) = \sum_{i=1}^{N=4} z_i(t) + W(t)$. Since $W(t)$ is the summation of the energy use of multiple devices, we may assume that $W(t) \sim U(0, W_{max} = 0.45)$. Accordingly, we reset $\epsilon = 0.15 + 0.45 = 0.6$ and rerun the simplified Viterbi Algorithm. As shown in the Table 6.10, the disaggregation

Disagg. Accuracy	Norm. Abs. Err.	D_{decode}	D_{proc}	D
88.17%	96.5%	180s	35.58s	215.58s

Table 6.10: Disaggregation Performance of Disaggregation based on Simplified Viterbi Algorithm with Multiple Unknown Devices

accuracy drops and, more importantly, the normalized absolute error goes up dramatically. This is because all the energy consumptions of these unknown devices are counted as the mismatch between the actual measurements and our disaggregation solutions according to the equation 6.10. Moreover, the processing delay is increased greatly as well due to the large ϵ and huge codebook size $M(t)$.

In sum, it is strongly suggested that we need to understand the power consumption behavior of each electrical appliance and capture its two-dimensional correlations before we include it into the disaggregation algorithm. Fortunately, in practice, we may download these information from the manufacturer as we introduce it into our residential power system.

6.4 Conclusions

In this Chapter, we propose a real-time disaggregation algorithm based on Markov Chain model and the Viterbi Algorithm. The model captures the inherent two dimensional correlations of minute-resolution power consumption behavior of each individual electrical appliance, that allows reliable estimation of their disaggregated power consumption status with short delay.

Chapter 7

CONCLUSIONS AND FUTURE WORKS

In this dissertation, the MAC protocol design and data analytics in Smart Metering Network (SMN) are discussed.

After introducing the Advanced Metering Infrastructure (AMI) applications and SMN architecture briefly, we explain the various traffic types and the scalability issue in SMN in details, which make the traditional MAC protocols not perform well in such a densely populated network like SMN.

In order to solve the scalability issue for event-driven data communication, we propose two grouping based MAC protocols: TDMA-DCF and Group Leader DCF-TDMA, which can both reduce the competitive random channel contentions in SMN effectively by dividing all the Smart Meters into several groups. After conducting comprehensive throughput and delay analysis on these two schemes, we can observe that they significantly outperform the traditional random access protocols from the numerical results.

In order to solve the scalability issue for periodic data report, a modified PCF scheme with the aid of cognitive radio technology is proposed. In this method, the Smart Meters are allowed to employ the white space to report their periodic data as secondary users. The numerical and simulation results show that the performance of this modified PCF with cognitive radio is much better than that of traditional one in SMN.

For inclusion of our NS-3 simulation code into a future distribution, we need to follow the syntax format specified by the NS-3 core developers group, inclusive of:

- Complying with the variable naming rules.
- Complying with the data structure selection and implementaions rules.
- Writing self-contained testing file.

- Writing other documentations and so on.

In order to solve the scalability issue for periodic and time-variant power factor measurement report, we propose a new MAC protocol by using compressive sensing. The simulation results prove that the new proposed scheme can decrease the transmission delay effectively compared to the traditional MAC protocols. In the future, we may investigate the performance of this protocol under the scenario with communication noise.

In order to support the demand response more effectively, one of the most important applications in SMN, it is required for the customers to determine the disaggregated power consumption at individual appliance level. Therefore, we propose a real-time disaggregation algorithm based on Markov Chain model and implement it with Viterbi Algorithm, which proves to achieve the accurate estimation of disaggregated power consumption with short delay as shown in the simulation results.

In the future, we may develop this real-time disaggregation algorithm by considering the following three scenarios:

- If we care more about the power consumption statuses of some specific appliances among all the devices involved in the algorithm, we may set non-uniform weights for different appliances and polish their Markov Chains accordingly. Furthermore, the performance metric may also be modified to fit our goal.

- If we care less about the power consumption status on transient stages (steady level jumps), we may polish the Markov Chain of each electrical appliance by removing the states with multiple levels. Furthermore, we should also pre-operate the aggregated measurements before feeding them into the disaggregation algorithm block by detecting and filtering out the samples with transient stages measurements.

- In addition to using the real power value, we may study the two-dimensional correlations of other energy related parameters as our behavior patterns, such as real and reactive power and power factor measurement, and regenerate the Markov Chains and Mapping Tables accordingly. The disaggregation performance by using these different parameters as templates needs to be evaluated.

BIBLIOGRAPHY

[1] IEEE 802.11ah TG. Association id management for tgah. *IEEE 802.11-11/0088r1*, 2011.

[2] IEEE 802.11ah TG. Potential compromise for 802.11ah use case document. *IEEE 802.11-11/0457r0*, 2011.

[3] IEEE 802.11ah TG. Tgah channel model proposed text. *IEEE 802.11-11/0968r3*, 2011.

[4] IEEE 802.11ah TG. Specification framework for tgah. *IEEE 802.11-11/1137r15*, 2013.

[5] A. Ghassemi, S. Bavarian, and L.Lampe. Cognitive radio for smart grid communications. *2010 IEEE International Conference on Smart Grid Communications*, 2010.

[6] A.A.Sreesha, S.Somal, and I.Lu. Cognitive radio based wireless sensor network architecture for smart grid utility. *2011 IEEE Systems, Applications and Technology Conference*, 2011.

[7] A.I.Cole, and A.Albicki. Algorithm for non-intrusive identification of residential appliances. *Proceeding of IEEE International Symposium on Circuits and Systems (ISCAS 98)*, 1998.

[8] National Electrical Manufacturers Association. American national standard for utility industry end device data tables. 2008.

[9] C.Foh, M.Zukerman and J.Tantra. A markovian framework for performance evaluation of ieee 802.11. *IEEE Transactions on Wireless Communications*, 6, 2007.

[10] C.Lima. Smart grid communications logical reference architecture. *IEEE P2030-09-0110-00-0011*, 2009.

[11] D.L.Donoho. Compressed sensing. *IEEE Transactions on Information Theory*, 2006.

[12] E.J.Candes and M.B.Wakin. People hearing without listening: An introduction to compressive sampling. *IEEE Signal Processing Magazine*, 2008.

[13] E.J.Candes, and T.Tao. Near optimal signal recovery from random projections: Universal encoding strategies. *IEEE Transactions on Information Theory*, (12), 2006.

[14] E.J.Candes, J.Romberg, and T.Tao. Robust uncertainty principles: Exact signal reconstruction from highly incomplete frequency information. *IEEE Transactions on Information Theory*, 2006.

[15] E.Ziouva, and T.Antonakopoulos. Csma/ca performance under high traffic conditions: Throughput and delay analysis. *Computer Communications*, (25), 2008.

[16] F.Daneshgaran, M.Laddomada, F.Mesiti, and M.Mondin. Unsaturated throughput analysis of ieee 802.11 in presence of non ideal transmission channel and capture effects. *IEEE Transactions on Wireless Communications*, 7(4), 2008.

[17] F.Liu, J.Wang, Y.Han, and P.Han. Cognitive radio networks for smart grid communications. *2013 Asian Control Conference*, 2013.

[18] G.Bianchi. Performance analysis of the ieee 802.11 distributed coordination function. *IEEE Journal on Selected Areas in Communications*, 18(3), 2000.

[19] G.W.Hart. Nonintrusive appliance load monitoring. *Proceeding of the IEEE*, 80(12), 1992.

[20] H.Li, R.Mao, L.Lai, and R.C.Qiu. Compressed meter reading for delay-sensitive and secure load report in smart grid. *IEEE 2010 International Conference in Smart Grid Communications*, 2010.

[21] H.Ma, H.Alazemi, and S.Roy. A stochastic model for optimizing physical carrier sensing and spatial reuse in wireless ad hoc networks. *IEEE International Conference on Mobile Adhoc and Sensor Systems*, 2005.

[22] H.Tan, H.Lee, and V.Mok. Automatic power meter reading system using gsm network. *IEEE International Conference on Control Application*, 2007.

[23] IEEE 802.11 TG. Ieee standard for wireless lan medium access control (mac) and physical layer (phy) specifications. 1997.

[24] Electric Power Research Institute. Summary of epri test circuits. *www.epri.com.*

[25] J.Froehlich, E.Larson, S.Gupta, and G.Cohn, M.S.Reynolds, and S.N.Patel. Disaggregated end-use energy sensing for the smart grid. *IEEE Transactions on Pervasive Computing*, 10(1), 2010.

[26] J.G.Proakis. *Digital Communications, Fifth Edition.* McGraw Hill Publishing House, 2009.

[27] J.Z.Kolter, S.Batra, and A.Y.Ng. Energy disaggregation via discriminative sparse coding. *Proceeding of 2010 Conference on Advances in Neural Information Processing Systems*, 2010.

[28] K.Clement, K.V.Reusel, and J.Driesen. The consumption of electrical energy of plug-in hybrid electric vehicles in belgium. *Proceeding of 2nd Conference of European Ele-Drive Transportation*, 2007.

[29] K.Mets, T.Verschueren, W.Haerick, C.Develder, and F.Turck. Optimizing smart energy control strategies for plug-in hybrid electric vehicle charging. *2010 IEEE Networks Operations and Management Symposium Workshops*, 2010.

[30] M.Berges, E.Goldman, H.S.Matthews, and L.Soibelman. Training load monitoring algorithms on highly sub-metered home electricity consumption data. *Tsinghua Science and Technology*, 13, 2008.

[31] M.Berges, L.Soibelman, and H.S.Matthews. Building commissioning as an opportunity for training non-intrusive load monitoring algorithms. *Proceeding of 16th International Conference of Innovation in Architecture, Engineering and Construction*, 2010.

[32] M.Collins. The naive bayes model, maximum-likelihood estimation, and the em algorithm. *Lecture Notes, www.cs.columbia.edu/m̃collins/em.pdf.*

[33] M.Costanzo, D.Archer, E.Aronson, and T.Pettigrew. Energy conservation behavior: The difficult path from information to action. *American Psychologist*, 41(5), 1986.

[34] M.Gulati, S.S.Ram, and A.Singh. An in depth study into using emi signatures for appliance identification. *Proceedings of the 1st ACM Conference on Embedded Systems for Energy-Efficient Buildings*, 2014.

[35] M.Pipattanasomporn, M.Kuzlu, S.Rahman, and Y.Teklu. Load profiles of selected major household appliances and their demand response opportunities. *IEEE Transactions on Smart Grid*, 5(2), 2014.

[36] M.Roberts, and H.Kuhns. Towards bridging the gap between the smart grid and smart energy consumption. *Proceeding of 2010 ACEEE Summer Study on Energy Efficiency in Buildings*, 2010.

[37] O.Ekici, and A.Yongacoglu. Ieee 802.11a throughput performance with hidden nodes. *IEEE Communications Letters*, 12(6), 2008.

[38] Office of Energy Efficiency of Natural Resources Canada. 2003 survey of household energy use-detailed statistical report. 2003.

[39] Pecan Street's Inc. Pecan street's dataport. *https://dataport.pecanstreet.org*.

[40] Research Report of SBI Research. http://www.sbireports.com/smart-grid-utility-2496610/.

[41] R.P.Lewis, P.Igic, and Z.Zhongfu. Assessment of communications methods for smart electricity metering in the uk. *IEEE PES/IAS Conference of Sustainable Alternative Energy (SAE)*, 2009.

[42] R.Shinghal and G.Toussaint. Experiments in text recognition with the modified viterbi algorithm. *IEEE Transactions on Pattern Analysis and Machine Intelligence*, 1979.

[43] R.Yu, Y.Zhang, S.Gjessing, C.Yuen, S.Xie, and M.Guizani. Cognitive radio based hierarchical communications infrastructure for smart grid. *IEEE Magazine on Network*, 2011.

[44] S.B.Leeb, S.R.Shaw, and J.L.Kirtley Jr. Transient event detection in spectral envelope estimates for nonintrusive load monitoring. *IEEE Transactions on Power Delivery*, 3(3), 1995.

[45] S.Chen, D.L.Donoho, and M.Saunders. Atomic decompositions by basis pursit. *SIAM Journal on Scientific Computing*, (1), 1999.

[46] Seattle City Light and University of Washington. Pacific northwest smart grid demonstration project. *http://www.pnwsmartgrid.org/docs/UWseattle.pdf*, 2014.

[47] S.Gupta, M.S.Reynolds, and S.N.Patel. Electrisense: single-point sensing using emi for electrical event detection and classification the home. *Proceedings of the 12th ACM International Conference on Ubiquitous Computing*, 2010.

[48] T.Adame, A.Bel, B.Bellalta, J.Barcelo. J.Gonzalez, and M.Oliver. Capacity analysis of ieee 802.11ah wlans for m2m communications. *Proceedings of 6th International Workshop, MACOM*, 2013.

[49] AEIC Team. Aeic/smartgrid ami interoperability standard guidelines for ansi c12.19 communications. *Version 2.0*, 2010.

[50] T.Khalifa, K.Naik, and A.Nayak. A survey of communication protocols for automatic meter reading applications. *IEEE Communications Survey and Tutorials*, 13(2), 2011.

[51] U.Madhow. Fundamentals of digital communications. *Cambridge University Press*, 2008.

[52] V.C.Gungor, D.Sahin, T.Kocak, and S.Ergut. Smart grid communications and networking. *Turk Telekon Technology Report*, 2011.

[53] V.C.Gungor, D.Sahin, T.Kocak, S.Ergut, C.Buccella, C.Cecati, and G.P.Hancke. Smart grid technologies: Communication technologies and standards. *IEEE Transactions on Industrial Informatics*, 7(4), 2011.

[54] W.Kempton and L.Montgomery. Folk quantification of energy. *Energy*, 7(10), 1982.

[55] W.Wang, Y.Xu, and M.Khanna. A survey on the communication architectures in smart grid. *Computer Networks*, 55(16), 2011.

[56] Y.G.Goutam, M.Girish Chandra, K.Srinivasarengan, and S.Kadhe. On electrical load disaggregation using factor graphs. *Proceedings of 2013 International Conference on Advances in Computing, Communications and Informatics*, 2013.

[57] Y.Peizhong, A.Iwayemi, and C.Zhou. Developing zigbee deployment guideline under wifi interference for smart grid applications. *IEEE Transactions on Smart Grid*, (1), 2011.

[58] Y.Yang, and S.Roy. Grouping based mac protocols for ev charging data transmission in smart metering network. *IEEE Journal of Selected Area on Communications*, 32(7), 2014.

[59] Y.Yuan, W.Arbaugh, and S.Lu. Towards scalable mac design for high-speed wireless lans. *EURASIP Journal on Wireless Communications and Networking*, 2007.

[60] Z.Abichar. Group-based medium access control for ieee 802.11n wireless lans. *IEEE Transactions on Mobile Computing*, 2013.

VITA

Yue Yang receives his B.S degree in Electrical and Computer Engineering from Shanghai Jiaotong University, Shanghai, China, in 2011. He is at present working towards his Ph.D. degree in Electrical Engineering from University of Washington, Seattle, WA, US. His current work focuses on the MAC protocols design and data analysis algorithm in Smart Metering Network. He is an IEEE student member. His Ph.D. thesis is titled Contributions to Transport and Analysis of Smart Metering Data.

Publications:

- Yue Yang and Sumit Roy, "Grouping Based MAC Protocols for EV Charging Data Transmission in Smart Metering Network", *IEEE Journal of Selected Area on Communications*, vol 32, no 7, July 2014.

- Yue Yang and Sumit Roy, "PMU Deployment for Three-Phase Optimal State Estimation Performance", *IEEE International Conference on Smart Grid Communications*, Vancouver, Canada, 2013.

- Yue Yang and Sumit Roy, "PMU Deployment for Optimal State Estimation Performance", *IEEE GLOBECOM*, Anaheim, CA, USA, 2012.

- Yue Yang and Sumit Roy, "Real-time Disaggregation of User Power Consumption using the Viterbi Algorithm", *IEEE Transactions on Smart Grid*, under review.

- Yue Yang and Sumit Roy, "MAC Protocol Design for Periodic Power Factor Measurement Report with Compressive Sensing", *IEEE Transactions on Communications*, to be submitted.

- Yue Yang and Sumit Roy, "Smart Grid Communication R&D Program, DOE FOA-0000313: Networked Communication for Distributed Energy Resource Management

System (DERMS)".